PhD Thesis

Membrane properties of ceramide: a fluorescence spectroscopic and microscopic study

Biofisika Institute (UPV/EHU, CSIC)
Department of Biochemistry and Molecular Biology
Faculty of Science and Technology
University of the Basque Country (UPV/EHU)

Ibai Artetxe González

Supervisor: Prof. Félix M. Goñi Urcelay

Leioa 2017

CONTENTS

ABBREVIATIONS

ΔH	enthalpy
$\Delta T_{1/2}$	width at half-height phase transition (in calorimetry)
3KdhSph	3-ketodihydrosphingosine
9,10-DPA	9,10-diphenylanthracene
α	pre-exponential factor (in time-resolved fluorescence)
α_F	pre-exponential factor of free calcein lifetime (in calcein assay)
α_E	pre-exponential factor of entrapped calcein lifetime (in calcein assay)
γ	edge tension
λ	wavelength
λ_{em}	emission wavelength
λ_{ex}	excitation wavelength
η	viscosity
τ	fluorescence lifetime
τ_F	free calcein lifetime (in calcein assay)
τ_E	entrapped calcein lifetime (in calcein assay)
ANTS	8-aminonaphtalene-1,3,6-trisulfonic acid
BHT	butylated hydroxytoluene
BODIPY	4,4-difluoro-4-bora-3a, 4a-diaza-s-indacene
BSA	bovine serum albumin
C	crystalline lipid phase
C2-Cer	acetylceramide
C12-Cer	lauroylceramide
C16-Cer	palmitoylceramide
C24:1-Cer	nervonoylceramide
CDase	ceramidase
Cer	ceramide
Cer1P	ceramide-1-phosphate
CerS	(dihydro)ceramide synthase
CERT	ceramide transfer protein
Chol	cholesterol
CK	ceramide kinase

CL	cardiolipin
CoA	coenzyme A
C_p	heat capacity
DAG	diacylglycerol
DeoCer	1-deoxyceramide
DeodhCer	1-deoxydihydroceramide
DeometdhCer	1-deoxymethyldihydroceramide
dhCer	dihydroceramide
dhSph	dihydrosphingosine
DiD	1,1'-Dioctadecyl-3,3,3',3'-tetramethylindodicarbocyanine perchlorate
DiI	1,1'-dioctadecyl-3,3,3',3'-tetramethylindocarbocyanine perchlorate
DiO	3,3'-dioctadecyloxacarbocyanine perchlorate
DLS	dynamic light scattering
DMSO	dimethyl sulfoxide
DOPC	1,2-dioleoyl-L-α-phosphatidylcholine
DOPS	1,2-dioleoyl-L-α-phosphatidylserine
Doxyl	4,4-dimethyl-3-oxazolinidyloxy
DPG	1,2-dipalmitoyl-*sn*-glycerol
DPH	1,6-diphenyl-1,3,5-hexatriene
DPhPC	1,2-diphytanoyl-L-α-phosphatidylcholine
DPPC	1,2-dipalmitoyl-L-α-phosphatidylcholine
DPX	*p*-xylene-bis-pyridinium bromide
DRM	detergent-resistant membrane
DSC	differential scanning calorimetry
DSPC	1,2-distearoyl-L-α-phosphatidylcholine
E	efflux
eCer	egg ceramide
EDTA	ethylenediaminetetraacetic acid
ePC	egg phosphatidylcholine
ePE	egg phosphatidylethanolamine
eSM	egg sphingomyelin
FAPP2	four-phosphate-adaptor protein 2
FRET	Föster resonance energy transfer
GABA	*gamma*-aminobutyric acid

GCase	glucosylceramidase
GCS	glucosylceramide synthase
GluCer	glucosylceramide
GPI	glycosylphosphatidylinositol
GSL	glycosphingolipid
GUV	giant unilamellar vesicles
H	hexagonal lipid phase
H_I	type I hexagonal lipid phase
H_{II}	type II hexagonal or inverted hexagonal lipid phase
HEPES	4-(2-Hydroxyethyl)piperazine-1-ethanesulfonic acid
ITO	indium tin oxide
k_B	Boltzmann constant
L	lamellar lipid phase
L_α	fluid or liquid-crystalline lamellar lipid phase
L_β	gel or solid ordered lamellar lipid phase
$L_{\beta'}$	tilted lamellar lipid phase
L_c	lamellar crystalline lipid phase
L_d	liquid-disordered lamellar lipid phase
L_o	liquid-ordered lamellar lipid phase
LUV	large unilamellar vesicles
M	micellar lipid phase
M_I	type I micellar lipid phase
M_{II}	type II micellar or inverted micellar lipid phase
MLV	multilamellar vesicles
MOM	mitochondrial outer membrane
NBD	N-7-nitrobenz-2-oxa-1,3-diazol-4-yl
P	oblique lipid phase
PA	phosphatidic acid
PC	phosphatidylcholine
pCer	palmitoylceramide
PDI	polydispersity index
PE	phosphatidylethanolamine
PG	phosphatidylglycerol
PI	phosphatidylinositol

PI(4)P	phosphatidylinositol-4-phosphate
PI(4,5)P	phosphatidylinositol-4,5-biphosphate
PIPES	piperazine-1,4-bis(2-ethanesulfonic acid)
POPC	1-palmitoyl-2-oleoyl-L-α-phosphatidylcholine
PS	phosphatidylserine
pSM	palmitoylsphingomyelin
PTFE	polytetrafluoroethylene
Q	cubic lipid phase
Q_I	type I cubic lipid phase
Q_{II}	type II cubic or inverted cubic lipid phase
Q_{STAT}	static quenching
r	pore radius
R	vesicle radius
R_h	hydrodynamic radius of spherical particles
Rho-PE	18:1 phosphatidylethanolamine-N-(lissamine rhodamine B sulfonyl)
SM	sphingomyelin
SMase	sphingomyelinase
SMS	sphingomyelin synthase
SK	sphingosine kinase
Sph	sphingosine
Sph1P, S1P	sphingosine-1-phosphate
SPPase	sphingosine phosphate phosphatase
SPT	serine phosphoryltransferase
SUV	small unilamellar vesicles
T	temperature
THF	tetrahydrofuran
T_m	phase transition temperature
tPA	*trans*-parinaric acid
Triton-X-100	octylphenoxypolyethoxyethanol

Chapter 1:

GENERAL INTRODUCTION AND OBJECTIVES

Chapter 1: GENERAL INTRODUCTION AND OBJECTIVES

1.1 Cell membranes

Biological membranes play a key role in the structure and function of both prokaryotic and eukaryotic cells. They mainly act as semipermeable barriers separating two compartments while allowing selective exchange of substances between them. They are also important for the generation of chemical and charge gradients, regulation of enzyme activity and signaling. Some membranes can even have specialized functions such as nutrient uptake in the intestines, insulation in the nerves and light perception in the retinal rods. The plasma membrane separates the cell cytoplasm from the external environment and defines the shape of the cell through interactions with the cytoskeleton. Additionally, eukaryotic sub-cellular organelles and both endocytic and exocytic vesicles are also delimited by a membrane (Figure 1.1) (Stillwell, 2013).

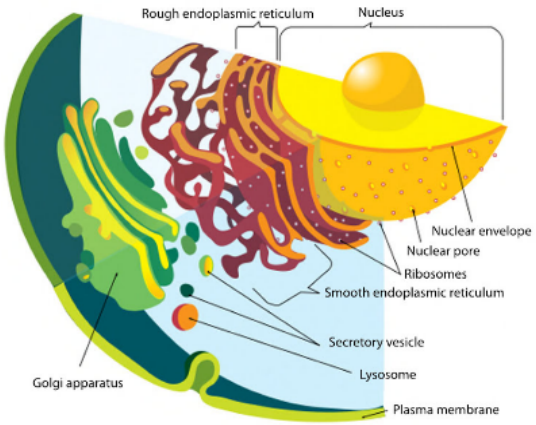

Figure 1.1. The endomembrane system of an animal cell. Taken from Stillwell (2013).

The fundamental architecture of the membrane is based on a lipid bilayer, composed of amphipathic lipids that contain both polar (headgroup) and nonpolar moieties. These molecules cannot be dissolved in water and upon dispersion into aqueous media most of them aggregate into two opposed layers with their polar headgroups in contact with the water molecules and their hydrophobic tails buried in the core of the bilayer, facing each other. This aggregation happens spontaneously, driven by the unfavorable interaction of the hydrophobic moieties of the lipids with the water molecules (known as the hydrophobic effect). The main function of the lipid bilayer is compartmentalization by means of creating a non-selective permeability barrier for most polar molecules (although permeable to water). This allows the cells to maintain specific internal pH and ionic conditions, which are essential for the correct function of intracellular components and/or organelles (Luckey, 2008).

Although lipids can have specific functions such as second messengers in signaling processes, most of the diverse activities exhibited by biological membranes are carried out by proteins in association with or inserted into the lipid bilayer. For example, proteins are crucial for the selective permeability of the membrane. While small uncharged molecules such as oxygen and carbon dioxide can freely diffuse across the membrane, the diffusion of larger molecules is restricted by the lipid bilayer. Specific transport proteins allow these molecules to cross the membrane. Some of the transport proteins just facilitate diffusion by forming pores or channels, but others can actively transport molecules against their concentration gradient, thus promoting the accumulation of solutes and the creation of solute gradients. Membrane proteins also perform different kinds of enzymatic activity, supporting cell metabolism, as well as communication across the membrane without transport of molecules (Yeagle, 2012).

One of the earliest studies on membrane properties was performed in 1895 by Ernest Overton. His observation that non-polar molecules could diffuse across a cell membrane led him to the conclusion that this was a lipidic structure (Kleinzeller, 1998). Later, in 1925, Gortel and Grendel discovered that the basic architecture of membranes was a lipid bilayer, based on the fact that the surface area of a monolayer formed by a lipid extract from erythrocytes was twice the surface area corresponding to those erythrocytes (Gorter and Grendel, 1925). The presence of proteins was detected and included in the "sandwich" model proposed by Danielli and Davson (1935). This model postulated a membrane structure with globular proteins on the outer surfaces of a lipid bilayer (Figure 1.2A). This "sandwich" model was well accepted and only slightly modified by replacing the globular proteins with proteins in an extended β-sheet conformation (Figure 1.2B), which led to the concept of the "unit membrane" common to all biological membranes defended by Robertson in the light of results obtained by electron microscopy (Robertson, 1959). However, the work of Benson and Green on thylakoid and mitochondrial membranes led to a completely different model where the membrane was constituted by lipoprotein subunits devoid of a lipid bilayer (Figure 1.2C) (Benson, 1966; Vanderkooi and Green, 1970). Finally, in 1972 Singer and Nicolson proposed what is now the accepted paradigm of the structure of the biological membrane: the fluid mosaic model (Figure 1.2D) (Singer and Nicolson, 1972).

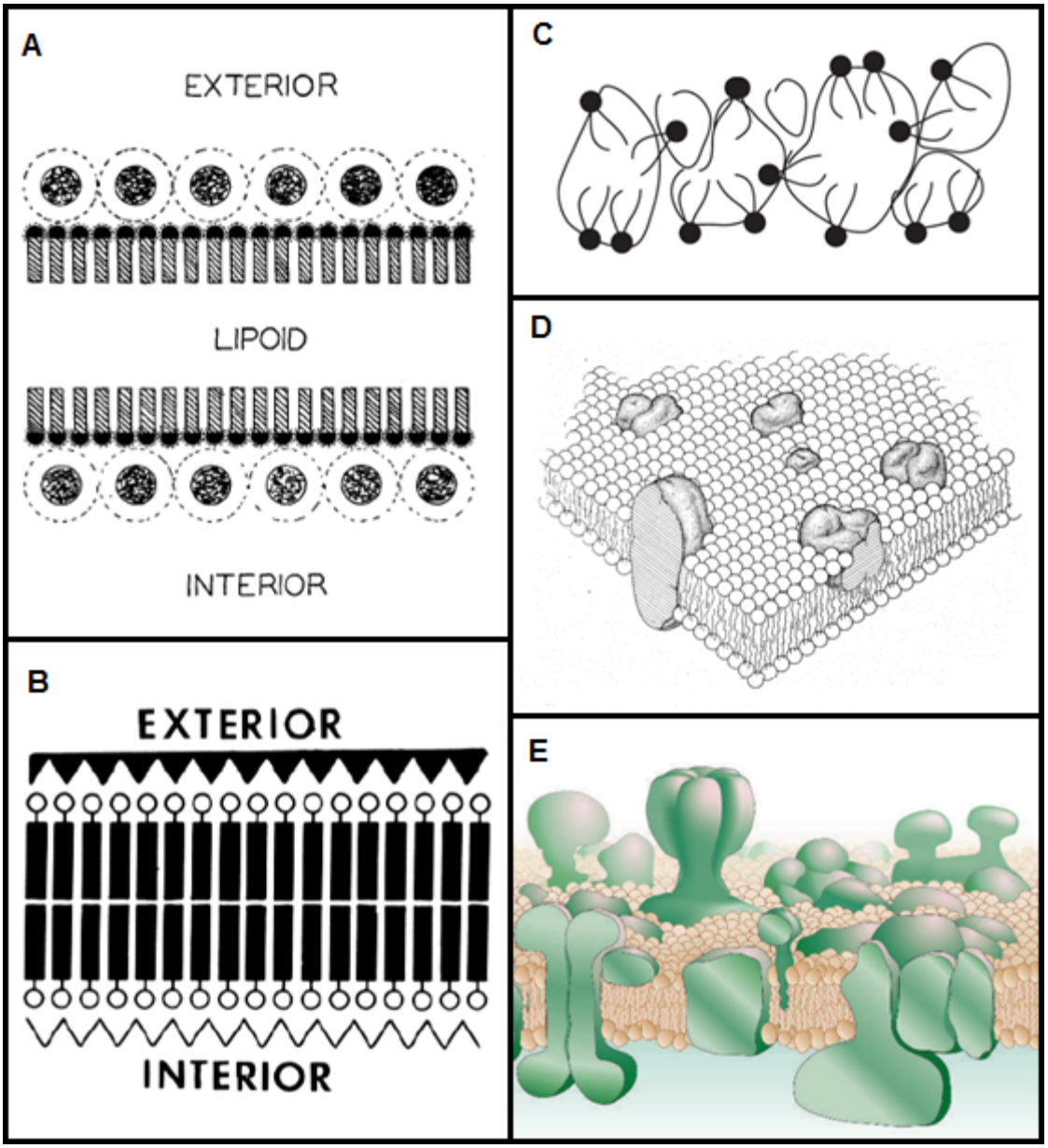

Figure 1.2. Architecture of membrane models. (A) The Davson-Danielli model showing a lipid bilayer enclosed between layers of globular proteins. Taken from Danielli and Davson (1935). (B) The unit membrane proposed by Robertson, with proteins still enclosing the lipid bilayer but in a β-sheet conformation. Taken from Robertson (1981). (C) The Benson-Green Lipoprotein Subunit membrane model for photosynthetic thylakoids and mammalian mitochondria, with large protein particles arranged in complexes and solvated by few lipid molecules (no lipid bilayer present). Taken from Stillwell (2013). (D) The Fluid Mosaic model of Singer and Nicolson composed of a lipid bilayer where intrinsic proteins are integrally embedded. Taken from Singer and Nicolson (1972). (E) An updated version of the membrane structure showing a high density of transmembrane proteins and a highly perturbed bilayer due to this protein crowding. Taken from Engelman (2005).

The fluid mosaic model describes the membrane as a lipid bilayer which will act as a solvent for embedded amphiphilic proteins, also called integral proteins (Figure 1.2, D), while some other proteins are electrostatically bound to the membrane surface. It is a mosaic in the sense that proteins are scattered across the bilayer and along its surface. This model also emphasizes that the lipid bilayer is fluid, so lipids and proteins can diffuse laterally in the plane of the membrane. This dynamism facilitates interactions between lipids and proteins, important for membrane function. Translocation between leaflets, on the contrary, was proposed to be highly limited. Another property described by the fluid mosaic model is the asymmetry of cell membranes, which can be observed in most membrane constituents and also contributes to membrane function. Membrane carbohydrates, for example, are only present in the outer leaflet of the bilayer where they participate in cellular recognition. Additionally, lipids heterogeneously accumulate between the two monolayers of the lipid bilayer, the composition of each leaflet being different (see section 1.4.1 Lipid distribution). Asymmetry is also applied to integral proteins, which always show the same orientation.

The fluid mosaic model remains as the paradigm of membrane structure, yet decades of experimentation in the field of membranes have brought several novel concepts that have complemented and expanded the original model (Goni, 2014). Now it is known that membranes are highly crowded with proteins (Figure 1.2, E), whose mobility can be limited by the cytoskeleton in eukaryotic cells, and which can also create large complexes to carry out many functions in the membrane. This high protein density will thus result in a strong perturbation of the lipid bilayer. Indeed, the lipid bilayer is no longer seen as a static homogeneous structure. Trans-bilayer lipid motions, membrane curvature, the appearance of transient non-lamellar phases, lipid lateral heterogeneity and the presence of laterally segregated membrane domains have contributed to a shift in the paradigm into a more dynamic view of the lipid bilayer. An important contribution regarding the lateral heterogeneity of membranes was the proposal by Simons and Ikonen in 1997 of the existence of lateral sphingolipid- and cholesterol-enriched lipid structures that could serve as platforms for protein attachment during signal transduction (Simons and Ikonen, 1997). These structures, denoted as “lipid rafts”, are believed to have profound effects on the nature of the membrane and opened the door to the now well accepted view on the importance of membrane domains for its biological function (see section 1.4 Lipid domains).

1.2 Membrane lipids

Natural membrane lipids are amphipathic biomolecules that upon dispersion in aqueous solutions self-aggregate forming bilayer structures, thus being the basic components of cell membranes. In the early membrane models, lipids were only considered to be the solvent in which proteins are embedded. A small number of different species should be enough to play that role. However, membrane lipids show a large diversity, from simple fatty acids to complex sphingoglycolipids, each species showing important biological functions (Yeagle, 2012).

The basic units of most membrane lipids are the fatty acids. They can be saturated or unsaturated. Double bonds of natural fatty acids are always *cis*, so they produce a kink in the acyl chain which leads to packing defects, making lipids and membranes more fluid and disordered. The single C-C bonds can also be in two conformations: *trans* or *gauche*. *All-trans* acyl chains are linear, allowing a dense packing and favoring ordered phases. On the contrary, *gauche* conformation induces a kink in the acyl chain that promotes a disordering effect and disordered phases. As temperature is increased, *gauche* isomers increase, leading to a phase transition from a solid, densely packed, ordered phase to a fluid, disordered phase (see section 1.2.2 Lipid polymorphism) (Luckey, 2008). The main natural fatty acids present in membrane lipids are summarized in Table 1.1. Note that the melting temperature (i.e. the temperature at which the solid phase become fluid) increases for saturated fatty acids and those with longer hydrocarbon chains. Although some free fatty acids can be found in the membrane, most of them are part of complex membrane lipids as hydrophobic acyl chains covalently bound to a polar headgroup.

Structure (x:y) Δ	Common name	Melting temperature (°C)
12:0	lauric acid	44,2
14:0	myristic acid	52
16:0	palmitic acid	63,1
18:0	stearic acid	69,6
20:0	arachidic acid	75,4
22:0	behenic acid	81
24:0	lignoceric acid	84,2
16:1 Δ9	palmitoleic acid	-0,5
18:1 Δ9	oleic acid	13,4
18:2 Δ9,12	linoleic acid	-9
18:3 Δ9,12,15	linolenic acid	-17
20:4 Δ5,8,11,14	arachidonic acid	-49,5
24:1 Δ15	nervonic acid	39

Table 1.1. Main fatty acids found in membrane lipids. x: number of carbon atoms, y: number of double bonds, Δ: position of the double bond.

1.2.1 Lipid classification

Membrane lipids can be classified into three main groups: glycerolipids, sphingolipids and sterols.

1) Glycerolipids are structurally based on a glycerol molecule and can be further classified into two groups: glycerophospholipids and glyceroglycolipids. Glycerophospholipids are the main lipids constituting the bulk of the membrane. These lipids present two fatty acids, usually one saturated and one unsaturated, bound to carbons in *sn*-1 and *sn*-2 position of a glycerol molecule, respectively. Then a phosphate group is linked to the carbon in the glycerol *sn*-3 position. Finally, esterification of the phosphate group with different headgroups gives rise to the variety of glycerophospholipids that are found in natural membranes (Figure 1.3). The properties of each type of glycerophospholipids depend mainly on the headgroup and the acyl chain composition. While phosphatidylcholine (PC) is generally responsible for the constitution of the bulk of the bilayer, lipids such as phosphatidylethanolamine (PE), phosphatidylserine (PS) and phosphatidylinositol (PI) have more specific functions. The acyl chain composition affects mainly the order, fluidity and melting temperature of the lipid bilayer. Additionally, acyl chains can have specific functions when released by lipases, as it happens with the bioactive arachidonic acid (Brash, 2001).

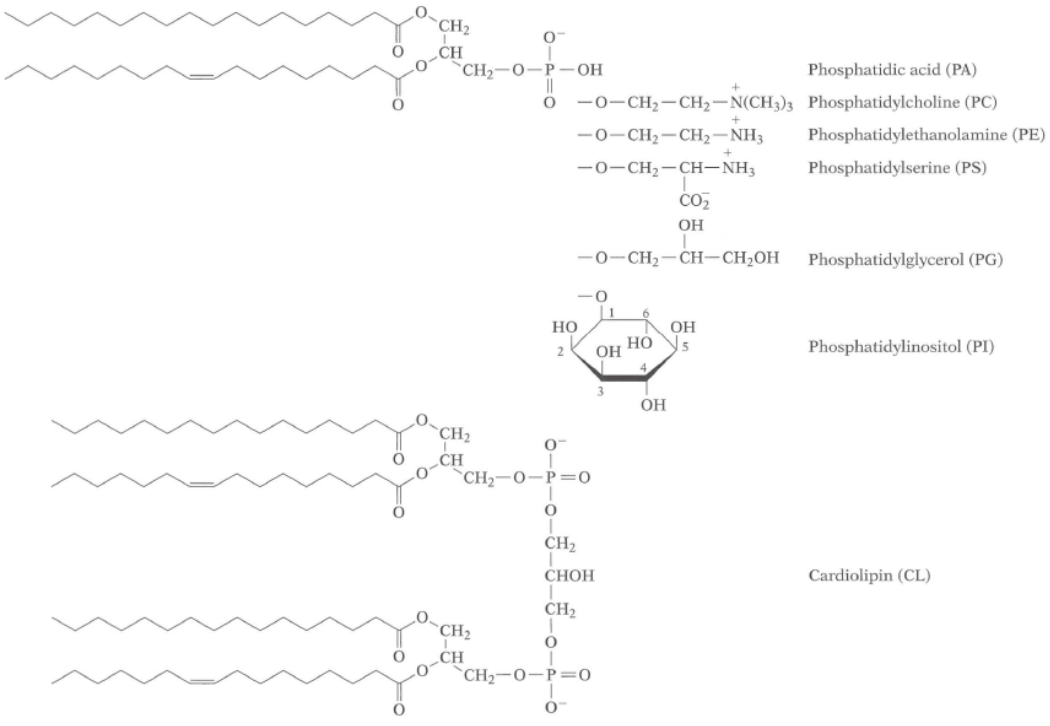

Figure 1.3. Structure of common glycerophospholipids. Taken from Luckey (2008).

The second class of glycerolipids is that of glyceroglycolipids. These are less abundant in animal cell membranes but highly present in plants and bacteria. The difference with glycerophospholipids is that, instead of a phosphate group, they contain a mono- or oligosaccharide group bound to carbon *sn*-3 of glycerol. The major glyceroglycolipid is monogalactosyldiacylglycerol, a lipid present in thylakoid membranes and one of the most abundant lipids in nature (Holzl and Dormann, 2007).

2) Sphingolipids are similar to glycerolipids, but they have a long-chain base as its backbone, instead of glycerol. The long-chain base is an amino alcohol, usually sphingosine, the simplest sphingolipid. Binding of a fatty acid (usually saturated) to the sphingosine moiety by amide linkage generates ceramide (Figure 1.4), an important lipid in several cellular processes such as apoptosis (Castro *et al.*, 2014; Goni *et al.*, 2014). Attachment of a phosphorylcholine residue to the ceramide molecule results in the formation of sphingomyelin (Figure 1.4), a common lipid in the external leaflet of plasma membranes. Other common sphingolipids are glycosphingolipids, which show one or more sugar residues as polar headgroup. Apart from their role in membrane structure, sphingolipids have more specific functions than glycerolipids, for example, as second messengers in cell signaling processes (Carreira *et al.*, 2015; Hannun and Obeid, 2008).

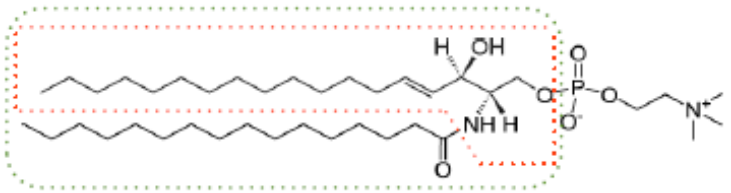

Figure 1.4. Structure of sphingomyelin (whole structure), ceramide (green dotted box) and sphingosine (red dotted box).

3) The third group of membrane lipids comprises the sterols, highly hydrophobic molecules based on a four-ring structure with a free hydroxyl group (Figure 1.5). This small polar headgroup orients the molecule so the hydrophobic part is buried in the bilayer and the hydroxyl group is located at the interface. The main type of sterol depends on the organism: ergosterol in yeast, stigmasterol and β-sitosterol in plants and cholesterol in animals. Replacement of sterol in organisms shows that each sterol has a non-specific function (that any sterol can perform) and a specific effect (exclusive of each sterol).

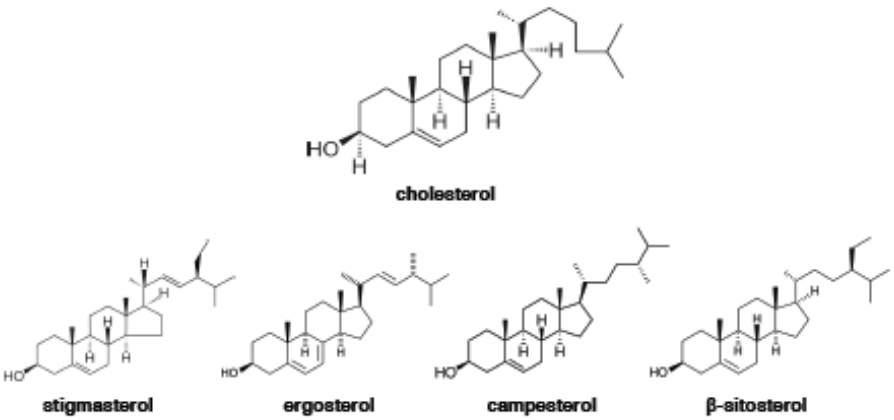

Figure 1.5. Structure of cholesterol and other common sterols.

The best known sterol is cholesterol, principally found in plasma membranes where it can account for up to 30 mol% of the total lipid, being present in even higher amounts in red blood cells and ocular lens membranes. Cholesterol cannot form bilayers, the small head group being unable of effectively shielding the hydrophobic part from water (Huang and Feigenson, 1999). This is why it favors interaction with phospholipids of large headgroups (Bjorkbom *et al.*, 2010). Cholesterol regulates the lipid bilayer fluidity and increases membrane thickness. Additionally, it can also regulate the lateral organization of membranes by associating with sphingolipids to generate membrane domains, such as "rafts" (Simons and Ikonen, 1997).

1.2.2 Lipid polymorphism

Membranes are always in the form of a bilayer, but this is not the only structure that can be formed by lipids in solution. Actually, the formation of transient non-lamellar structures is known to be essential for biological processes such as membrane fusion and fission (Gilbert, 2016). Due to their low water solubility, lipids tend to self-aggregate when dispersed in an aqueous solution following the hydrophobic effect (Stillwell, 2013), the structure adopted by the lipid assembly depending on pH, temperature, pressure, ionic strength, hydration level and the geometry of the lipid. Lipids at that point are said to exist in a particular phase: a thermodynamic idealization defined under equilibrium conditions and characterized by particular physical dimensions. Lipidic phases are classified according to three criteria: (i) kind of lattice, (ii) order of the acyl chains and (iii) overall structure curvature.

The most accepted nomenclature was proposed by Vittorio Luzzati based on x-ray studies (Luzzati, 1968). This nomenclature uses a capital letter to define the kind of lattice: unidimensional micellar (M) or lamellar (L), bidimensional hexagonal (H) or oblique (P) and tridimensional cubic (Q) or crystalline (C). Additionally, subscripts are used to classify the unidimensional lamellar phases according to the acyl chain order: disordered or fluid (L_α), ordered and perpendicular to the plane of the membrane (also called gel) (L_β), ordered and tilted with respect to the plane of the membrane ($L_{\beta'}$) and crystalline (L_c). Later, a new lamellar phase with intermediate properties between fluid disordered and gel was described: the liquid-ordered phase (L_o). Finally, non-lamellar phases can be classified using subscripts according to their overall curvature as type I or II: type I corresponds to an overall positive curvature (oil-in-water) and the type II, or inverted, describes an overall negative curvature (water-in-oil). Permutations between phases, also called phase transitions, can occur with changes in temperature (thermotropic transitions), pressure (barotropic transitions) or solvent proportions (lyotropic transitions) among others. An overview of the different phases can be seen in Figure 1.6. Among them, the most biologically relevant phases are the lamellar and the inverted hexagonal phases.

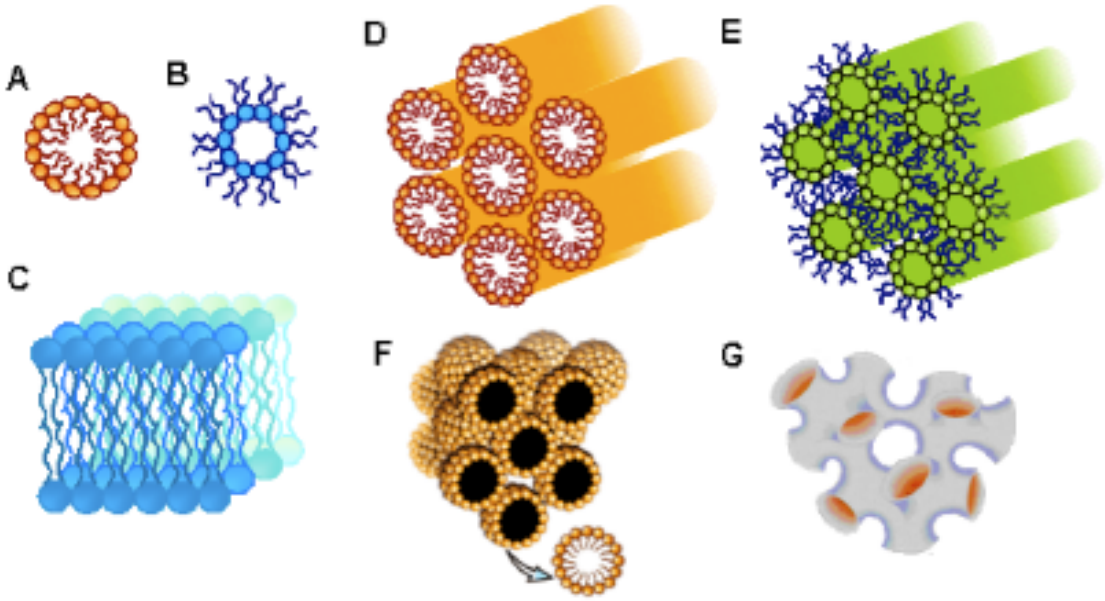

Figure 1.6. Lipid polymorphism. A, micellar type I (M_I); B, inverted micellar (M_{II}); C, lamellar (L); D, hexagonal type I (H_I); E, inverted hexagonal (H_{II}); F, cubic type I (Q_I); G, inverted cubic (Q_{II}).

The basic structure of biological membranes under equilibrium conditions is a lipid bilayer in a lamellar phase. This lamellar phase is usually liquid crystalline (L_α, also called liquid-disordered or L_d), gel (L_β), or sometimes a phase with intermediate properties named liquid-ordered (L_o). The L_α phase is characterized by the ability of lipids to freely diffuse laterally or rotationally, and by the acyl chains being in a complete disordered state, with most carbon-carbon conformers in a *gauche* conformation. This phase usually corresponds to lipids with at least one unsaturated acyl chain. Saturated lipids, on the contrary, are generally present in a L_β phase when in the pure state. The acyl chains are highly ordered, with a high proportion of *trans* C-C conformers, so lateral and rotational motion is restricted. When a lipid bilayer in a gel state is heated, the C-C *gauche* conformer proportion increases and the acyl chain order decreases until a disordered phase is formed, usually coupled to a decrease in the bilayer thickness (Figure 1.7). The phase transition from L_β to L_α is commonly known as the main phase transition or gel-fluid transition and the temperature at which that transition occurs is the main transition temperature or melting temperature (T_m). The T_m and the thermodynamics of the main phase transition of pure or lipid mixtures can be easily studied using differential scanning calorimetry (DSC) (Figure 1.7B).

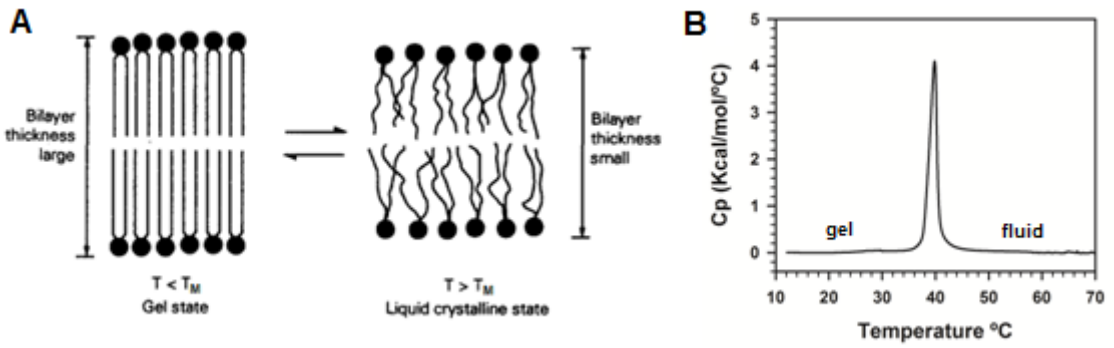

Figure 1.7. Lamellar gel-fluid phase transition. (A) Changes in thickness and chain order due to phase transition. (B) DSC thermogram of the main transition of palmitoylsphingomyelin (pSM).

While most membrane lipids are fluid at the physiological temperature, some of them (mainly saturated sphingolipids) have the ability to form gel domains in the bilayer phase due to their high T_m. The third phase, called liquid-ordered (L_o), was described on lipid mixtures of phospholipids with sterols (Ipsen *et al.*, 1987). This phase shows intermediate properties between the gel and the liquid-disordered phases: most C-C conformers are *trans* but lateral diffusion is allowed. This is the phase in which membrane rafts are supposed to exist (Brown and London, 1998).

Although the lipid bilayer of a natural cell membrane resembles the structure of a lamellar phase, transient generation of non-lamellar structures appears to be important for several mechanisms such as fusion or fission processes, the most relevant non-lamellar structure being the hexagonal phase. This is a bidimensional structure with large parallel cylinders with a hexagonal packing. Hexagonal phases can be of type I, the acyl chains of the lipids placed towards the centre of the cylinder, or they can also be an inverted phase (type II), when the polar headgroups are in the center of the cylinder and the acyl chains are in contact with hydrophobic tails from other cylinders.

While most lipids in cell membranes (the most abundant being PC) tend to form a lamellar phase, some lipids with a cone-shaped geometry such as PE (see section 1.2.3 Lipid geometry) can promote inverted hexagonal phase formation. Therefore the ratio of lamellar vs. hexagonal phase-forming lipids (usually PC/PE ratio) influences the propensity of hexagonal phases for being generated within the bilayer. Interestingly, processes of lipid- and protein-mediated pore and/or channel formation seem to recruit non-lamellar phase-forming lipids for stabilization of the structure, while lipids with propensity for hexagonal phase formation are also required in contact sites between membranes in fusion events and for the final neck generation before fission processes (Gilbert, 2016).

1.2.3 Lipid geometry

The lipid phase formed by lipids will depend highly on the structure or geometry of the lipid involved. This was proposed in 1980 by Jacob Israelachvili, suggesting that the structures of lipid aggregates are determined by the cross-sectional area between the polar headgroup and the hydrophobic tail of the lipid (Israelachvili *et al.*, 1980). According to this, the lipids can be classified into three shapes depending on the morphological parameter $S = V/A_0L_c$, where "V" is the volume of the lipid molecule, "A_0" the area of the molecule at the lipid-water interface and "L_c" the length of the extended acyl chain. This parameter depends on the relationship between the area at the interface (A_0) and the cross-sectional area in the hydrophobic tail (A_H), since $V = A_HL_c$ for a lipid displaying cylindrical shape, determining the shape of the lipid and the structure it forms upon aggregation, as described in Figure 1.8:

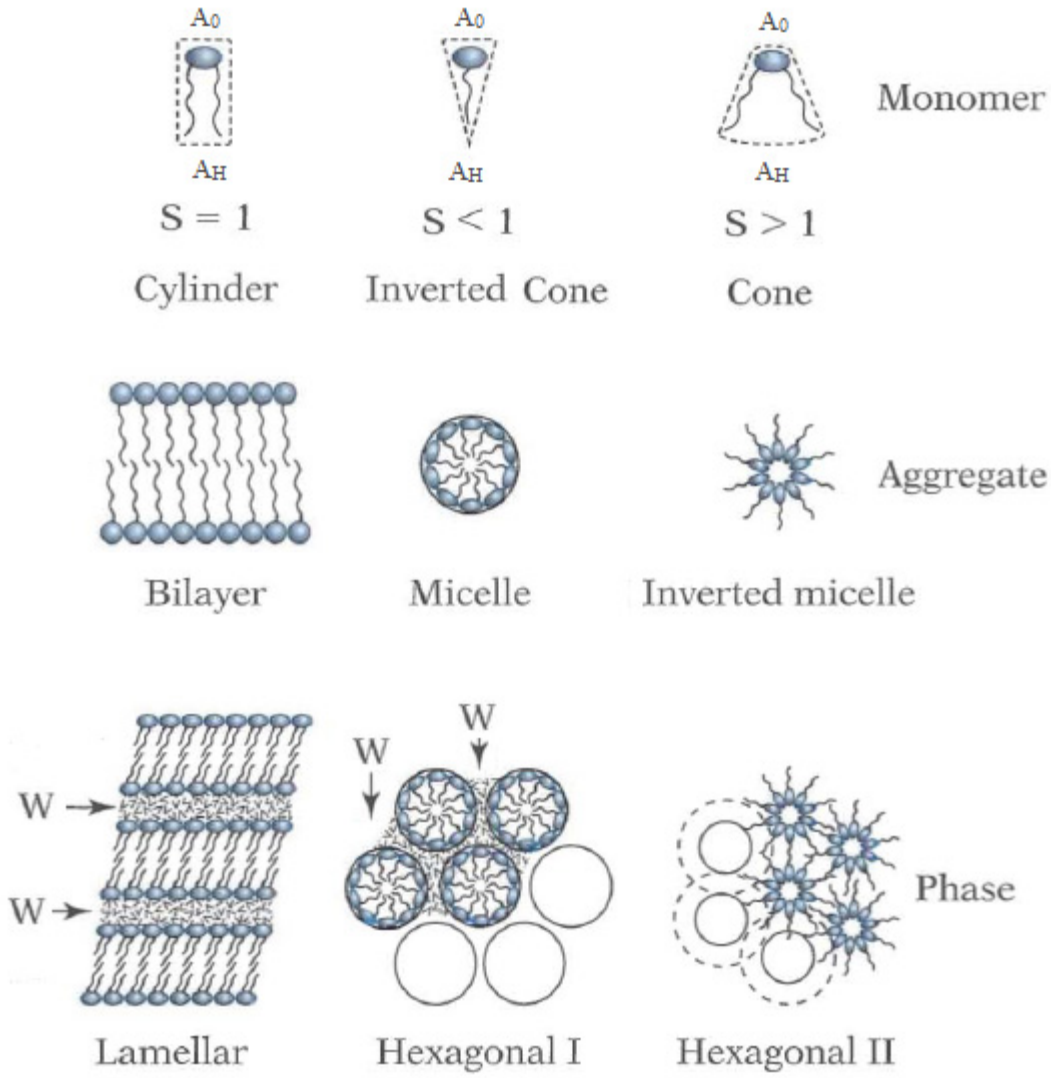

Figure 1.8. Relationship between lipid geometry and the resulting lipid aggregate and phase. W: water. Adapted from Luckey (2008).

-When $A_0 = A_H$ (S = 1) the lipid presents a cylindrical shape. These lipids (PC, SM) induce the formation of lamellar bilayers with zero curvature.

-When $A_0 > A_H$ (S < 1) the lipid presents an inverted cone shape. Lipids with this shape (lysophospholipids) aggregate into micelles and promote type I hexagonal phases. When present in membranes they induce positive curvature.

-When $A_0 < A_H$ (S > 1) the lipid presents a cone shape. These lipids (PE, ceramide, diacylglycerol, sterols) induce negative curvature on the membrane and promote the formation of inverted hexagonal phases.

1.3 Sphingolipids

Sphingolipids are a family of lipids structurally based on sphingosine, or (2S, 3R, 4E)-2-amino-4-octadecene-1,3-diol. They were discovered in 1884 by Johann L.W. Thudichum, who isolated a brain-derived compound that he named after the mythological sphinx, with regard to its enigmatic nature (Thudichum, 1884). Initially they were merely considered as inert structural lipids for decades, until they started to attract the attention of many scientists after the discovery of the sphingolipid signaling pathway (Hannun *et al.*, 1986; Kolesnick, 1987). Nowadays, many sphingolipids are considered to be bioactive molecules that act as secondary messengers in different signaling pathways (Carreira *et al.*, 2015; Hannun and Obeid, 2008).

Sphingolipid biosynthesis (Figure 1.9) starts in the endoplasmic reticulum, where L-serine and acyl-coenzyme A are condensed to 3-ketosphinganine. This molecule will then be converted into sphinganine (or dihydrosphingosine), which will be in turn acylated to dihydroceramide and desaturated to obtain ceramide. Dihydrosphingolipids have been considered to be inert lipids, so they have not been has extensively studied as their counterpart bioactive sphingolipids. However, recent studies in the last decade suggest that dihydroceramide may be biologically active, showing a different function than its counterpart, ceramide (Fabrias *et al.*, 2012; Siddique *et al.*, 2015). Additionally, the enzyme catalyzing desaturation of dihydroceramide to ceramide, thus a key regulator of the equilibrium between dihydrosphingolipids and common sphingolipids in cell homeostasis, is emerging as a novel therapeutic target in cancer and HIV-1 infection (Fabrias *et al.*, 2012; Vieira *et al.*, 2010). Once ceramide has been formed, it will be transported via specific protein transport to the Golgi, where sphingomyelin and the complex glycosphingolipids will be synthesized and delivered to the plasma membrane via vesicular transport (Figure 1.9).

Constitutive degradation of sphingolipids occurs in acidic compartments, i.e. in late endosomes or lysosomes (Figure 1.9). However, fast sphingomyelin degradation to ceramide can also occur in the plasma membrane (Figure 1.9) in response to several stress-induced extracellular and intracellular stimuli (Henry *et al.*, 2013). This pathway allows a fast and highly regulated generation of lipid messengers that can act in different signaling pathways of the cellular stress response.

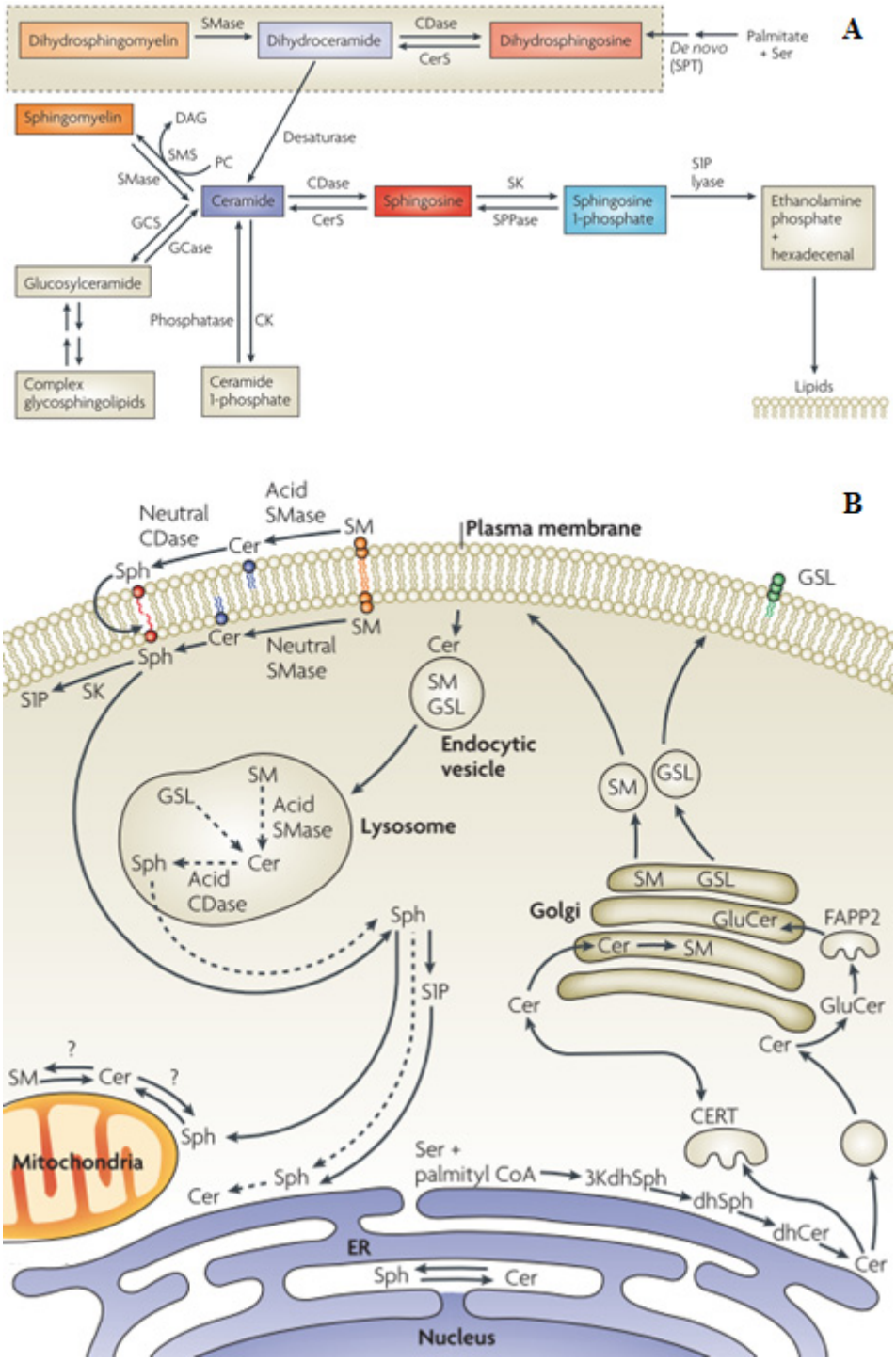

Figure 1.9. Sphingolipid metabolism. (A) Diagram of sphingolipid metabolism showing enzymatic pathways. (B) Compartmentalization of sphingolipid metabolism. Abbreviations: CDase = ceramidase, CerS = (dihydro)ceramide synthase, CERT = ceramide transfer protein, CK = ceramide kinase, FAPP2 = four-phosphate-adaptor protein 2, GALC = galactosylceramidase, GCase = glucosylceramidase, GCS = glucosylceramide synthase, SK= sphingosine kinase, SMase = sphingomyelinase, SMS = sphingomyelin synthase, SPPase = sphingosine phosphate phosphatase, SPT = serine phosphoryltransferase. Adapted from Hannun and Obeid (2008).

The principal bioactive sphingolipids are sphingosine, ceramide and their phosphate analogues sphingosine-1-phosphate (Sph1P) and ceramide-1-phosphate (Cer1P) (Gomez-Munoz *et al.*, 2016; Goni *et al.*, 2014). These are simple sphingolipids with unique biophysical properties (Table 1.2) that can have a profound impact on the physical properties of cell membranes, which is suggested to be the basis for some of their physiological functions (Goni *et al.*, 2014).

Table 1.2. Biophysical properties of simple sphingolipids. Adapted from Goni *et al.* (2014).

Sphingolipid	Property
Sphingosine	Net positive charge at physiological pH
	Increases membrane permeability
	Rigidifies bilayer acyl chains
	Facilitates cubic phase formation (with negatively charged lipids)
Sph-1-P	Somewhat water-soluble (critical micellar concentration 12 μM)
	Stabilizes lipid lamellar structure
Ceramides	Increase lipid chain order
	Segregate laterally into rigid domains
	Increase membrane permeability
	Induce flip-flop motion of lipids
	Facilitate H_{II} phase formation
Cer-1-P	Spontaneously forms bilayers
	pK_a very sensitive to phospholipid composition

Sphingosine, the simplest sphingolipid, was the first one identified as a bioactive lipid due to its ability to interact with protein kinases (Hannun *et al.*, 1986). This sphingolipid has been shown to induce membrane permeabilization, a recent study suggesting this as a possible pathogenic mechanism for the Niemann-Pick disease type C1 (Jimenez-Rojo *et al.*, 2014c). Ceramide is also well known as a bioactive lipid, deeply involved in cellular stress response pathways (Obeid *et al.*, 1993). Its ability to laterally segregate into domains could create membrane platforms clustering receptor molecules that mediate in signal transduction processes (Cremesti *et al.*, 2001; Zhang *et al.*, 2009). Additionally, phosphorylation of sphingosine and ceramide generates Sph1P and Cer1P respectively, both of them potent bioactive lipids with anti-apoptotic effects and deeply involved in several cellular processes such as cell migration and inflammatory responses (Gomez-Munoz *et al.*, 2016). Interestingly, Sph1P and Cer1P can exert both pro- and anti-inflammatory responses, depending on the cell type where they are generated (Gomez-Munoz *et al.*, 2016).

1.3.1 Ceramide

N-acylsphingosine, or ceramide, is one of the best studied sphingolipids and the main focus of the present thesis. This simple sphingolipid is well known for its role in several biological processes such as cell proliferation, apoptosis, and inflammatory responses (Castro *et al.*, 2014; Gomez-Munoz *et al.*, 2016; Goni *et al.*, 2014). Ceramide levels in resting membranes are very low, yet they can significantly increase under cellular stress conditions or upon several stimuli (such as death receptor ligands, cytokines or ionizing radiation) and act as second messengers in different intracellular response pathways (Hannun, 1996; Kolesnick *et al.*, 2000). Additionally, ceramides are noted by their unusual physico-chemical properties, being able to cause profound changes in the biophysical properties of membranes. These alterations may be the underlying mechanism behind ceramide function in cellular processes.

Ceramide constitutes the basic hydrophobic structure of sphingomyelin and other complex sphingolipids. It consists of a sphingoid base with a fatty acid of variable chain length in its amino group. Most common ceramides have sphingosine as their sphingoid base and long (C16-24) saturated acyl chains. Nevertheless, ceramides with different sphingoid bases and acyl chains can also be naturally found. Interestingly, the biophysical properties of ceramides have been shown to be highly dependent on the length and unsaturation degree of both the sphingoid base (Fabrias *et al.*, 2012; Maula *et al.*, 2012) and the acyl chain (Chiantia *et al.*, 2007; Jimenez-Rojo *et al.*, 2014a; Megha *et al.*, 2007; Pinto *et al.*, 2011; Sot *et al.*, 2005a; Sot *et al.*, 2005b). Additionally, a novel category of bioactive sphingolipids, sphingoid bases without the 1-hydroxy group, was recently described to be synthesized in mammalian cells and animals (Zitomer *et al.*, 2009), and found to be related to diabetes mellitus (Bertea *et al.*, 2010; Zuellig *et al.*, 2014). Acylation of such sphingoid bases gives rise to 1-deoxyceramides, which showed interesting biophysical properties in a recent study (Jimenez-Rojo *et al.*, 2014b).

Ceramide generation follows two principal mechanisms (Figure 1.9). One is the *de novo* synthesis in the endoplasmic reticulum from serine and acyl-CoA. Ceramide generated in this compartment will then be transported to the Golgi where it will serve as the basis for the generation of complex sphingolipids such as sphingomyelin and glycosphingolipids. A further pathway is sphingomyelin hydrolysis by a

sphingomyelinase (SMase), which will generate ceramide and phosphorylcholine. The latter pathway can occur in the plasma membrane and in acidic compartments such as lysosomes (Henry *et al.*, 2013). The regulation of ceramide generation is highly important, since accumulation of this lipid can lead to profound changes in the biophysical properties of the membrane, and is also considered as a strong apoptotic signal. Indeed, several apoptotic stimuli are known to activate both ceramide generation pathways (Henry *et al.*, 2013; Mullen and Obeid, 2012; Wang *et al.*, 2015). Therefore, ceramide and the enzymes that regulate its production and degradation are becoming important targets in the medical and pharmaceutical fields and especially in cancer treatment (Jacobi *et al.*, 2016; Li and Zhang, 2015).

As previously stated, ceramide can deeply alter the biophysical properties of membranes (Castro *et al.*, 2014; Goni *et al.*, 2014). For example, they induce negative curvature in the lipid bilayer due to their cone geometry, thus facilitating the formation of inverted hexagonal phases (Sot *et al.*, 2005a; Veiga *et al.*, 1999), which could be important in membrane fusion processes (Basanez *et al.*, 1997). Additionally, contrary to what was postulated by Singer and Nicolson in their fluid mosaic model, ceramides show a fast transmembrane (flip-flop) lipid motion (Lopez-Montero *et al.*, 2005) and can even induce generalized flip-flop motion in the membrane (Contreras *et al.*, 2005; Contreras *et al.*, 2003).

Another interesting property of ceramides is their ability to induce membrane permeabilization (Montes *et al.*, 2002; Ruiz-Arguello *et al.*, 1996; Siskind and Colombini, 2000), which could be directly related to the ability of ceramide to induce permeabilization of mitochondria to cytochrome c, promoting apoptosis (Di Paola *et al.*, 2000). The mechanism behind this process is still debated, though. Chapter 5 in this thesis is intended to clarify this topic.

Finally, ceramide is well known for its ability to increase acyl chain order and laterally segregate in highly ordered gel-like domains (Busto *et al.*, 2009; Castro *et al.*, 2007; Catapano *et al.*, 2011; Sot *et al.*, 2006). These domains could generate large membrane platforms working as recruiting sites for different proteins that would then act in signal transduction processes (Cremesti *et al.*, 2001; Zhang *et al.*, 2009), in a similar way to the proposed mechanism for the activation of apoptotic machinery by the drug edelfosine (Mollinedo and Gajate, 2006).

1.4 Lipid domains

1.4.1 Lipid distribution

Lipids do not distribute homogeneously in the membrane. Each cell type has a different lipid composition, and even within the same cell lipids are present in different proportions depending on the organelle. Additionally, the cell membrane is asymmetric, a property that was already described in the fluid mosaic model of Singer and Nicolson (1972). Human erythrocytes, for example, show larger amounts of zwitterionic lipids such as PC and SM in the external leaflet of the membrane, while charged and/or amino-group containing phospholipids (mainly PE, PS and PI) are more abundant in the internal leaflet (Figure 1.10). Thus, membranes are asymmetric not only for the lipid composition but also for the electrical charge.

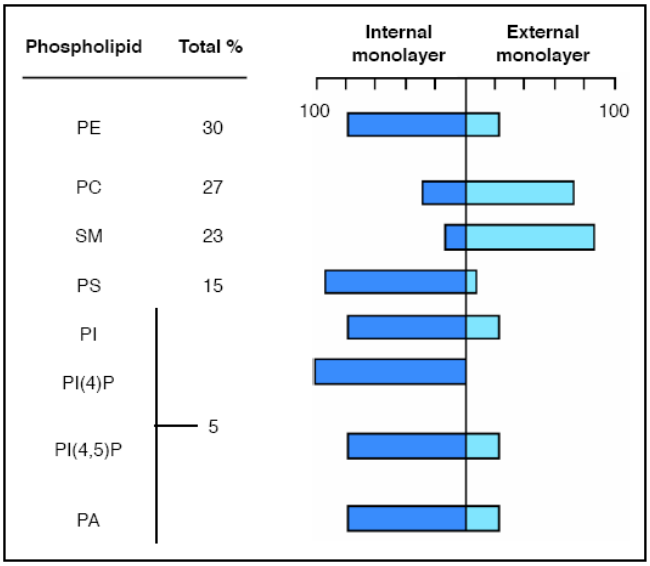

Figure 1.10. Asymmetric distribution of phospholipids in the erythrocyte plasma membrane.

Membrane asymmetry is a result of the active synthesis of lipids being located only in a specific leaflet and also due to the work of specific lipid translocases. This asymmetry is crucial for membrane function. For instance, PI and its derivatives specifically interact with several internal proteins and act as key players in important cellular processes (Irvine, 2016). Additionally, under certain specific stimuli, transverse diffusion of the lipids can happen. This can be seen during the apoptotic response in a cell, when PS residing in the inner monolayer of the cell membrane is externalized, becoming a signal for macrophage recruitment (Fadok *et al.*, 1998).

Lipids can also be heterogeneously distributed in the plane of the bilayer, giving rise to laterally segregated regions, commonly referred to as membrane domains, with different composition and properties as compared to the rest of the membrane. The concept of "membrane rafts", proposed by Kai Simons and collaborators, is a widely known example of membrane domains (Simons and Ikonen, 1997). Rafts are described as transient structures or microdomains in the plane of the bilayer with profound biological implications. They are proposed to exist in the liquid-ordered phase, an intermediate between the liquid-disordered and the gel phase. Membrane rafts are also proposed to be generally enriched in sphingolipids, cholesterol and also in some proteins that associate through lipid-anchors or structural characteristics that favor partition into such ordered domains (Figure 1.11). In this way, such microdomains could bring proteins together so that they can interact, acting as signaling platforms. The existence of rafts, however, is still controversial and not completely accepted.

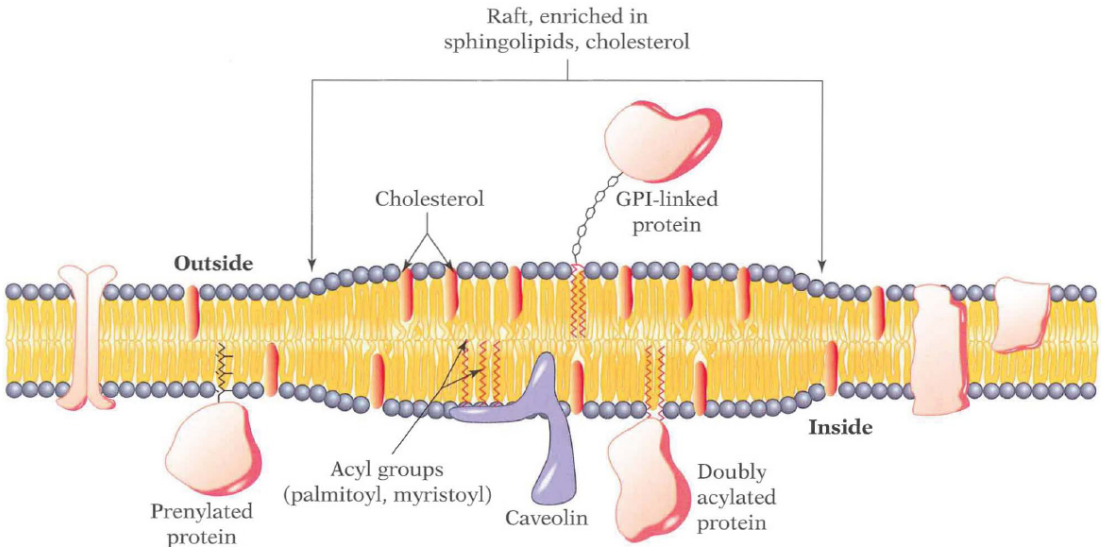

Figure 1.11. Representation of lipid rafts. Taken from Luckey (2008).

One of the problems in this field is probably the confusion when addressing the concepts of lipid rafts, the liquid-ordered phase and detergent-resistant membranes (DRMs) (Lichtenberg *et al.*, 2005). A DRM is a non-solubilized membrane fraction remaining after detergent treatment of membranes. Although rafts are not solubilized by detergents at low temperatures, DRMs should not be identified with such membrane domains. Additionally, the L_o phase is a lipid phase observed in bilayers with high amounts of cholesterol. Thus, although rafts are considered to be in the L_o phase due to their high cholesterol content, those concepts should not be used as synonyms.

Many relevant signaling processes have been associated to the formation of membrane rafts (Stillwell, 2013). However, not all the laterally segregated domains are rafts. The previously explained ceramide-enriched domains are one example of such raft-unrelated membrane domains, which could be important in apoptotic events.

1.4.2 Lipid-lipid interactions

The generation of lateral membrane domains is strongly associated to specific lipid-lipid interactions and depends on the lipid physical properties. Lipids with saturated acyl chains and high T_m tend to induce the formation of ordered lipid domains. One example is sphingomyelin, which is also known to interact favorably in model membranes with other lipids such as cholesterol forming raft-like SM- and Chol-enriched domains in a L_o phase. This interaction is probably a result of: i) acyl chain saturation of SM, ii) the large phosphocholine headgroup of SM effectively shielding the hydrophobic body of Chol and iii) hydrogen bonding between both lipids (Garcia-Arribas *et al.*, 2016; Slotte, 2016).

First of all, cholesterol is known to preferentially associate with saturated lipids to segregate into L_o domains. This has been shown not only for sphingomyelin but also for other saturated lipids such as dipalmitoylphosphatidylcholine (DPPC), its glycerophospholipid analogue (de Almeida *et al.*, 2003; Halling *et al.*, 2008; Veiga *et al.*, 2001). Additionally, cholesterol favors interactions with phospholipids showing large headgroups which help shielding its large hydrophobic body from unfavorable interactions with water (Bjorkbom *et al.*, 2010; Huang and Feigenson, 1999). Finally, the association between SM and Chol is probably stabilized by hydrogen bonding, due to the presence of both hydrogen bond donor and acceptor groups in the former that could bind to the hydroxyl group of the latter (Garcia-Arribas *et al.*, 2016; Slotte, 2016). Glycerophospholipids, on the contrary, only have acceptor groups, so their interaction with Chol should be weaker. Indeed, it was recently shown that Chol has a higher affinity for SM than for an acyl-matched PC at equal acyl chain order (Lonnfors *et al.*, 2011). In addition to cholesterol, ceramide is also able to induce lateral segregation in mixtures with either low T_m or high T_m lipids. When mixed with sphingomyelin, ceramide induces the formation of highly ordered gel-like domains (Figure 1.12) (Busto *et al.*, 2009; Castro *et al.*, 2007; Catapano *et al.*, 2011; Sot *et al.*, 2006).

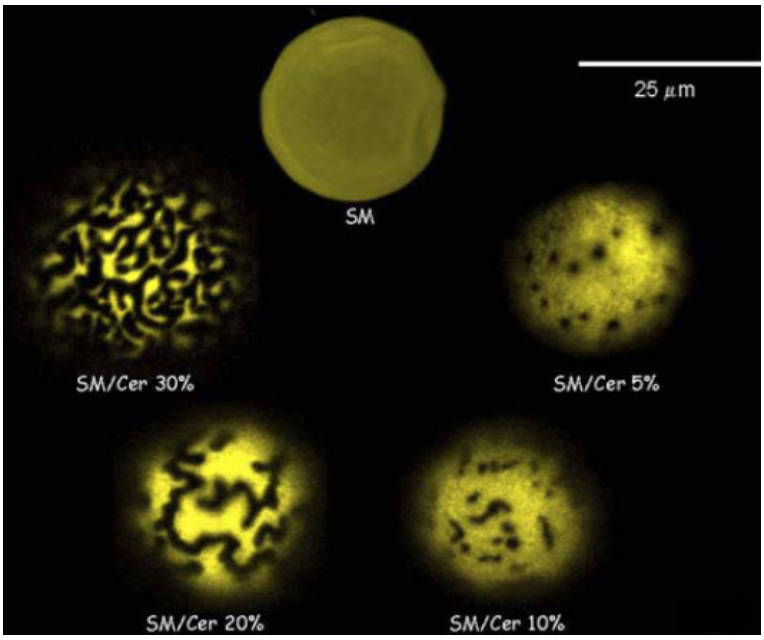

Figure 1.12. Ceramide-enriched domains (black, probe-depleted) in SM:Cer GUV. Taken from Sot *et al.* (2006).

As previously described, ceramide generation in the plasma membrane happens upon activation of sphingomyelinases that degrade SM to ceramide, a process that occurs during apoptosis (Henry *et al.*, 2013; Mullen and Obeid, 2012). Therefore, ceramide platforms formed by the association of both lipids could be involved in apoptotic signal pathways. As it happens with cholesterol, the interaction between ceramide and SM is probably driven by the ordered nature and large headgroup of SM and it is stabilized through hydrogen bonding (Slotte, 2016). However, a recent study showed that the headgroup size of SM was much less important for the interaction of this sphingolipid with ceramide than for association with cholesterol (Artetxe *et al.*, 2013). This could partly be due to ceramide having also both hydrogen bond donors and acceptors, thus more extensive hydrogen networks can be created with SM, producing a stronger interaction than in the case of cholesterol.

SM on the plasma membrane is primarily interacting with cholesterol, so ceramide generation by sphingomyelinases would give rise to platforms enriched in these three lipids, their interactions being crucial for the resulting effects on the membrane. In this regard, Megha and London made an important observation in 2004 on the behavior of both cholesterol and ceramide in the presence of sphingomyelin: ceramide showed the ability to displace cholesterol from raft-like structures, a result that was confirmed by further studies using a wide range of techniques (Alanko *et al.*, 2005;

Chiantia *et al.*, 2006; Megha and London, 2004; Nyholm *et al.*, 2010; Sot *et al.*, 2008). This could be seen as the result of an enhanced affinity of SM for ceramide due to the higher hydrogen bonding ability of the latter, as compared to that of cholesterol. However, when the cholesterol amount of the bilayer is increased, ceramide domains are solubilized (Silva *et al.*, 2007; Silva *et al.*, 2009). Hence, cholesterol and ceramide seemed to compete with each other for association with sphingomyelin. Another study showed the same effect in the absence of sphingomyelin (Castro *et al.*, 2009), suggesting that instead of competing for association with SM, cholesterol and ceramide were more likely to interact.

In line with this hypothesis, cholesterol and ceramide were shown to interact with each other in SM bilayers without a disordered phase (Busto *et al.*, 2010). Further work in our laboratory has shown that cholesterol and palmitoylceramide (pCer) incorporation into bilayers of either palmitoylsphingomyelin or its glycerophospholipid analogue DPPC results in the formation of a homogenous ternary phase with unique properties (Busto *et al.*, 2014; Garcia-Arribas *et al.*, 2016; Garcia-Arribas *et al.*, 2015). These ternary mixtures will be further studied in chapter 4 of this thesis.

1.5 Aims

The present work is focused on the study of the lipid ceramide, using principally (but not exclusively) fluorescence spectroscopy and microscopy techniques. The aims of the present thesis are:

- To characterize pentaene ceramide analogues as fluorescent membrane probes for membrane biophysics studies.

- To describe the physical properties of bilayers composed of ternary mixtures including a saturated phospholipid (pSM or DPPC), cholesterol and palmitoylceramide.

- To explore the ceramide-induced membrane permeabilization mechanism and to evaluate the ability of deoxyceramides to permeabilize membranes.

- To measure the effect of ceramide on membrane edge tension.

Chapter 2:

EXPERIMENTAL TECHNIQUES

Chapter 2: EXPERIMENTAL TECHNIQUES

2.1 Model membrane systems (liposomes)

Cell membranes are highly complex systems as they are composed of many different molecules: proteins, phospholipids, sterols… Thus, it is not easy to assess the properties and behavior of each component. That is the reason why many membrane studies rely on model membranes. These can be moderately complex as membrane extracts (with or without proteins) or as simple as a pure lipid monolayer. Their main disadvantage is that these model systems are a very simplified version of a natural membrane, so the conclusions obtained may not be directly applicable to the more complex systems. However, they allow a reasonably good control of membrane composition under desired conditions, so they are still extremely useful tools for studying membrane components and their interactions.

The model membrane systems used in this work have been lipid vesicles or liposomes. These are lipid bilayers enclosing an aqueous solution that generate spontaneously when cylindrically shaped lipids are dispersed in aqueous solutions (Bangham and Horne, 1964). Not only the lipidic composition of these models is easily controlled, but proteins can also be reconstituted into them, generating proteoliposomes. Depending on the procedure, liposomes of different sizes with either a unique or several bilayers or lamellae can be obtained (Figure 2.1).

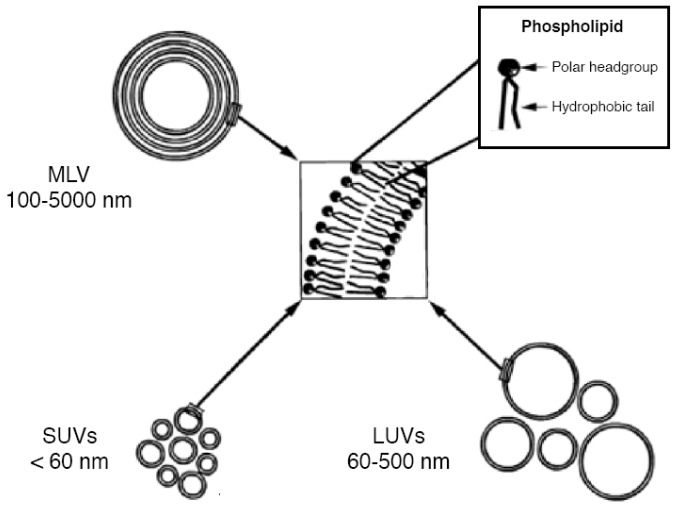

Figure 2.1. Representation of different sized liposomes and their phospholipid organization (not drawn to scale).

Liposomes are widely used to measure biophysical phenomena such as membrane fusion, fission, solubilization, leakage, lipid flip-flop, or lipid-protein interactions. Additionally, they are also being used as carriers of encapsulated molecules by pharmaceutical, cosmetic, food and nutritional industries. An interesting application can be seen in recent studies using liposomes for drug administration in anticancer therapies (see Yingchoncharoen *et al.* (2016) for a recent review on the use of liposomes in cancer treatment).

2.1.1 Multilamellar vesicles (MLV)

Multilamellar vesicles (MLV) are lipid vesicles with multiple concentric bilayers formed after lipid hydration and sample shaking. They usually contain between 7 and 10 concentric bilayers separated by a thin water layer, and they are also quite heterogeneous in size (Figure 2.1). MLV are the easiest and fastest liposomes to prepare, so they are frequently used in studies that are not affected by the presence of multiple lamellae, such as characterization of lipid phases by DSC, nuclear magnetic resonance (NMR), x-ray diffraction techniques, or measurement of the fluorescence emission of membrane probes…

A detailed protocol for multilamellar vesicle preparation as used in the present work is described below (Protocol 1).

Protocol 1 – Multilamellar vesicles (MLVs)

1) Pure lipid stocks are prepared by diluting lipids in powder in chloroform/methanol (2:1 v/v) to the desired concentration.
2) The desired amount of lipids is pipetted from the stock in organic solution into a glass test tube.
3) The organic solvent is evaporated under a stream of nitrogen gas until a lipid film is formed.
4) The sample is then introduced into a high vacuum desiccator for 2 h to completely remove any residual solvent.
5) The resulting lipid film is hydrated by addition of the desired buffer solution followed by vigorous vortex mixing. Both sample and buffer are maintained at a temperature above the lipid main phase transition temperature, so that all the lipids are in a fluid phase state.

6) Although this method is often enough for MLV preparation, MLV for fluorometric studies are also sonicated in a bath sonicator at the same temperature as hydration for 10 min, in order to obtain a more homogeneous sample.
7) In this study, the hydration step was performed in a slightly different way in the case of MLV for DSC experiments. Instead of adding the buffer solution at once, increasing amounts of the solution are added, helping the dispersion by stirring with a glass rod. Then, the vesicles are homogenized by forcing the sample 50-100 times between two syringes through a narrow tube (0.5 mm internal diameter, 10 cm long).

2.1.2 Large unilamellar vesicles (LUV)

MLV are easy and fast to prepare, but they are not suitable for experiments that require a single bilayer, such as the leakage experiments performed in this study where unilamellar vesicles are needed. These are classified according to their size (Figure 2.1): small unilamellar vesicles (SUV) with an average diameter of less than 60 nm, large unilamellar vesicles (LUV) with an average diameter between 60 and 500 nm, and giant unilamellar vesicles (GUV) with a micrometer-ranged diameter (not shown). Each of them differs not only in size but also in the method of preparation.

Large unilamellar vesicles were chosen for the leakage experiments in this work due to their intermediate size and their low curvature stress so that, in contrast with the highly curved SUV, the lipid distribution is homogeneous through both monolayers. There are several methods to obtain large unilamellar vesicles, the one used in this work being the mechanical extrusion of MLV through polycarbonate filters (Mayer *et al.*, 1986). For further detail, see Protocol 2 below.

Protocol 2 – Large unilamellar vesicles (LUV)

1) MLV are prepared (steps 1-5 of Protocol 1).
2) The MLV are subjected to 10 freeze/thaw cycles by introducing the sample tube first in liquid nitrogen for 1 min, and then into a water bath at a temperature above that of the lipid with the main phase transition, until the sample is defrosted and equilibrated. Then, the sample is vortexed and subjected to the same procedure another 9 times.

3) The vesicles are then extruded by passing the sample 10 times through polycarbonate filters with the desired pore diameter (100 nm in this work). The sample is still to be maintained at a temperature above the main phase transition temperature of the lipid mixture.
4) Finally, due to the loss of lipids that this methodology may cause, a lipid phosphorous assay is performed to check the lipid concentration (Protocol 6).

2.1.3 Giant unilamellar vesicles (GUV)

While SUV and LUV are commonly used membrane models, their size does not make them suitable for microscopy. Studies with this kind of technique rely instead on giant unilamellar vesicles (GUV). These are liposomes with a single bilayer and a diameter ranging from 5 to 100 micrometers. Therefore, they are comparable in size to a cell and direct microscopy can be performed on individual vesicles, obtaining additional information not available with smaller membrane model systems.

GUV can be generated by different procedures. The most common and the one used in this study is electroformation, developed by Angelova and Dimitrov based on the exposure of dry lipid films to an aqueous solution under electric fields (Angelova and Dimitrov, 1986) (Figure 2.2). Initially, this procedure could only be used with aqueous solutions with very low ionic strengths. However, improvements to this method allow nowadays using physiological salt solutions and even generating giant vesicles from erythrocyte membranes (Montes *et al.*, 2007).

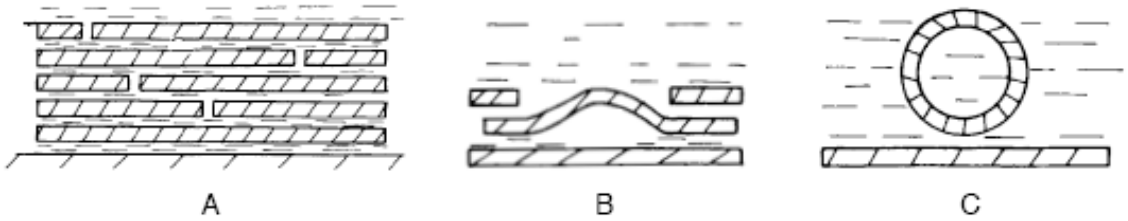

Figure 2.2. Liposome electroformation. A lipid film is deposited onto platinum wires (A) then an electric field is applied to make the lipid bilayers grow (B) and detach (C). Adapted from Angelova and Dimitrov (1986).

In this work, three different GUV generation procedures based on electroformation have been applied, as described below:

I. GUV in suspension for electroporation studies were generated by electroformation on glass slides coated with indium tin oxide (ITO-glasses) (Protocol 3)

II. GUV in suspension for permeabilization studies were generated by electroformation on platinum electrodes (Protocol 4)

III. GUV attached to platinum wires for direct visualization of lipid lateral domain segregation were generated by electroformation on platinum electrodes (Protocol 5).

Protocol 3 – Giant unilamellar vesicles (GUV) in solution [ITO-glasses]

1) Stocks of the lipid mixtures under study are prepared from pure lipid stocks to a final concentration of 4 mM in chloroform.
2) 10 µl of the desired stock solution are deposited on the conducting sides of glass slides coated with indium tin oxide.
3) The glasses are kept under high vacuum for 30 minutes in order to remove any residual solvent.
4) The glasses are then assembled into a chamber, spaced by a 2 mm-thick PTFE frame, and equilibrated at a temperature above the T_m of the lipid mixture.
5) The chamber is filled with a sucrose solution (240 mM sucrose, 1 mM HEPES, pH 7) previously equilibrated at the same temperature as the chamber.
6) The slides are then connected to a generator via copper stripes and a sinusoidal voltage of 25 mV peak-to-peak is applied at 10 Hz. The voltage is increased in 100 mV steps every 5 min to a value of 1225 mV and maintained under these conditions for 2 h.
7) Vesicles are generated attached to the ITO-glasses and the frequency is decreased to 5 Hz for 30 min so the vesicles detach.
8) The electric field is disconnected and the vesicles are left to equilibrate at room temperature for 30 min.
9) The vesicle solution is finally pipetted from the formation chamber into an isosmotic glucose buffer (255 mM glucose, 1 mM HEPES, 1 mM NaCl, pH 7) in a homemade electroporation chamber (see section 2.7 GUV electroporation).

The second procedure for obtaining GUV in solution (Protocol 4) is similar to the previous one (Protocol 3). The main differences are: (1) the use of chambers with platinum electrodes instead of ITO-glasses, and (2) electroformation starting at a high voltage value, instead of slowly increasing it.

Protocol 4 – Giant unilamellar vesicles (GUV) in solution [platinum electrodes]

1) 10 µg of the desired lipid mix plus the desired fluorescent probe dissolved in chloroform is spread on the surface of platinum electrodes built in a specially designed chamber and the residual solvent is allowed to dry.
2) The chambers are then equilibrated above the highest transition temperature of the lipid mixture for 15 min.
3) The platinum wires are immersed in a 300 mM sucrose solution, previously equilibrated at the same temperature as the chamber. The chambers are designed so they can be tightly closed to avoid evaporation.
4) The platinum wires are then connected to a generator that applies the desired electric field for 2 h: 10 Hz and 1.5 V.
5) Vesicles are generated attached to the platinum wires, and the frequency is decreased to 2 Hz for 1 h so the vesicles detach from the electrodes.
6) The electric field is disconnected and the vesicles are left to equilibrate at room temperature for 30 min.
7) The vesicle solution is finally pipetted from the formation chamber into an isosmotic buffer in special visualization microscopy chambers with a glass bottom. The higher density of the enclosed sucrose will make the vesicles sediment onto the bottom of the chambers, so the vesicles can be visualized using an inverted confocal microscope. The glass bottom is previously treated with casein to immobilize the vesicles.

The procedure for obtaining GUV attached to platinum wires (Protocol 5) is similar to the previous one for vesicles in solution (Protocol 4). The main differences are: (1) a special chamber designed for direct microscopy is used, based on the design by Prof. Luis A. Bagatolli (University of Southern Denmark, Odense, Denmark) (Figure 2.3), and (2) the vesicles are generated directly in the desired buffer.

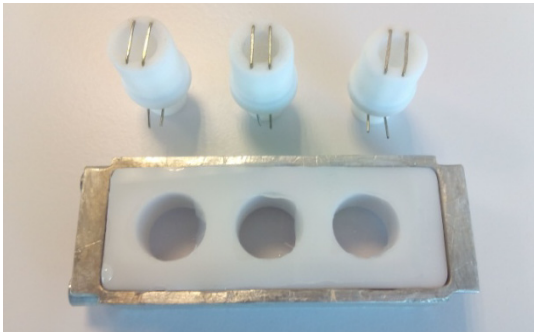

Figure 2.3. Electroformation chamber and PTFE-made round cells for obtaining GUV attached to platinum wires.

Protocol 5 –GUV attached to a platinum wire

1) Stocks of the lipid mixtures under study are prepared from pure lipid stocks to a final concentration of 0.2 mM in chloroform/methanol (2:1 v/v), plus the desired fluorescent probe.
2) 5 µl of the desired stock solution are added onto the surface of platinum electrodes attached to specially designed round cells made of polytetrafluoroethylene (PTFE) (Figure 2.3).
3) The round units containing the platinum wires are kept under high vacuum for 90 minutes in order to remove any residual solvent.
4) The round cells are then fitted into wells within a specially designed chamber (Figure 2.3) to which a cover glass has been previously attached by the use of epoxy glue, so that the platinum wires stay in close contact with the glass.
5) Using a water bath, the chamber is equilibrated at a temperature above the highest transition temperature of the lipid mixture for 15 min.
6) The platinum wires are then covered with the desired buffer, previously equilibrated at the same temperature as the chamber. The wells are closed with tightly fitting caps to avoid evaporation.
7) The platinum wires are then connected to a generator that applies the desired electric field for 2 h: the frequency is maintained to 500 Hz and the amplitude is set to 0.22 V (peak-to-peak) for 6 minutes, to 1.9 V for 20 min and finally to 5.3 V for 90 min.
8) The electric field and water bath are disconnected and the chamber is left to equilibrate for 30 min.
9) The chamber is finally mounted on top of an inverted confocal microscope and the vesicles attached to the platinum wire are directly observed.

2.2 Phospholipid concentration determination (Fiske assay)

An accurate determination of lipid concentration both in primary lipid stocks and in final liposome samples is of uttermost importance. In the case of phospholipids, concentration is routinely determined by a well established method based on the assay of inorganic phosphorous, developed by Fiske and Subbarow (1925) and later modified (Bartlett, 1959; Böttcher *et al.*, 1961). The method consists on the hydrolysis of phospholipids so that the phosphate groups are cleaved free and interact with specific reagents that will color the solution in a concentration-dependent manner. See below for the detailed protocol (Protocol 6).

Protocol 6 – Phospholipid concentration determination assay

1) A calibration curve is prepared with 0, 25, 50, 75 and 100 nmol phosphorous pipetted into duplicate separate test tubes from a NaH_2PO_4 standard solution.
2) The sample is then pipetted into separate test tubes (triplicate at least) so that each of them contains around 50-60 nmol phosphorus, corresponding to the middle of the calibration curve.
3) 500 µl of perchloric acid ($HClO_4$) is added to each tube. These are then vortexed and introduced into a heating block at 200 ºC for 45-60 min. This step causes the hydrolysis of the phospholipid headgroups, yielding free inorganic phosphate.
4) Tubes are cooled down and then 4 mL of an ammonium heptamolybdate solution (22 g $[(NH_4)_6Mo_7O_{24}.4H_2O]$, 143 ml H_2SO_4, 857 ml H_2O) and 500 µl of 10% ascorbic acid solution are added to each tube, followed by vigorous vortexing. The inorganic phosphate reacts with molybdate, which in turns reacts with ascorbic acid generating a yellow-colored solution.
5) The tubes are introduced into a boiling water bath and kept for 6 min. The presence of phosphorous will shift the color of the solution to blue in a concentration-dependent manner.
6) Finally, the tubes are cooled down and absorbance at 812 nm is measured for each sample using an Ultrospec 500 Pro spectrophotometer from Amersham Biosciences (Piscataway, NJ, USA).
7) The absorbance of the standards is plotted against the phosphorous concentration and adjusted with a linear regression method. The corresponding equation will be used together with the sample absorbance to determine the sample concentration.

2.3 Dynamic light scattering (DLS)

Liposome formation and vesicle size were determined by measuring the Brownian motion of the particles in the sample using dynamic light scattering (DLS). The measured particle speed can then be used to determine the particle size according to the Stokes-Einstein equation:

$$D = k_B T / 6 \pi \eta R_h \qquad \text{[Eq. 2.1]}$$

where D is the diffusion coefficient, k_B is the Boltzmann constant, T is the temperature, η is the viscosity of the medium and R_h is the hydrodynamic radius of spherical particles.

In this methodology, the sample is illuminated with a laser beam and the intensity fluctuations of the scattered light produced by the movement of the particles (in our case vesicles) are measured. This provides a correlation function from which, using several algorithms, a vesicle size distribution can be obtained (Figure 2.4). A polydispersity index (PDI) is also provided, a determination of the homogeneity of the size distribution of the sample. This value varies between 0 and 1, values close to 0 indicating homogenous monodisperse solutions.

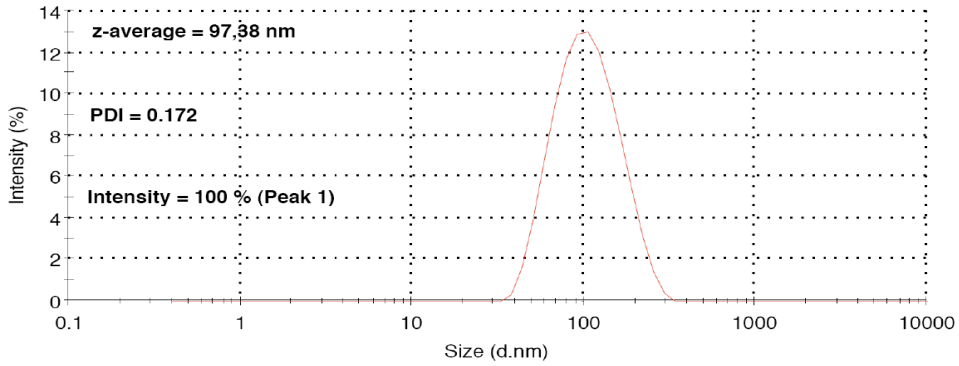

Figure 2.4. Size distribution of an ePC vesicle sample extruded through 100 nm filters.

Measurements have been performed in a Malvern Zeta-Sizer Nano ZS (Malvern Instruments, Malvern, UK) with a detection range for sizes between 0.6 nm to 6 µm and a He-Ne laser beam of 5 mW (λ = 633 nm). 50 µl of the samples (usually 0.3 mM in lipid) were measured in standard acryl-cuvettes at room temperature and the scattered light was detected with a photomultiplier placed at 173º to the beam. The results were analyzed by the commercial software of the instrument.

2.4 Fluorescence spectroscopy

Fluorescence spectroscopy is a frequently used technique in the field of membrane biophysics, mainly due to the sensitivity of many fluorophores to the surrounding environment (Lakowicz, 2006b). Both soluble fluorophores and hydrophobic probes that insert into the lipid bilayer can be used to characterize several biophysical properties of the membrane. Depending on the characteristics and behavior of each fluorophore different experiments and fluorescence measurement types can be used.

2.4.1 Quantum yield measurements

One of the most important characteristics of a fluorophore is the brightness of its emission, i.e. the quantum yield. Quantum yield is the number of photons a fluorophore emits relative to the number of absorbed photons (Brouwer, 2011). Probes with high quantum yields will then be preferable over fluorophores with low quantum yields, since experiments relying on the latter will need highly sensitive detection systems and more careful sample manipulation to avoid working with a low fluorescence/noise ratio.

The quantum yields of a fluorophore can be calculated measuring the fluorescence spectrum and comparing its integrated intensity with the same quantity for a reference system with a known quantum yield. The quantum yield will be then calculated from equation 2.2 below (Brouwer, 2011), where Φ_F^S and Φ_F^{ref} are the quantum yield of the sample and that of the standard, respectively. F_s and F_{ref} represent the area of fluorescent emission in units of photons; η_s and η_{ref} are the refractive indices of the solvent. β_s and β_{ref} are the correction absorption factors, $\beta=1-10^{-A}$ where A= absorbance.

$$\Phi_F^S = \frac{F_s \cdot \beta_{ref} \cdot \eta_s^2}{F_{ref} \cdot \beta_s \cdot \eta_{ref}^2} \cdot \Phi_F^{ref} \qquad \text{[Eq. 2.2]}$$

Absorption and fluorescence spectra were registered in a SpectraMax M5 spectrophotometer (Molecular Devices, Sunnyvale, CA) using a 1-cm path length quartz cuvette. Quantum yields of GABA-pentaene fluorophores were calculated by measuring the integrated emission area of the fluorescent spectra, related to the area measured for the reference 9,10-diphenylanthracene (9,10-DPA) in ethanol after excitation at 346 nm (Φ_F = 0.95) (Morris *et al.*, 1976).

In order to minimize reabsorption effects, the solutions for quantum yield measurements were prepared such that the optical density was generally about A=0.04 at λ_{ex}=346 nm, but was never higher than 0.05. Quantum yields calculated by this method are reliable to ± 10% (Mateo *et al.*, 1996; Patalag and Werz, 2012).

2.4.2 Fluorescence spectra

Another important characteristic of fluorescent probes is their excitation and emission fluorescence spectra. Experiments should always be carried out with the highest fluorescence intensity possible, i.e. at the maximum excitation and emission wavelength, which can be easily determined from the spectra. When using several fluorophores, it is also important that their spectra do not overlap to avoid contribution of other probes in the measured emission; or in the case of Föster resonance energy transfer (FRET) studies, a spectral overlap will be needed for the energy transfer to occur. Emission spectra can also be used to detect alterations in the environment that cause a wavelength shift or quenching of the fluorescence emission.

Measurements of fluorescence spectra of pentaene ceramide analogues were performed under continuous stirring and at a constant temperature of 23 ºC using a QuantaMaster 40 spectrofluorometer (Photon Technology International, Lawrenceville, NJ) (λ_{ex} = 353 nm for emission spectra and λ_{em} = 474 nm for excitation spectra). Raw spectra were corrected using an internal reference for excitation intensity and also applying correction values for the differential excitation and emission monochromator efficiency at different wavelengths (provided by the instrument software).

2.4.3 Time-resolved tPA fluorescence

The most commonly used fluorescence measurement is steady state, i.e. with constant illumination and observation. Time-resolved measurement is less common because it requires more complex instrumentation, capable of recording in the nanosecond time scale. However, the latter gives molecular information that is lost in the former and it has been successfully applied to membrane studies, for example in vesicle content release assays (Jimenez-Rojo *et al.*, 2014c; Lete *et al.*, 2015; Patel *et al.*, 2009), and also in studies on membrane order and lateral heterogeneity using the fluorophore *trans*-parinaric acid (tPA) (Castro *et al.*, 2009; de Almeida *et al.*, 2002; Nyholm *et al.*, 2011; Silva *et al.*, 2007; Wolber and Hudson, 1981).

Time-resolved measurements are performed using a pulse of light to excite the sample and then the distribution of the emitted photons over time is recorded. This is the intensity decay of a fluorophore, and it is usually exponential (Figure 2.5). The lifetime or decay time (τ) is the average amount of time a fluorophore spends in the excited state prior to the emission of a photon and can be calculated from the slope of a plot of log *I(t)* versus *t*.

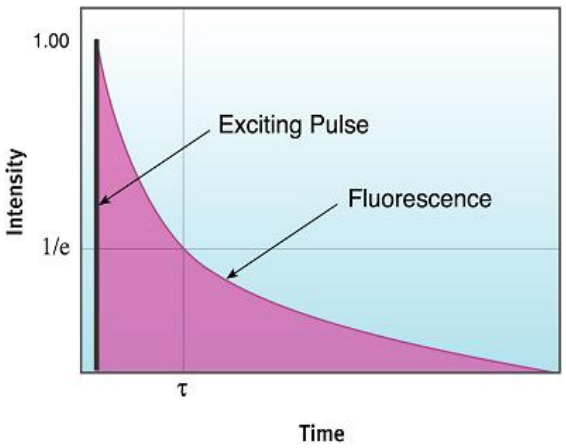

Figure 2.5. Diagram of an intensity decay of a fluorophore.

The lifetime of a fluorophore can change depending on the environment (for example, the molecular order of a bilayer or the presence of quenchers), as it happens with the emission spectra. However, the main advantage of time-resolved fluorescence is that, compared to steady state fluorescence, it can distinguish between fluorophores in different states or environments. When such a situation happens, the intensity decay of the fluorophore becomes multi-exponential due to the fluorophores in each state displaying a different lifetime. Therefore, while steady state measurements can only give averaged information, time-resolved fluorescence can be used to study fluorophores in different states or environments within the same sample.

tPA is a fluorescent lipid whose lifetimes are highly informative of the molecular order of the lipid bilayer. When present in a fluid bilayer tPA shows two short lifetimes (below 10 ns), while an intermediate lifetime around 15 ns and a long lifetime above 30 ns are observed in gel bilayers (de Almeida *et al.*, 2002; Ruggiero and Hudson, 1989; Wolber and Hudson, 1981). tPA average lifetime can therefore be used to measure changes in membrane order. Additionally, tPA shows at least three lifetimes in bilayers with domain coexistence (Artetxe *et al.*, 2013; Castro *et al.*, 2007; de Almeida *et al.*, 2002), becoming a useful probe in lateral heterogeneity studies. Another important property of this fluorophore is its high preference towards gel domains that, even at very low fractions, will give rise to a fingerprinting long-lifetime component above 30 ns (Castro *et al.*, 2007; Maula *et al.*, 2012; Silva *et al.*, 2007), thus becoming highly useful in studies using ceramide.

Time-resolved measurements of tPA fluorescence were performed using MLV at 0.2 mM in lipid with 1 mol% tPA in a 1-cm path length quartz cuvette using a Fluoromax-3 spectrofluorometer with a time-correlated single-photon counting (TCSPC) accessory (Horiba Jobin Yvon, Edison, NY), under continuous stirring. The samples were excited with a pulsed 289 nm LED and the emission was recorded at 430 nm. The emission slit was adjusted so that the count rate was always 0.6-0.3% (0.6-0.3 photons detected per 100 excitation pulses). The instrument response function, i.e. the response of the instrument to a zero lifetime sample, was measured for each sample at each temperature at an emission of 289 nm using a scattering solution of colloidal silica. Data were analyzed with the DAS6 software using the nonlinear least squares analysis method (Lakowicz, 2006c) and the intensity decays measured were fitted to a bi-exponential decay model (equation 2.3):

$$\mathbf{I(t) = \alpha_1 \exp(-t/\tau_1) + \alpha_2 \exp(-t/\tau_2)} \qquad \text{[Eq. 2.3]}$$

where τ_1 and τ_2 are the lifetime components and α_1 and α_2 their respective pre-exponential factors. When $\sum\alpha_i$ is normalized to unity, α_1 and α_2 represent the fractional amplitude of their corresponding lifetimes.

Choosing the suitable multi-exponential model for fitting the intensity decay of tPA is not an easy task. As previously described, it is well known that tPA shows two lifetimes even in isotropic solvents and in bilayers in either fluid or gel state. However, at least three lifetimes have been described in complex bilayers with coexistence of different domains or bilayers of a single lipid near their transition temperature. The tPA intensity decays of the samples studied in this work were adequately fitted to a bi-exponential decay model at room temperature. In experiments where the temperature was increased, coexistence of gel and fluid domains should appear when the samples were heated at around their transition temperature, a three-exponential decay being the most appropriate model for those cases. However, there were no clear and objective parameters in the data to decide at which temperature the decay model should be changed, the results for some samples being significantly different depending on the temperature range where the three-exponential model had been used. Therefore, bi-exponential decays were used at all temperatures to avoid introducing a judgment bias in the analysis of the results. It has to be noted, however, that changes in the results according to the model used would not affect the conclusions drawn.

2.4.4 Vesicle content efflux measurement (Leakage assay)

One of the main functions of cell membranes is compartmentalization by means of creating a non-selective permeability barrier. However, there are several agents such as electrical fields, detergents, pore-forming proteins and also lipids that can cause membrane permeabilization. A simple approach to study the ability of molecules to permeabilize the lipid bilayer is to enclose fluorescent molecules within liposomes. Membrane permeabilization will then cause vesicle content efflux or leakage, which will be measured by changes in the fluorescence intensity. Two different leakage assays have been used in this thesis: ANTS/DPX assay and calcein assay.

2.4.4.1 ANTS/DPX leakage assay

This assay is based on the ANTS/DPX system: the low-weight fluorophore 8-aminonaphtalene-1,3,6-trisulfonic acid (ANTS) and its quencher *p*-xylene-bis-pyridinium bromide (DPX) (Ellens *et al.*, 1985). When both of them are encapsulated within a liposome, ANTS emission is quenched by DPX. Therefore, content efflux can be measured as an increase in ANTS emission due to the loss of interaction with DPX after dilution on the external medium (Figure 2.6).

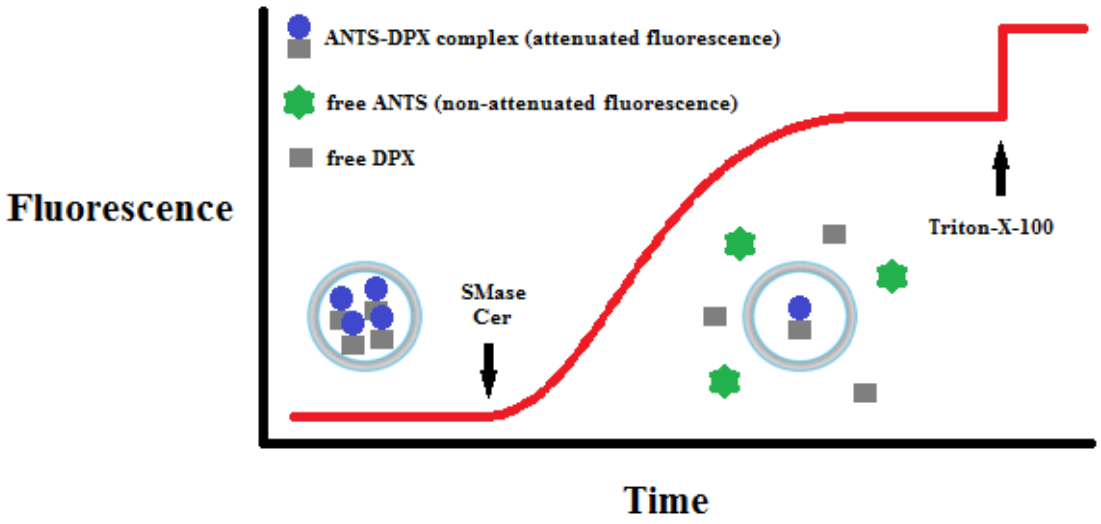

Figure 2.6. Schematic overview of the ANTS/DPX leakage assay. ANTS emission remains quenched while encapsulated together with DPX. Addition of the permeabilizing agent (in our case SMase or ceramide) causes ANTS and DPX efflux, which results in the dilution of these molecules, decrease of interaction between then and therefore an increase of ANTS fluorescence. Triton-X-100 is generally used for complete vesicle solubilization (100% leakage value).

For this assay, 100 nm LUV are prepared as previously described (Protocol 2) in a buffer containing 20 mM ANTS and 70 mM DPX. A high ANTS/DPX ratio is used to ensure complete quenching inside the vesicles. Then, non-entrapped ANTS and DPX are removed from the vesicle suspension by gel filtration in a PD-10 desalting column containing Sephadex G-25 resin, eluting with a previously adjusted isosmotic buffer without ANTS or DPX. ANTS fluorescence of a vesicle solution 0.3 mM in lipid will then be measured using a 1-cm path length quartz cuvette in a QuantaMaster 40 spectrofluorometer (Photon Technology International, Lawrenceville, NJ), under continuous stirring. The fluorophore is excited at 355 nm and emission is collected at 520 nm. The initial fluorescence of vesicles, without permeabilizer, is used to determine 0% leakage, while 100% leakage is determined by the fluorescence measured after complete vesicle solubilization by 0.1% Triton-X-100.

2.4.4.2 Calcein leakage assay

This assay is based on calcein, a fluorophore that self-quenches at high concentrations. Therefore, efflux from calcein-loaded vesicles can be followed as an increase in the steady state fluorescence emission of this dye in a similar way to ANTS/DPX assays. Additionally, time-resolved fluorescence measurements in calcein leakage assays allow not only determination of solute efflux, but also characterization of the membrane permeabilization mechanism (Patel *et al.*, 2009).

The intensity decay measured from calcein-loaded liposomes shows a bi-exponential behavior: fully entrapped calcein shows a lifetime around 0.4 ns (τ_E), while free calcein shows a lifetime of 4 ns (τ_F). In the absence of a permeabilizer, the decay is dominated by a high pre-exponential factor or fractional amplitude corresponding to entrapped calcein (α_E), with a weak pre-exponential factor corresponding to free calcein (α_F) due to spontaneous dye release. When permeabilization occurs, the efflux increase can be followed as a decrease in α_E and a concomitant increase in α_F. Furthermore, partial unloading of vesicles leads to an increase in the τ_E value due to reduced self-quenching, which allows determination of the leakage mechanism (Figure 2.7). When all-or-none leakage occurs (Figure 2.7A), only some of the vesicles are leaky and release all their content (not contributing to τ_E), while the rest remain intact and loaded with fully self-quenched calcein (τ_E = 0.4 ns). In graded leakage (Figure 2.7B) all the vesicles release part of their contents, becoming partially unloaded (τ_E > 0.4 ns).

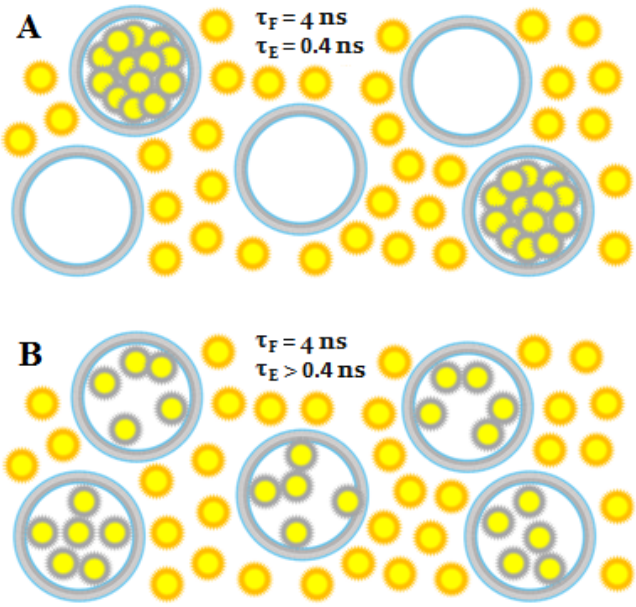

Figure 2.7. Leakage mechanism in calcein-loaded vesicles. (A) All-or-none leakage, results in calcein efflux but no change in τ_E. (B) Graded leakage, results in calcein efflux together with an increase in τ_E.

For this assay, 100 nm LUV were prepared as previously described (Protocol 2) in a buffer containing 70 mM calcein. Calcein-loaded vesicles were separated from unencapsulated dye by gel filtration in a 1 × 30 cm column packed with Sephacryl HR-500 resin, eluting with a previously adjusted isosmotic calcein-free buffer. Calcein fluorescent decays were measured in vesicle solutions at 30 μM in lipid using small 1 ml glass tubes in a FluoroMax-3 spectrofluorometer equipped with a time-correlated single photon counting (TCSPC) system (Horiba Jobin Yvon, Edison, NY), under continuous stirring. The fluorophore is excited using a pulsed LED at 467 nm and emission is collected at 515 nm. The instrument response function was measured at an emission of 467 nm using a scattering solution of colloidal silica. Data analysis was performed using DAS 6 software (Horiba Jobin Yvon).

The curve for free calcein (100% efflux control, with 0.1 % Triton-X-100) was fitted to a mono-exponential model, and the decay curves for the liposome samples were fitted to a bi-exponential model, keeping the τ_F fixed at the value obtained with the 100% efflux control. The efflux value (E) was determined according to equation 2.4 below (Patel *et al.*, 2009), where α_{F0} is the pre-exponential factor of free calcein in a spontaneous efflux control without permeabilizer and Q_{stat} is the static quenching factor.

$$E = \frac{(\alpha_F - \alpha_{F0})}{(\alpha_F - \alpha_{F0} + Q_{stat}\alpha_E)} \qquad \text{[Eq. 2.4]}$$

2.4.5 Fluorescence anisotropy

When in homogeneous solution, all ground-state fluorophores are randomly oriented. Upon exposition to polarized light, those fluorophores whose absorption transition moments are oriented along the electric vector of the incident light are preferentially excited, so excited-state population will be partially oriented. Emission from these fluorophores will be therefore polarized too. However, the emission can become depolarized by different processes, e.g. energy transfer or rotational diffusion. The anisotropy value (r) describes the polarization extent of this emission (Figure 2.8).

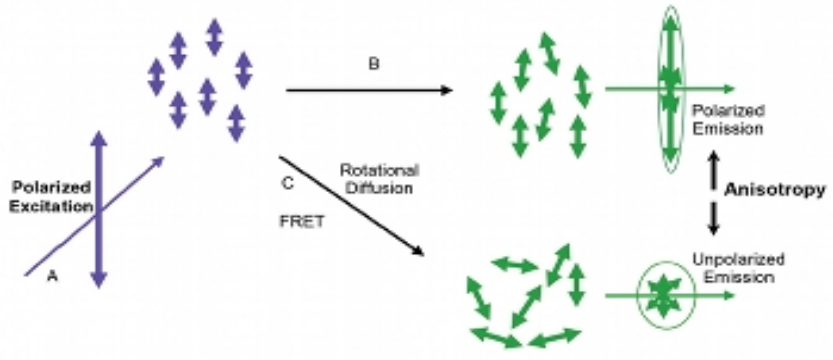

Figure 2.8. Fluorescence polarization and anisotropy. (A) Polarized excitation selectively excites dipole-aligned fluorophores. (B) Fluorophores bound or in high viscosity media diffuse or rotate more slowly, resulting in highly polarized emission and high anisotropy. (C) Rotational diffusion or resonance energy transfer reduces polarization, resulting in lower anisotropy.

Measurements of fluorescence anisotropy are performed with vertically polarized excitation light. The emission intensity is measured through a polarizer: when this is oriented parallel to the direction of the polarized excitation intensity $I_{\parallel}$ is obtained, and when the orientation is perpendicular, then the $I_{\perp}$ intensity is obtained. The anisotropy is then calculated using these two intensities according to equation 2.5 (Lakowicz, 2006a):

$$r = (I_{\parallel} - I_{\perp}) / (I_{\parallel} + 2I_{\perp}) \qquad \text{[Eq. 2.5]}$$

If the light passing through the emission polarizer is completely polarized along the transmission direction of the polarizer, then $I_{\perp} = 0$ and $r = 1$. This value can be observed for scattered light or oriented samples but never for unoriented samples. In fact, in a homogeneous unoriented sample, when the absorption and emission dipoles are collinear and there are no depolarization-causing processes, the value of $I_{\perp}$ is one-third the value of $I_{\parallel}$, so the anisotropy is equal to 0.4. If the emission is completely depolarized, then $I_{\parallel} = I_{\perp}$ and $r = 0$.

When performing the measurements, it is important to note that the emission is observed through a monochromator, and this usually has different transmission efficiency for vertically and horizontally polarized light. Thus, the measured intensities are not the desired parallel and perpendicular intensities since they are also proportional to the transmission efficiency of the monochromator for each polarized component. In fact, the ratio between the vertically and horizontally measured polarized intensities differs from the true ratio by a factor G, this G factor being equal to the ratio of sensitivities of the detection system for vertically and horizontally polarized light. Therefore, the G factor must be first calculated in order to obtain a correct anisotropy. The G factor is measured using horizontally polarized excitation, since under these conditions the ratio between the measured intensities is equal to this factor. Then, the real ratio ($I_{\parallel}/ I_{\perp}$) can be calculated and this will be used to obtain the correct anisotropy.

The dependence of fluorescence anisotropy on fluorophore motions and rotational diffusion has allowed a large number of applications for biochemical research. For example, fluorescence anisotropy can be used to measure the association of proteins with other macromolecules, which alters their motility. Anisotropy measurements can also be used to follow the unwinding of DNA by action of helicases. In the membrane biophysics field, fluorescence anisotropy of the hydrophobic probe diphenylhexatriene (DPH) is commonly used to determine the molecular order of lipid bilayers. When present in a highly ordered bilayer, DPH rotational diffusion is restricted and a high anisotropy near 0.4 is observed. When present in a disordered bilayer, on the contrary, DPH freely rotates and a low anisotropy is observed. DPH anisotropy is, therefore, highly useful in studies on membrane order and can be also used to detect gel-fluid transitions of bilayers.

In this work, both DPH and tPA anisotropies have been measured with MLV at 0.1 mM plus 1 mol% DPH or tPA using a 1-cm path length quartz cuvette in a QuantaMaster 40 spectrofluorometer (Photon Technology International, Lawrenceville, NJ) under continuous stirring. tPA was excited at 305 nm and its emission recovered at 410 nm, while DPH was excited at 360 nm and its emission recovered at 430 nm. The anisotropy was calculated by the instrument software (PTI FelixGX) from an average of measurements for each experimental point, automatically correcting for the G factor, which was measured for every sample at each temperature.

2.5 Fluorescence microscopy

Fluorescence spectroscopy can provide a large amount of information, but this will always be averaged information of all the processes happening in the sample. Fluorescence microscopy, on the contrary, allows direct visualization of single objects.

Confocal microscopy is an advanced fluorescence microscopy technique that allows detection of fluorescence coming from an individual thin in-focus plane of the sample, thus enabling the construction of three-dimensional images. The ability to avoid out-of-focus plane fluorescence is obtained by the use of a pinhole next to the detector that only allows emission from the focal plane to reach the detector. Figure 2.9 shows a schematic depiction of the main components of a fluorescence confocal microscope. The sample is excited by a laser beam focused into a dichroic mirror, which selects the light that will be directed into a small spot in the sample. Emitted fluorescence will then be directed across the same dichroic mirror into a pinhole that will let in-focus plane fluorescence pass to the detector while it blocks out-of-focus fluorescence.

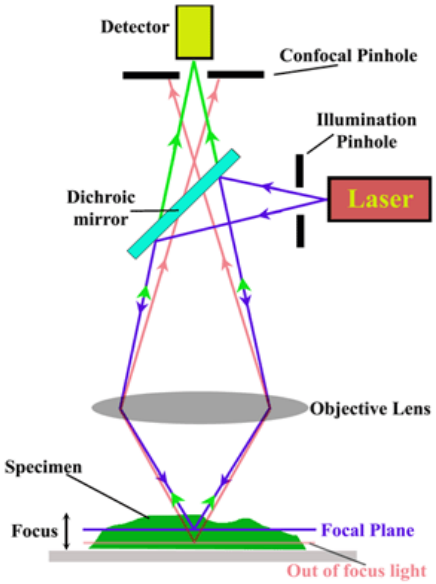

Figure 2.9. Central components of a fluorescence confocal microscope

An advance on conventional fluorescence microscopy came with the development of the multiphoton excitation mode. This technique uses a pulse laser with femtosecond pulse widths to excite fluorophores by two-photon absorption, the wavelength of the photons being twice that of the absorption band of the fluorophore (Figure 2.10). The two-photon absorption process only occurs at the focal point of the laser beam, so it is an alternative to confocal microscopy for avoiding out-of-focus fluorescence. Multiphoton excitation mode can still be applied on a confocal microscope though, as in the system used in this work. The main advantage of multiphoton excitation is that it uses infrared excitation, avoiding the problems of using UV light. Additionally, only the focal point is excited, so photobleaching of the fluorophore is minimized.

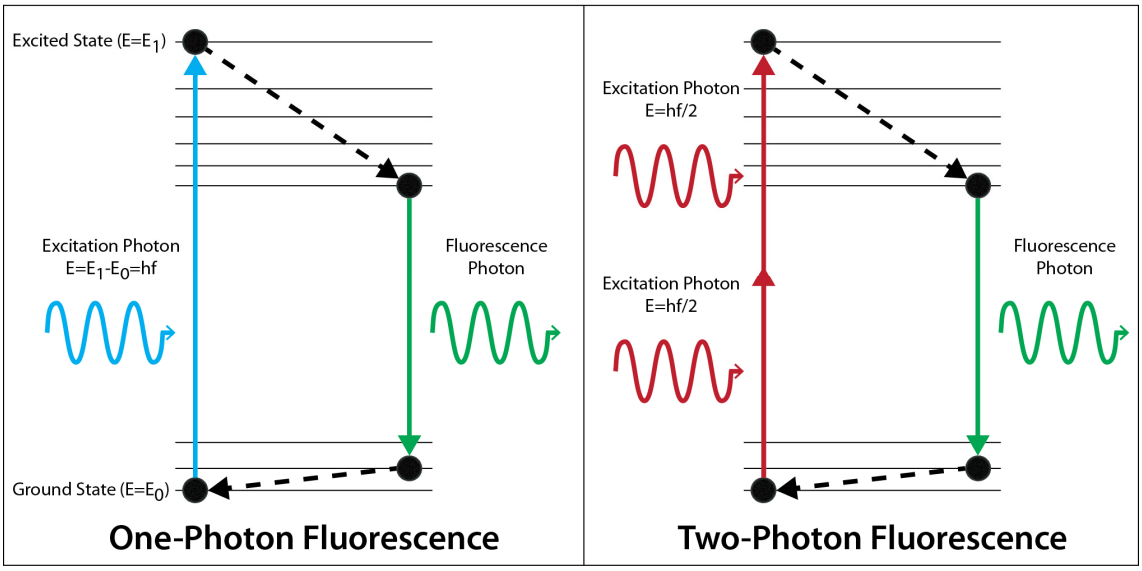

Figure 2.10. Two-photon excitation. Normally, a fluorophore is excited by absorption of one photon of a wavelength corresponding to its absorption band (left panel). In two-photon fluorescence, the fluorophore is excited by absorption of two photons of twice that wavelength (right panel).

Confocal/multiphoton microscopy is commonly used in the characterization of membrane lateral heterogeneity in GUV (Bagatolli, 2006). Domain segregation can be visualized in giant liposomes using fluorescent probes with differential partitioning between domains with different properties. Most fluorescent dyes, such as the fluorescently labeled lipid Rhodamine PE or the hydrophobic probe DiI, partition favorably into the most disordered domains present in the bilayer, while some probes such as naphtopyrene and the cholesterol analogue cholestatrienol show a preference for cholesterol-enriched domains (Baumgart *et al.*, 2007; Juhasz *et al.*, 2010). There are also probes, as for example NBD-ceramide, which distribute homogeneously between fluid and gel domains (Sot *et al.*, 2008). However, all such fluorescent probes are completely unable to enter the highly rigid ceramide-enriched domains, much less preferentially partitioning into them.

Working in this line, confocal/multiphoton microscopy has been used in chapter 3 to characterize the ability of pentaene ceramide analogues to preferentially stain different domains in giant liposomes and their potential use in membrane lateral heterogeneity studies. Multiphoton excitation was chosen for the pentaene probes due to the labile nature of these fluorophores and their high sensitivity to photobleaching.

For these experiments, GUV attached to platinum wires were prepared as described before (Protocol 5), with 2 mol% polyene probes and 0.3 mol% of DiD, DiO or Rho-PE (as reference probes with well known partitioning behavior). GUV were then directly visualized under an inverted confocal microscope with a high-efficiency spectral detector (Leica TCS SP5; Leica Microsystems, Manheim, Germany) and a two-photon excitation mode (MaiTai HP DS laser; Spectra Physics, Mountain View, CA). A 63X water immersion, N.A. 1.2 objective was used and the images were collected and analyzed with the LAS AF software. DiO, DiD and Rho-PE were excited at 488, 543 and 633 nm, and their emission was collected between 500-600, 550-650 and 650-700 nm respectively, with the pinhole set at 1 Airy unit in all cases. Polyene probes were excited using two-photon excitation mode at 706 nm and their emission was collected with the pinhole completely opened in the 467-499 nm range for Pentaene I and 400-550 nm for Pentaene Cer.

2.5.1 GUV permeabilization assay

Membrane permeabilization is most commonly studied using vesicle content release assays, as described above. However, this process can also be directly observed under a fluorescence microscope by addition of a soluble fluorophore to the external medium of a GUV suspension and imaging the fluorophore entry into the liposomes. The main advantage of this methodology is that it allows characterization of membrane permeabilization in single vesicles, and thus determination of the permeabilization mechanism. It can also be used to determine the stability of the membrane pores or defects that cause permeabilization, by addition of a second soluble fluorophore after the permeabilization to the first probe has taken place: stable pores or defects will cause the entry of the second dye into the liposomes, while no entry will be observed if the membrane has been resealed.

For this assay, GUV in solution were prepared as described before (Protocol 4), with 0.2% Rho-PE as a membrane marker, and mixed with 0.2 μM Atto 488. The samples were imaged using a LSM710 confocal microscope with a C-Apochromat × 40 NA. 1.2 water immersion objective (Zeiss, Jena, Germany), with excitation laserlines at 488 and 561 nm. A spectral beam guide was used to separate emitted fluorescence.

Images were processed with a homemade analysis software (Hermann *et al.*, 2014) detecting the filling degree of each GUV. At least a hundred GUV were analyzed per experiment. The degree of GUV filling was calculated as:

$$\% \text{ GUV filling} = [(F_t^{in} - F_0) / (F_t^{out} - F_0)] \times 100 \quad \text{[Eq. 2.6]}$$

where F_t^{in} and F_t^{out} are the average fluorescence intensities inside and outside a GUV at time t, and F_0 is the background fluorescence.

2.6 Differential scanning calorimetry (DSC)

Differential scanning calorimetry or DSC is a thermoanalytical technique based on measuring the difference in the amount of heat needed to increase the temperature of a sample relative to a reference solution. This technique is highly used in the field of membrane biophysics due to its ability to measure thermally-induced lipid phase transitions and their thermodynamic parameters.

DSC is performed in a calorimeter with two cells: one for a reference (usually buffer solution) and the other for the sample (in our case, a MLV suspension). The cells are closed and driven to a high pressure to avoid liquid boiling and bubble generation. The calorimeter contains a Peltier system for heating and cooling the cells at a controlled temperature rate, and is connected to a device that measures the difference in temperature between both cells. When both cells are heated, cell temperature is equally increased. If the sample undergoes a phase transition, either releasing or absorbing energy, it will result in a change in the sample cell temperature with respect to that of the reference cell. In order to keep the same temperature in both cells the calorimeter will give or remove heat from the sample cell. This will give a parameter known as heat capacity (C_p) in units of energy / temperature. Usually, the results are then normalized with the lipid molar concentration, so C_p will be given as kcal/mol/ºC. The resulting scan of a sample is called thermogram, and represents C_p vs. temperature. Lipid phase transitions typically display a peak on the thermogram (Figure 2.11). Three main thermodynamic parameters can be obtained from such data: phase transition temperature (T_m), phase transition width ($\Delta T_{1/2}$) and phase transition enthalpy (ΔH).

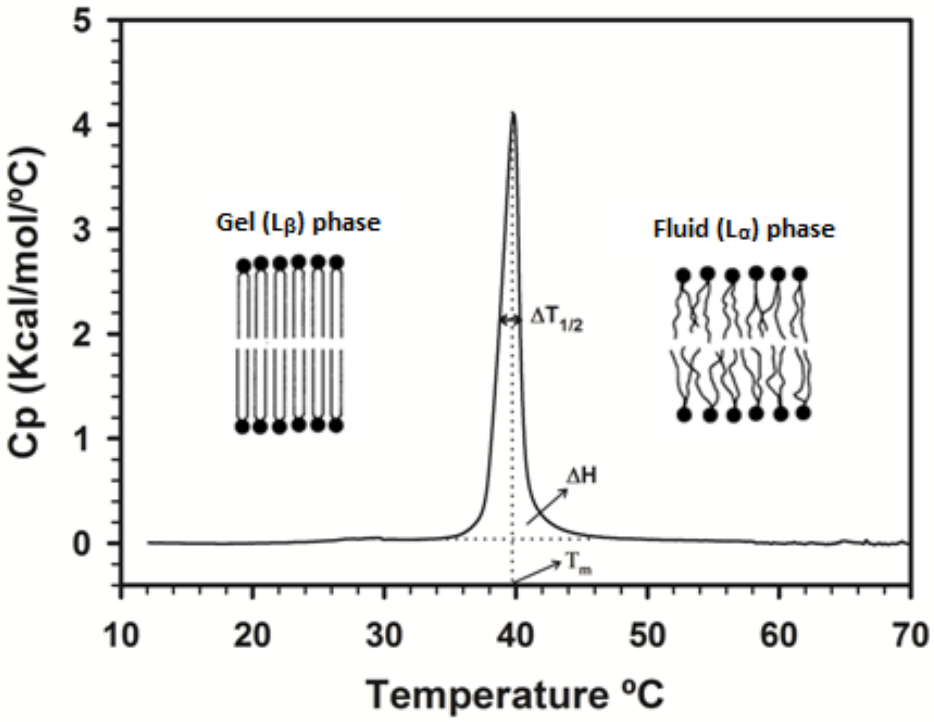

Figure 2.11. DSC thermogram of pure palmitoylsphingomyelin (pSM). The endothermic main phase transition and its associated thermodynamic parameters are shown.

T_m is usually given at the maximum of the transition, the center in the case of symmetric transitions. $\Delta T_{1/2}$ is the transition width in the middle of the transition height, and gives information about the transition cooperativity (molecular cooperation between lipid molecules): the lower the $\Delta T_{1/2}$ the higher the cooperativity. ΔH measures the amount of heat necessary to complete the phase transition, determined by integration of C_p over the whole phase transition temperature range.

In DSC experiments, first the buffer solution was degassed and introduced into both the reference and the sample cells of a VP-DSC high-sensitivity scanning microcalorimeter (MicroCal, Northampton, MA). A heating scan was then performed at the same conditions as the sample would: from 10 to 100 ºC, at 45 ºC/h. Once this scan had finished and during cooling and equilibration of the cells before the second scan, the sample cell was emptied and the MLV sample, previously degassed, was loaded. Then, at least seven heating scans were performed. Data was analyzed with the software ORIGIN 7.0 provided with the calorimeter, subtracting the reference buffer thermogram from the last heating scan and adjusting the resulting thermogram baseline. Sample concentration was then normalized and the thermodynamic parameters determined.

2.7 GUV electroporation

External perturbations such as exposure to electrical fields can induce membrane poration. This is a commonly used technique in the fields of biotechnology (Kotnik *et al.*, 2015) and medicine (Yarmush *et al.*, 2014) for cell transformation and drug delivery. When a pore is formed in the lipid bilayer, the hydrophobic core gets exposed to water so the lipid molecules at the pore edge will rearrange in order to shield their acyl chains from unfavorable interaction with water molecules. This process requires energy, which can be quantified and expressed as the bilayer edge tension (Boal, 2002). The edge tension depends on the properties of the lipid molecules of the bilayer and is highly relevant in biology, since it contributes to the self-assembly and self-healing ability of lipid bilayer structures.

Among the different methods that have been described for measuring the membrane edge tension, the one chosen in this thesis was described by Portet and Dimova (2010). This method is based on the use of electric pulses to porate giant vesicles and recording of the process using phase-contrast microscopy and a fast digital camera. Then, the pore closure dynamics is analyzed to obtain the edge tension value. The life of a pore in a spherical vesicle is composed of four consecutive stages: initial pore growth, stabilization at the maximal radius, slow decrease of the pore radius and final fast closure. Most of the lifetime of the pore is spent in the third regime, which will be used to determine the edge tension according to the following equation (Portet and Dimova, 2010):

$$R^2 \ln(r) = -\frac{2\gamma}{3\pi\eta}t + C \qquad \text{[Eq. 2.7]}$$

where R is the vesicle radius, r is the pore radius, t is the time, γ is the edge tension, η is the viscosity of the aqueous medium and C is a time-independent constant that varies for each experiment.

Determination of the edge tension is carried out by first plotting the porated area, $R^2 \ln(r)$ as a function of time (Figure 2.12, solid lines). Then, the slow closure stage of the pore lifetime will be fitted with a linear equation ($y = at + b$) (Figure 2.12, dashed lines) and the edge tension will thus be calculated from the slope of the linear fit according to the relation obtained from equation 2.7: $\gamma = -(3/2)\pi\eta a$.

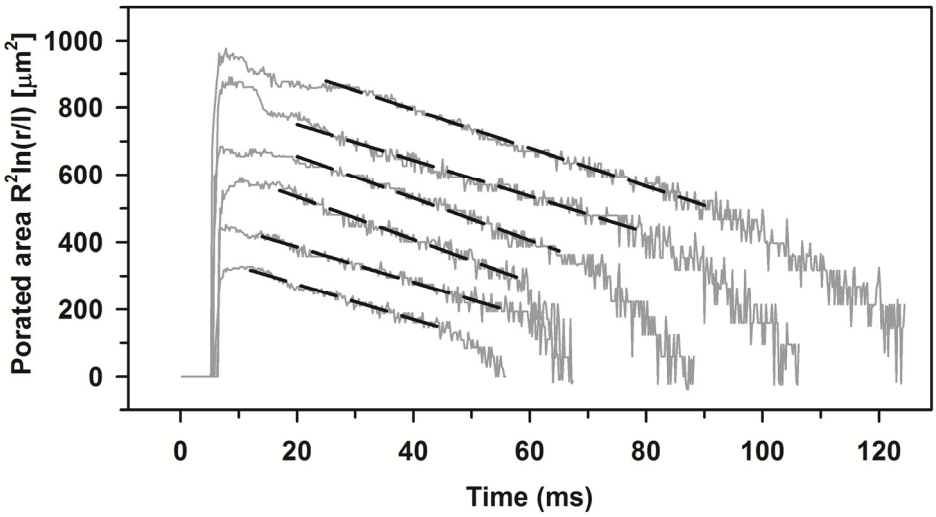

Figure 2.12. Evolution of the porated area as a function of time for different POPC vesicles subjected to a single electric pulse of 5 ms duration and 50-70 kV/m amplitude (applied at time = 0). l = 1 μm was introduced to avoid plotting a dimensional value in the logarithmic term. The solid lines correspond to the experimental data and the dashed lines correspond to the linear fitting of the slow closure regime.

Electroporation experiments were carried out using sucrose-containing GUV in solution (Protocol 3). A homemade electroporation chamber (Figure 2.13) was filled with 72 μl glucose buffer and 8 μl GUV solution, and mounted under an inverted microscope (Axiovert 135, Zeiss, Göttingen, Germany) equipped with a 20 x Ph2 objective and connected to a βtech pulse generator GHT-Bi500 (βtech, l'Union, France). The vesicles were then subjected to an electric pulse of 5 ms duration and around 60 kV/m amplitude directly under the microscope while phase-contrast images of vesicles were collected at an acquisition speed of 5000 frames/s (fps) with a fast digital camera (HG-100K, Redlake, San Diego, CA).

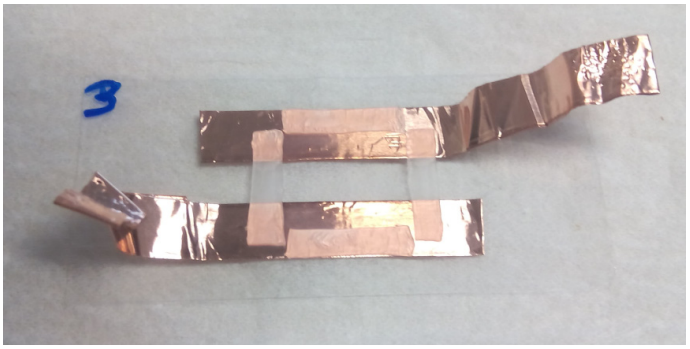

Figure 2.13. Electroporation chamber used in this study. The chamber is made of a rectangular glass coverslip where two copper stripes have been stuck 0.5 cm apart. Heated parafilm was used to create a cavity for deposition of the sample. The cavity was then covered with a smaller square coverslip.

The difference of the refractive indices of the inner sucrose and outer glucose solution allowed the visualization of vesicles as dark objects surrounded by a bright halo on a light gray background, pore opening leading to mixing of both solutions and interruption of the halo (Figure 2.14A). The vesicle radii were manually measured, while the pore radii were determined using an automatic image processing procedure to avoid bias in the pore-size determination. First, the raw images were transformed into a binary image, with the membrane represented by the non-zero pixel value (Figure 2.14B). Once the membrane contour was located (Figure 2.14B, inner white circle), the pore radii were determined via custom algorithms (Portet and Dimova, 2010). Finally, the pore dynamics were described as the evolution of the porated area [R^2 ln(r)] as a function of time (Figure 2.12, solid lines), the slow closure stage was fitted with a linear function (Figure 2.12, dashed lines) and the edge tension was determined from the slope of the linear fit as described above.

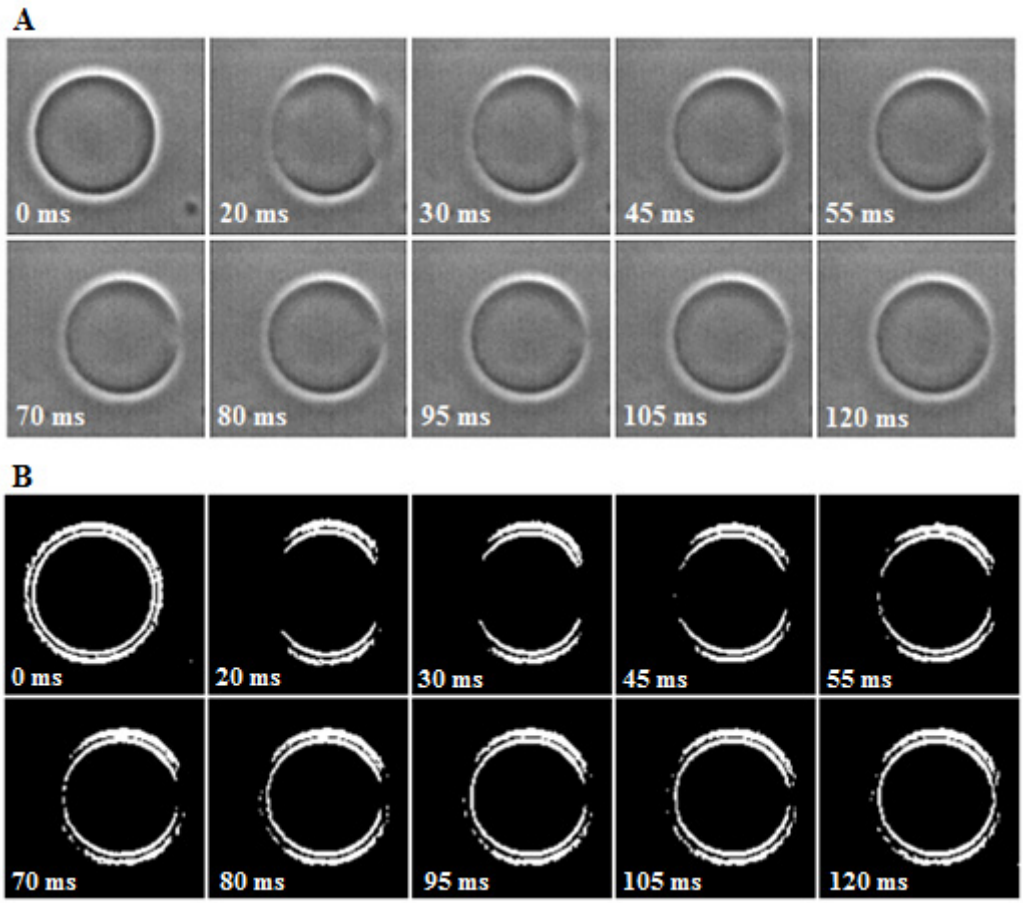

Figure 2.14. Time sequence of raw images (A) and processed binary images (B) of a POPC vesicle with a radius of 18.3 μm subjected to an electric pulse of 5 ms duration and 60 kV/m amplitude (applied at time = 0). Only the pore on the cathode side (right side) is taken into account when analyzing the data. In the processed binary images the membrane is represented by the inner white circle.

Chapter 3:

FLUORESCENT POLYENE CERAMIDE ANALOGUES AS MEMBRANE PROBES

Chapter 3: FLUORESCENT POLYENE CERAMIDE ANALOGUES AS MEMBRANE PROBES

3.1 Introduction

Ceramides (*N*-acylsphingosines) are lipids involved in important metabolic regulation events, such as apoptosis control (Kolesnick *et al.*, 2000; Mullen *et al.*, 2011). They are also noted by their unusual physico-chemical properties when incorporated into phospholipid bilayers, such as lateral segregation into ceramide-rich rigid domains (Carrer and Maggio, 1999; Huang *et al.*, 1996; Silva *et al.*, 2007; Veiga *et al.*, 1999). The studies of lateral phase separation in bilayers have benefited from the use of fluorescence techniques, both spectroscopic (Artetxe *et al.*, 2013; Megha and London, 2004; Pinto *et al.*, 2013) and microscopic (Fanani *et al.*, 2010; Fidorra *et al.*, 2009; Sot *et al.*, 2006). Nevertheless fluorescence studies of lipids suffer from the inherent limitation of requiring fluorescent probes. The probes are supposed to mimic the behavior of natural lipids, even if sometimes, as for example in the widely used diphenylhexatriene (DPH), structural similarities are remote.

In the case of ceramide analogues, molecules labeled with N-7-nitrobenz-2-oxa-1,3-diazol-4-yl (NBD) or 4,4-difluoro-4-bora-3a, 4a-diaza-s-indacene (BODIPY) have been used, even if the bulky fluorescent moieties are likely to provide the molecules with properties different from those of the natural lipid. For example, a ceramide containing NBD in the acyl chain was found to segregate laterally with the ceramide-poor domains, rather than with the rigid, ceramide-rich ones (Sot *et al.*, 2008). In an effort to provide fluorescent ceramide analogues that behave as closely as possible to the natural lipid, different ceramide analogues with a pentaene structure in the would-be sphingosine moiety (Figure 3.1) were prepared by Dr. Ingrid Nieves, from the research group lead by Prof. Antonio Delgado (Research Unit on Bioactive Molecules, Institute of Advanced Chemistry of Catalonia, Barcelona). Polyene derivatives are known to behave similarly to the natural lipids (Kuerschner *et al.*, 2005), and have already been extensively used in biophysical studies (Artetxe *et al.*, 2013; Bakht *et al.*, 2007; Pinto *et al.*, 2013; Silva *et al.*, 2007).

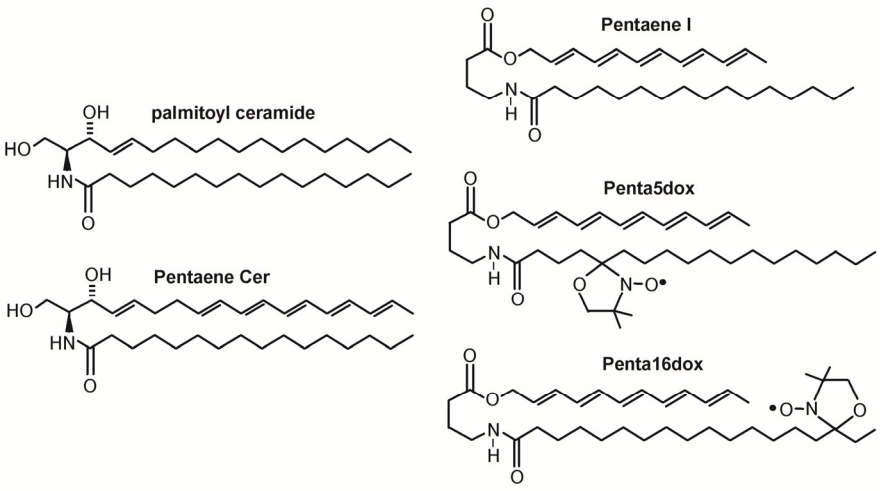

Figure 3.1. Structure of the pentaene probes and of palmitoylceramide (pCer).

First, a pentaene probe derived from *gamma*-aminobutyric acid (GABA) was synthesized as a structural analogue of ceramide which should behave rather similarly to the natural lipid (Figure 3.1, Pentaene I). Although the structural differences are clear, this simple synthetic molecule would help to determine the suitability of such probes for biophysical studies on membranes, before attempting the more challenging synthesis of a pentaenic ceramide. Additionally, two other GABA-pentaene probes were prepared containing a 4,4-dimethyl-3-oxazolinidyloxy (doxyl) radical in the *N*-acyl chain, at positions 5 or 16 (Figure 3.1, Penta5dox and Penta16dox). The doxyl radical is likely to quench the pentaene fluorescence when both the acyl and sphingosine-like chains are in close proximity, thus these doxyl-containing molecules were designed in order to test the intramolecular dynamics of these ceramide analogues. Once the usefulness of these molecules for the biophysical study of membranes was assessed, a pentaenic ceramide (Figure 3.1, Pentaene Cer) was synthesized and studied.

3.2 Materials and Methods

Materials

The pentaene fluorescent probes (Figure 3.1) were synthesized by Dr. Ingrid Nieves. Due to their labile nature, these fluorophores were dissolved in THF (tetrahydrofuran) stabilized with BHT (butylated hydroxytoluene) and stored at -80 ºC. Dioleoylphosphatidylcholine (DOPC), distearoylphosphatidylcholine (DSPC), egg phosphatidylcholine (ePC), dipalmitoylphosphatidylcholine (DPPC), egg

sphingomyelin (eSM), palmitoylsphingomyelin (pSM), palmitoylceramide (pCer), cholesterol (Chol) and 18:1 phosphatidylethanolamine-N-(lissamine rhodamine B sulfonyl) (Rho-PE) were purchased from Avanti Polar Lipids (Alabaster, AL). The fluorescent probes DiD (1,1'-Dioctadecyl-3,3,3',3'-tetramethylindodicarbocyanine perchlorate) and DiO (3,3'-dioctadecyloxacarbocyanine perchlorate) were from Molecular Probes (Eugene, OR). Stock solutions were prepared by dissolving pure lipids and (when required) DiD, DiO or Rho-PE in chloroform/methanol (2:1 v/v) and stored at -20 ºC. The buffer solution was HEPES 50 mM, pH 7.4.

Fluorescence spectroscopy

Lipid vesicles for spectrofluorometric assays (MLV) were prepared by mixing the desired lipids and fluorophores and evaporating the solvent under a stream of nitrogen. The sample was then kept under high vacuum for 90 min to remove any residual solvent. The resulting lipid film was hydrated by addition of the buffer solution at 65º C for DSPC samples and 45º C for DPPC, ePC and DOPC, followed by vigorous vortex mixing. The samples were then sonicated for 10 min in a bath sonicator at the same temperature to homogenize them.

Fluorescence measurements were performed with the polyene probes (0.9 μM) either in organic solvent or in liposome suspensions (0.3 mM in lipid) using a QuantaMaster 40 spectrofluorometer (Photon Technology International, Lawrenceville, NJ) (λ_{ex} = 353 nm, λ_{em} = 474 nm and a cut-off filter at 385 nm). The measurements were performed under continuous stirring and at a constant temperature of 23 ºC. For experiments involving temperature ramps, scanning from 20 to 50 ºC at a heating rate of 0.8 ºC/min was performed.

Fluorescence confocal and multiphoton microscopy

Giant unilamellar vesicles (GUV) were prepared following the electroformation method described previously (Montes *et al.*, 2007), using a homemade chamber that allows direct visualization under the microscope. Stock solutions of the lipid mixtures under study were prepared to a final concentration of 0.2 mM in chloroform/methanol (2:1 v/v), plus the desired fluorescent probe (0.3 mol% for DiD, DiO and Rho-PE and 2 mol% of the polyene probes). 5 μl of the desired stock solution were added to the surface of platinum electrodes and the solvent was removed under vacuum for 90 min.

Electroformation was then performed using a wave generator (TG330 function generator; Thurlby Thandar Instruments, Huntingdon, UK) at a temperature above the phase transition temperature (T_m) of the lipid mixture.

GUV attached to the platinum electrodes were visualized under an inverted confocal microscope with a high-efficiency spectral detector (Leica TCS SP5; Leica Microsystems, Manheim, Germany) and a two-photon excitation mode (MaiTai HP DS laser; Spectra Physics, Mountain View, CA). A 63X water immersion, N.A. 1.2 objective was used and the images were collected and analyzed with the LAS AF software. DiO, DiD and Rho-PE were excited at 488, 543 and 633 nm, and their emission was collected between 500-600, 550-650 and 650-700 nm respectively, with the pinhole set at 1 Airy unit in all cases. Polyene probes were excited using two-photon excitation mode at 706 nm and their emission was collected with the pinhole completely opened in the 467-499 nm range for Pentaene I and 400-550 nm for Pentaene Cer. Control GUV with only DiO and DiD were used to confirm that their emission did not significantly contribute to the signal observed on the polyene channel under the conditions of the experiments. Two independent experiments were carried out for each sample, and within each experiment duplicates or triplicates of the samples were prepared. During visualization, several images were taken at different points of the platinum wire in order to ensure that the sample did not display significant heterogeneity. In GUV exhibiting lateral phase separation, detected through differential fluorescence intensities, the intensity ratios between the different domains were calculated measuring local intensities with the Leica LAS AF software.

Differential scanning calorimetry (DSC)

All measurements were performed in a VP-DSC high-sensitivity scanning microcalorimeter (MicroCal, Northampton, MA). MLV to a final concentration of 1 mM were prepared as described above with a slightly different hydration step: instead of adding the buffer solution at once, increasing amounts of the solution were added, helping the dispersion by stirring with a glass rod. Then, the vesicles were homogenized by forcing the sample 50-100 times between two syringes through a narrow tube (0.5 mm internal diameter, 10 cm long). All the process was carried out at a temperature above the T_m of the lipid mixture.

Both the samples and buffer solutions were fully degassed before loading into the appropriate cell. Eight heating scans were performed for each sample at 45 ºC/h. The final lipid concentration, determined by a lipid phosphorus assay, and data from the last scans were used to obtain normalized thermograms. The data were processed using the software ORIGIN (MicroCal) provided with the calorimeter.

Quantum yield measurements

Absorption and fluorescence spectra were registered in a SpectraMax M5 spectrophotometer using a 1-cm path length quartz cuvette. 9,10-diphenylanthracene (9,10-DPA) was obtained from Sigma-Aldrich, and used without further purification. Ethanol (absolute for analysis) was deoxygenated thoroughly by argon bubbling prior to use. The fluorescence quantum yield of photoexcited fluorescence (Φ_F) is defined as the ratio of number of emitted photons *vs.* number of absorbed photons. Quantum yields were calculated by measuring the integrated emission area of the fluorescent spectra, related to the area measured for 9,10-DPA in ethanol after excitation at 346 nm (Φ_F = 0.95) (Morris *et al.*, 1976). Quantum yields for the aminobutyric polyene products were then calculated using equation 3.1 below (Brouwer, 2011) where Φ_F^S and Φ_F^{ref} are the quantum yield of the sample and that of the standard, respectively. F_s and F_{ref} represent the area of fluorescent emission in units of photons; η_s and η_{ref} are the refractive indices of the solvent. β_s and β_{ref} are the correction absorption factors, $\beta=1-10^{-A}$ where A= absorbance.

$$\Phi_F^S = \frac{F_s \cdot \beta_{ref} \cdot \eta_s^2}{F_{ref} \cdot \beta_s \cdot \eta_{ref}^2} \cdot \Phi_F^{ref} \qquad \text{[Eq. 3.1]}$$

In order to minimize reabsorption effects, the solutions for quantum yield measurements were prepared such that the optical density was generally about A=0.04 at λ_{ex}=346 nm, but was never higher than 0.05 for the 1-cm path length. The absorption spectra of polyene probes showed characteristic structured shapes between 270 and 360 nm in ethanol. This profile is consistent with that of other pentaene probes described in the literature. Quantum yields calculated by this method are reliable to ± 10% (Mateo *et al.*, 1996; Patalag and Werz, 2012). These experiments were carried out using freshly synthesized probes.

3.3 Results

Fluorescence of GABA-pentaene probes

The first step in the characterization of the GABA-pentaene probes (Figure 3.1, Pentaene I, Penta5dox and Penta16dox) was the measurement of the excitation and emission spectra in various environments. Both excitation and emission spectra of the three probes varied when dissolved in different organic solvents, absorption and emission intensities being lowest in hexane and highest in chloroform for the three probes (Figure 3.2). Absorption and emission intensities of all three probes in chloroform increased linearly with probe concentration, at least between 0.3 and 2.7 μM (Figure 3.3). A fluorescence quantum yield for Pentaene I of 0.060 in ethanol (relative to 9,10-DPA in ethanol) was determined as described above. Similarly, quantum yields of 0.031 and 0.048 for Penta5dox and Penta16dox, respectively, were also measured.

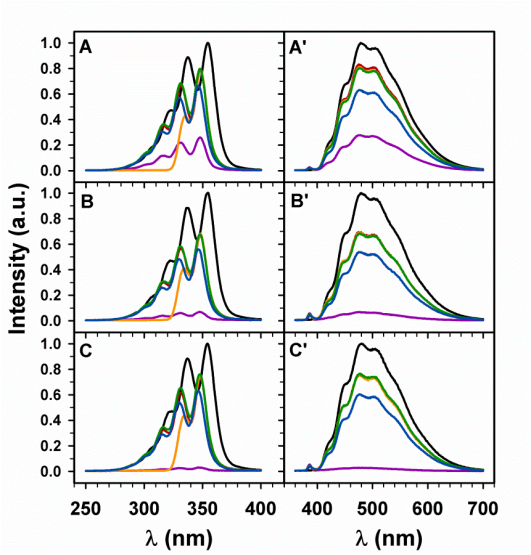

Figure 3.2. Fluorescence excitation (left panels) and emission (right panels) spectra for Pentaene I (A and A'), Penta16dox (B and B') and Penta5dox (C and C') in different solvents: hexane (purple), chloroform (black), ethyl acetate (red), acetone (orange), ethanol (green), methanol (blue).

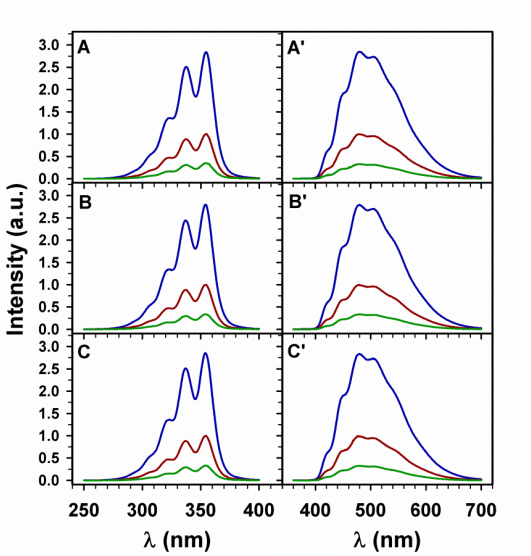

Figure 3.3. Fluorescence excitation (left panels) and emission (right panels) spectra for Pentaene I (A and A'), Penta16dox (B and B') and Penta5dox (C and C') in chloroform at different probe concentrations: 0.3 μM (green), 0.9 μM (red) and 2.7 μM (blue).

Fluorescence excitation and emission spectra of the three probes incorporated in pure lipid bilayers of different fluidities are shown in Figure 3.4. Pentaene I showed a maximum excitation at 353 nm and a maximum emission at 478 nm in DPPC (Figure 3.4 B, B´). In general, the maxima remained fairly constant for the three probes and the four lipid compositions. The absolute intensities (not shown) of Pentaene I were very similar, within ± 10 %, in all four lipids. Moreover, with lipids in the gel phase (Figure 3.4 A´, B´) the doxyl-containing probes exhibited clearly lower fluorescent emissions than Pentaene I, due to doxyl quenching, while this was less clear for the probes in fluid bilayers (Figure 3.4 C´, D´).

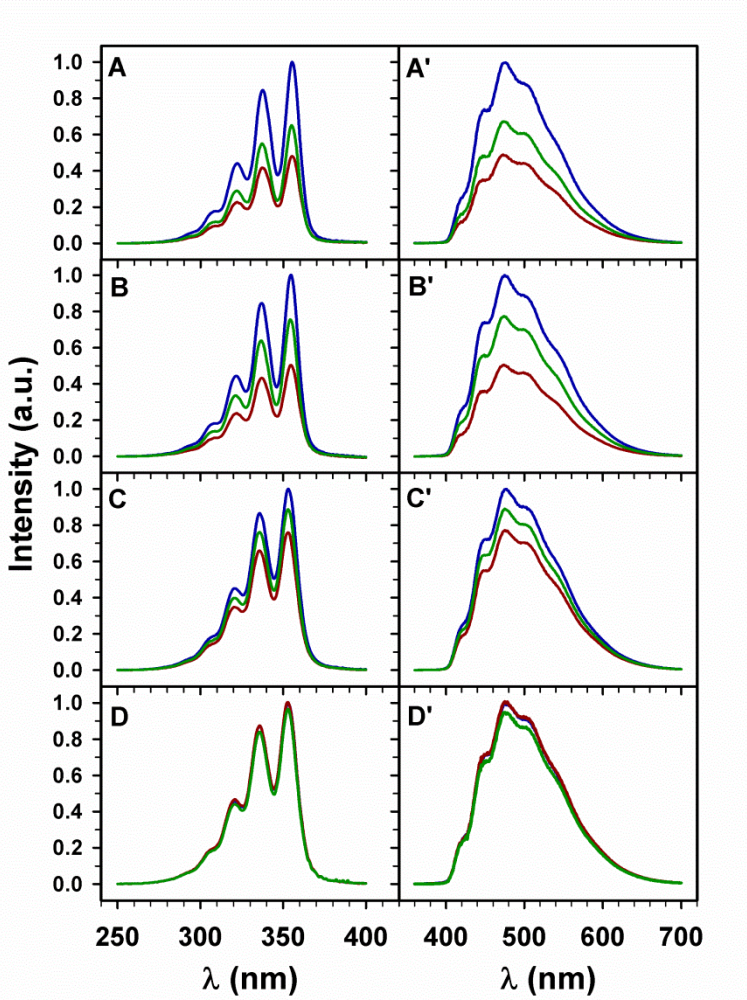

Figure 3.4. Fluorescence excitation (left panels) and emission (right panels) spectra for probes Penta16dox (red) and Penta5dox (green), normalized to Pentaene I (blue). Lipid bilayers were composed of: DSPC (A and A'), DPPC (B and B'), ePC (C and C'), and DOPC (D and D').

Quenching by the doxyl group of Penta16dox showed a high dependency on the fluidity of the bilayer: the degree of quenching reached 50% in gel liposomes but only 20 % in fluid liposomes (Figure 3.5). In contrast, the quenching ability of Penta5dox exhibited a more gradual sensitivity to the bilayer composition, from about 30-35 % quenching in liposomes made of DSPC to < 10 % in DOPC bilayers (Figure 3.5). The data are consistent with a tighter packing of the probes in the rigid bilayers, which reduces the conformational mobility of the doxylstearate chain and favors the spatial proximity of the doxyl radical to the polyene system.

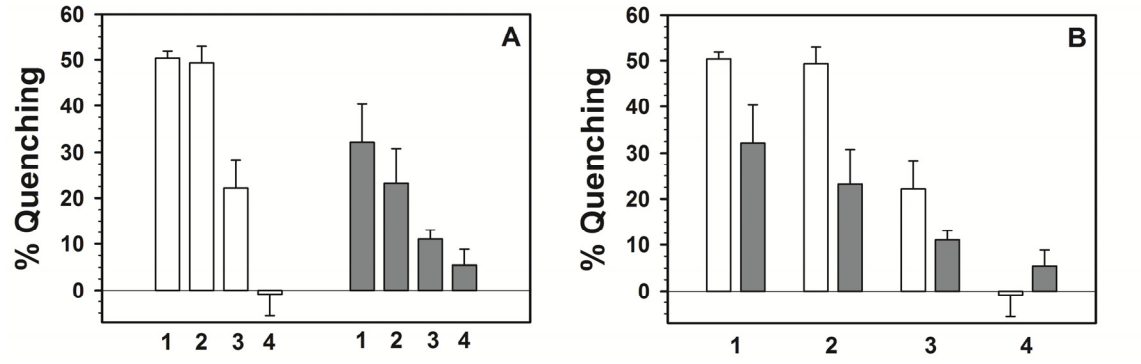

Figure 3.5. Quenching of pentaene fluorescence emission intensity in liposomes of varying compositions: DSPC (1), DPPC (2), ePC (3), and DOPC (4). The degree of quenching was calculated as the relative decrease of the emission intensity of Penta16dox (empty bars) and Penta5dox (full bars) as compared to the emission intensity of Pentaene I. (A) effect of lipid composition for each probe; (B) effect of the position of the doxyl quencher for each composition.

Absorption and emission intensities for all three probes in lipid bilayers were also dose-dependent, but the dependence was not linear, at variance with the observations in chloroform (Figure 3.3). Spectra of probes at different concentrations in DPPC are shown in Figure 3.6. Fluorescence of Pentaene I increases by 2.4-fold when probe concentration varies from 0.1 to 0.3 mol% and by 1.8-fold when concentration increases from 0.3 to 0.9 mol%. Fluorescence emission intensities of the doxyl probes also increase non-linearly with concentration.

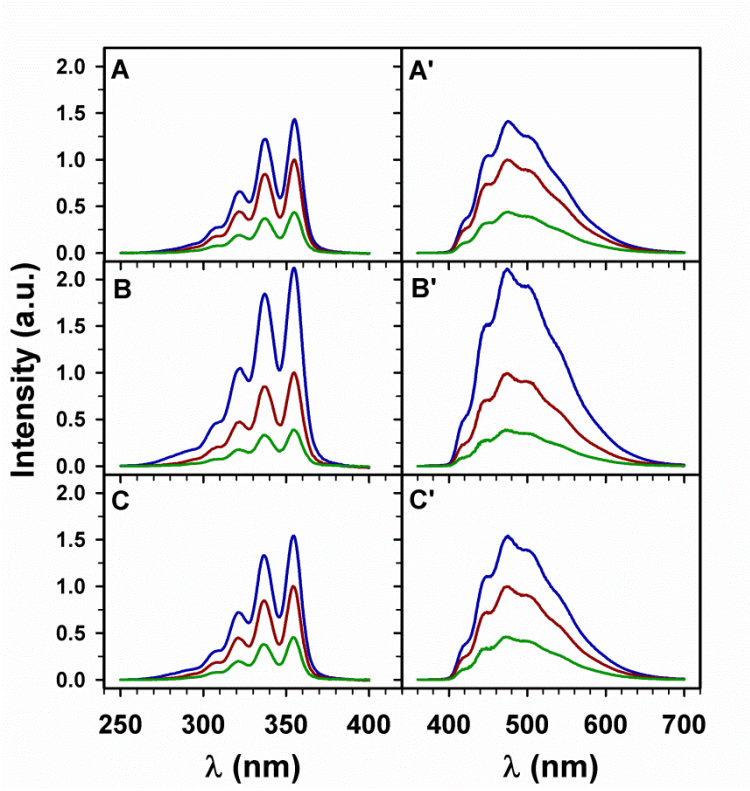

Figure 3.6. Fluorescence excitation (left panels) and emission (right panels) spectra for Pentaene I (A and A'), Penta16dox (B and B') and Penta5dox (C and C') in DPPC bilayers at different probe concentration: 0.1 mol% (green), 0.3 mol% (red) and 0.9 mol% (blue).

Three examples of the behavior of the three GABA-pentaene probes in bilayers composed of lipid mixtures are summarized in Figure 3.7 and 3.8. The mixture eSM:pCer (1:1) at 23º C will be predominantly in the gel phase (Sot *et al.*, 2006) and the spectra resemble very much those in DPPC or DSPC, also in the gel phase (Figure 3.4 A, B). The DOPC:DSPC (1:1 mol ratio) mixture gives rise to a coexistence of gel and fluid domains (Goni *et al.*, 2008), and the spectra were similar to those in ePC (Figure 3.4 C). A third example is constituted by the ternary mixture DOPC:eSM:Chol (2:1:1) in which fluid-ordered and fluid-disordered domains coexist (Goni *et al.*, 2008). In this mixture Penta-5-dox did not show any quenching capacity. Quenching values for the spectra in Figure 3.7 are summarized in Figure 3.8. The results are similar to those found in Figure 3.5 for pure lipids, in the sense that quenching was more efficient with Penta-16-dox than with Penta-5-dox and also in bilayers of higher order than in less ordered bilayers.

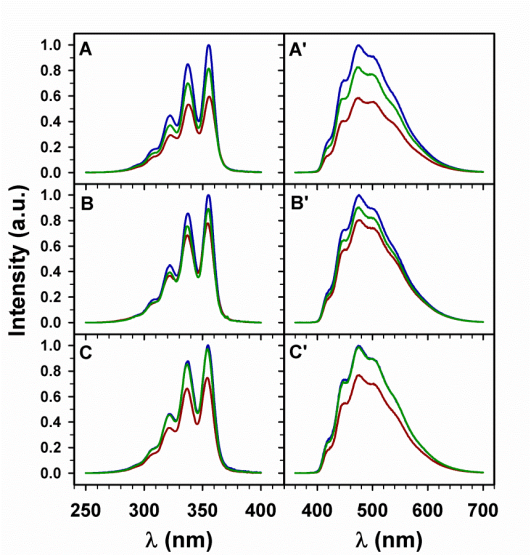

Figure 3.7. Fluorescence excitation (left panels) and emission (right panels) spectra for probes Penta16dox (red) and Penta5dox (green), normalized to Pentaene I (blue). Lipid bilayers were composed of: eSM:pCer (9:1) (A and A'), DOPC:DSPC (1:1) (B and B') and DOPC:eSM:Chol (2:1:1) (C and C').

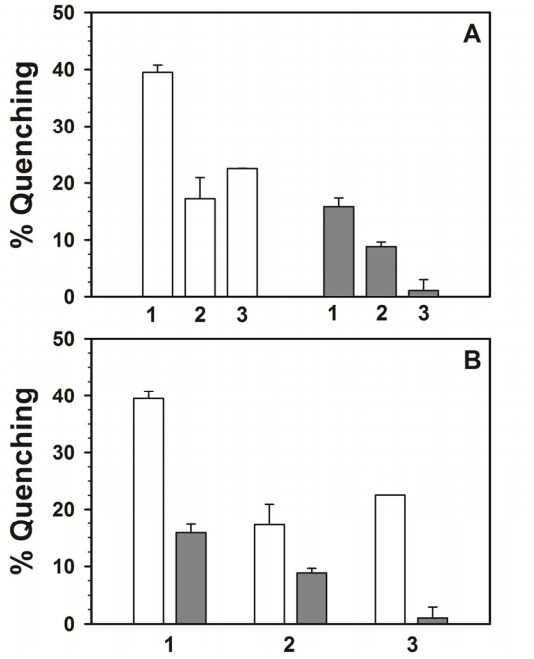

Figure 3.8. Quenching of pentaene emission intensity in liposomes of varying compositions: eSM:pCer (9:1) (1), DOPC:DSPC (1:1) (2), DOPC:eSM:Chol (3). The degree of quenching was calculated as the relative decrease of the emission intensity of Penta16dox (empty bars) and Penta5dox (full bars) as compared to the emission intensity of Pentaene I. (A) effect of lipid composition; (B) effect of the doxyl probe.

Differential scanning calorimetry of Pentaene I

Incorporation of Pentaene I into phospholipid bilayers was tested by differential scanning calorimetry. Pure DPPC, when fully hydrated, exhibits a main endothermic gel-fluid transition centered at about 41 ºC and a smaller pre-transition at about 33 ºC (Figure 3.9). However, Pentaene I did not exhibit any thermal signal in the temperature range under study (10-100 ºC) as it is common for polyunsaturated lipids (Figure 3.9). A mixture of DPPC and Pentaene I (85:15 molar ratio) gave rise to a single major endotherm, centered at 40.7 ºC, while the pre-transition endotherm does not appear in the mixture (Figure 3.9). The width at half-height of the main transition was 1.80 ºC vs. 0.69 ºC for the pure DPPC. The main transition enthalpy hardly changed, 13,000 cal/mol for DPPC vs. 12,900 cal/mol for DPPC + Pentaene I. Therefore, Pentaene I appears to behave in the same way as other amphipathic, unsaturated lipids, mixing well with phospholipids in bilayer form (Davis *et al.*, 1980; Goni and Alonso, 1999).

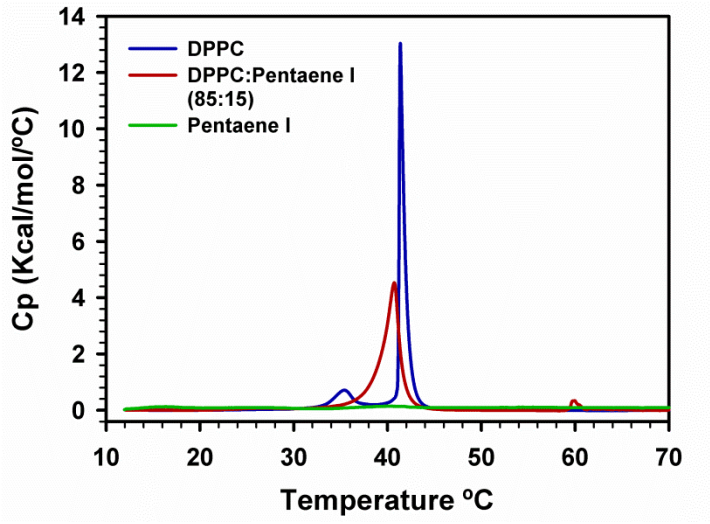

Figure 3.9. DSC of aqueous dispersions of DPPC, Pentaene I and DPPC + 15 mol% Pentaene I.

Pentaene I in microscopy studies.

Confocal/multiphoton microscopy was used to examine GUV composed of DOPC:eSM:Chol (2:1:1 molar ratio) with 2 mol% of GABA-pentaenes. The mixture exhibits lateral separation of liquid-disordered (L_d) and liquid-ordered (L_o) domains, respectively bright and dark when the vesicles are stained with DiO (Figure 3.10, left-hand panels). When the fluorescence of Pentaene I is examined the L_o domains are preferentially stained (Figure 3.10), suggesting a high partition of the polyene into this kind of domains, although a higher fluorescence yield in the ordered domains cannot be discarded. A quantitative study of the average intensity ratio of Pentaene I-stained L_o/L_d domains gave a value of 3.9 ± 1.8 (112 vesicles). The doxyl-containing pentaenes, however, homogeneously stained all the bilayer (Figure 3.10). This could be a result of the differential fluorescence quenching within domains of different order of these fluorophores, previously shown (Figure 3.4, 3.5), which could counteract the higher partition and/or fluorescence yield seen for Pentaene I in L_o domains. Additionally, all the probes showed a photoselection process. This occurs because the extent of excitation of a fluorophore usually depends on the orientation of its transition moment relative to the plane of polarization of the exciting light. Therefore, when the fluorophore keeps a fixed orientation (as it happens with lipids in an ordered bilayer) the excitation efficiency will depend on the location of the probe along the liposome. That is the reason why dark areas can be seen in the L_o domains in the pentaene channel, always located along an imaginary north-south axis (Figure 3.10, right-hand panels blue arrows), while the disordered domains do not exhibit such dark areas.

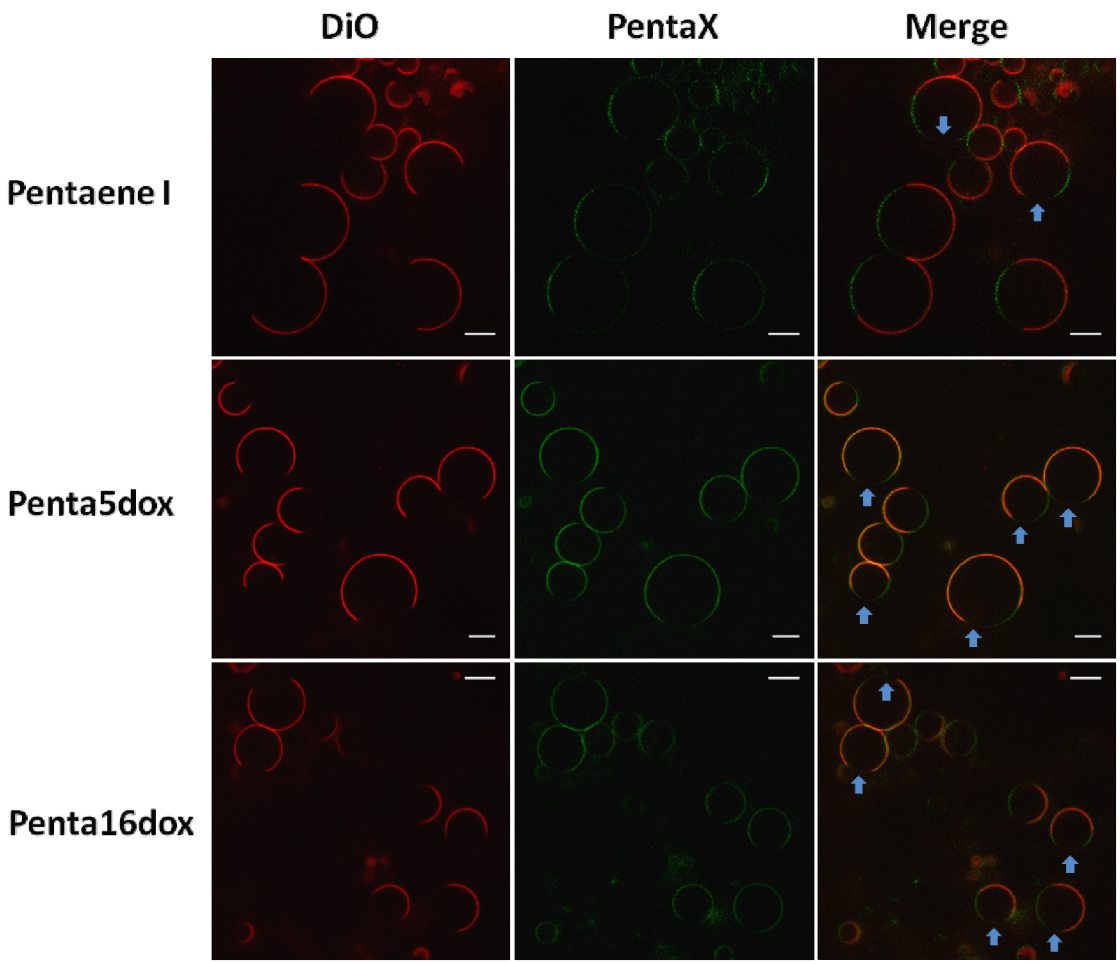

Figure 3.10. Staining of lipid domains by GABA-pentaenes. Representative confocal/multiphoton equatorial sections of GUV of DOPC:eSM:Chol (2:1:1) containing 0.3% DiO and 2% Pentaene I (top panels), Penta5dox (middle panels) or Penta16dox (bottom panels) are shown. Blue arrows show the effect of photoselection on L_o domains. Scale bar = 10 μm.

The ability of Pentaene I to preferentially stain ordered domains was further studied in mixtures of saturated and unsaturated phospholipids, where gel and fluid domains are formed. Pentaene I appears to emit more intensely in domains in the gel phase (Figure 3.11, bottom panels), with a measured intensity ratio of 2.6 ± 0.8 for the gel/fluid domains (27 vesicles). In bilayers consisting of mixtures of phospholipid:ceramide lateral phase separation occurs of ceramide-rich and –poor domains (Fanani *et al.*, 2010; Sot *et al.*, 2006; Sot *et al.*, 2008), the latter being preferentially stained by DiO (Figure 3.11). Pentaene I, however, appears to distribute rather evenly over the vesicle (Figure 3.11), so when both DiO and Pentaene I are excited the ceramide-rich domains appear stained by the polyene fluorescent probe.

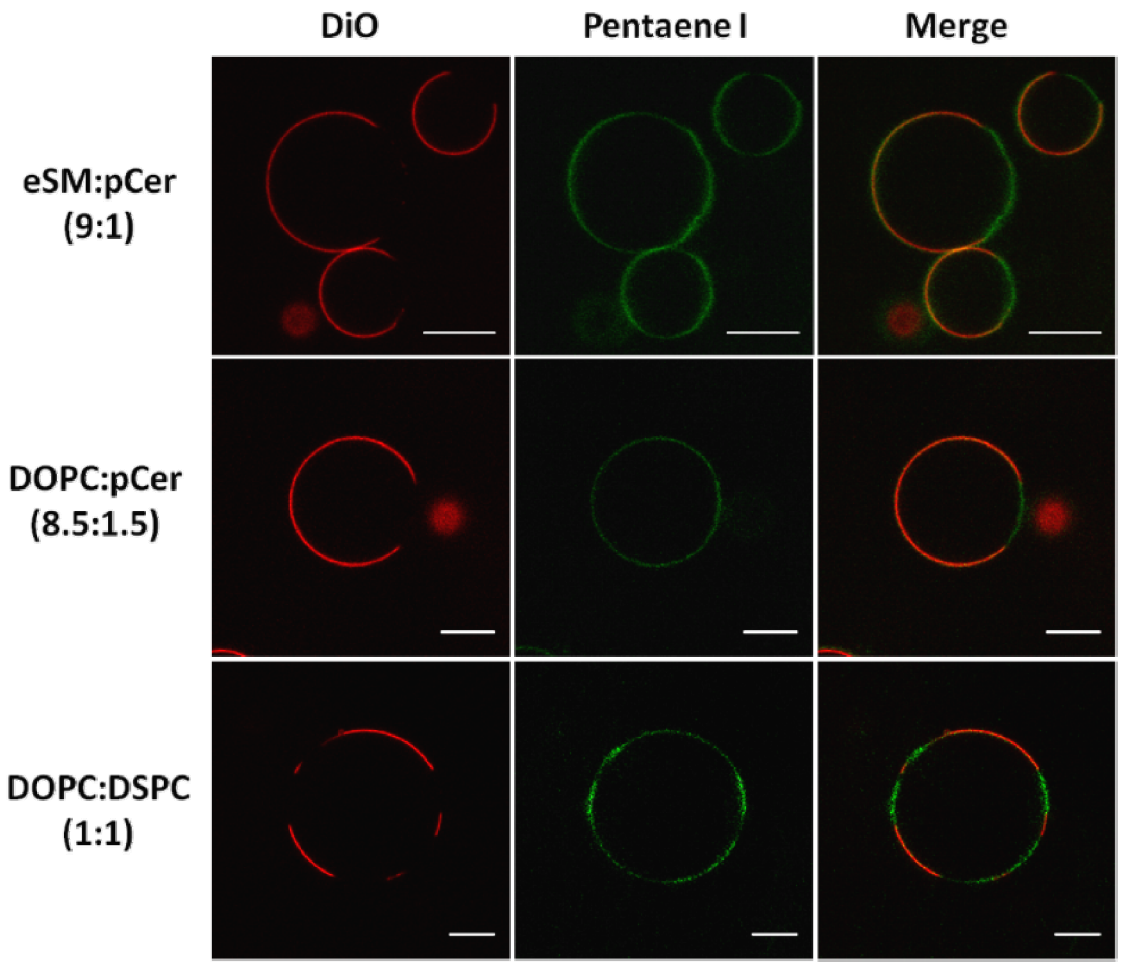

Figure 3.11. Staining of lipid domains by Pentaene I. Representative confocal/multiphoton images of GUV of different compositions containing 0.3% DiO and 2% Pentaene I are shown (equatorial sections). Scale bar = 10 µm.

GABA-pentaene doxyl probes in the study of phospholipid gel-fluid transitions.

The observation that pentaene fluorescence of Penta16dox was quenched more efficiently in gel than in fluid bilayers (Figure 3.5) suggested the possibility of using Penta16dox as a probe to detect gel-fluid transitions in aqueous phospholipid dispersions. As shown in Figure 3.12 (top curve) when the probe was incorporated into DPPC vesicles and quenching was recorded as a function of temperature two abrupt decreases, marked by arrows, were observed at ~ 33 ºC and 42 ºC, i.e. respectively the pre-transition and the main gel-fluid transition temperatures of DPPC (Figure 3.9). However with ePC, which does not undergo any phase transition in the temperature range under study, Penta16dox quenching did not exhibit any discontinuity (Figure 3.12, bottom curve). Thus, this probe appears to be suitable for the detection of this kind of thermotropic transitions in aqueous phospholipid systems.

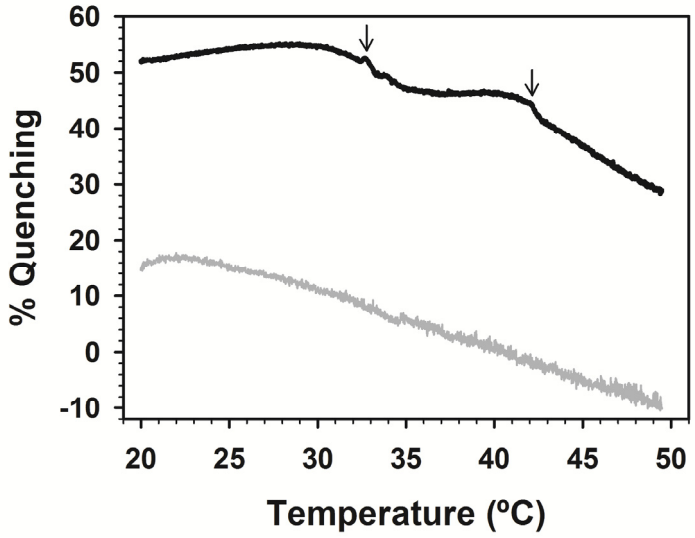

Figure 3.12. Quenching of the pentaene emission intensity of Penta16dox as a function of temperature in liposomes made of DPPC (top) or ePC (bottom). Representative curves of at least three separate experiments are shown. Heating rate: 0.8 C/min.

Pentaene ceramide

After assessing the suitability of GABA-pentaene molecules as fluorescent probes, the study focused on the characterization of the pentaenic ceramide. The excitation and emission spectrum of Pentaene Cer on DPPC vesicles was nearly identical to that observed for the other three pentaenes (Figure 3.13), suggesting that the structural differences between the probes does not markedly affect the spectral properties of the pentaene system within bilayers.

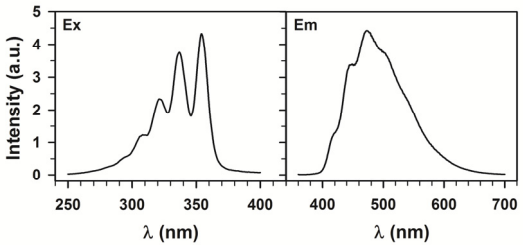

Figure 3.13. Fluorescence excitation (left panel) and emission (right panel) spectra for Pentaene Cer in DPPC bilayers.

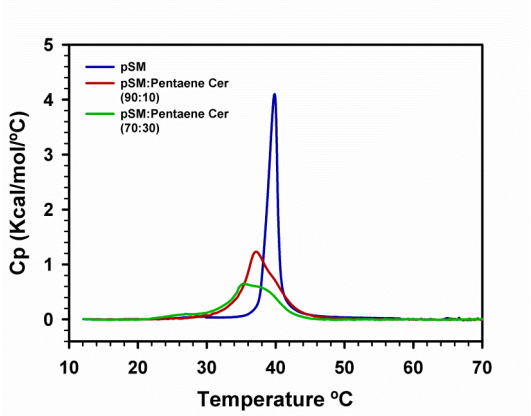

Figure 3.14. DSC of aqueous dispersions of pSM (blue), pSM + 10% Pentaene Cer (red) and pSM + 30 % Pentaene Cer (green).

DSC and microscopy experiments were performed to determine whether the pentaene moiety affects the biophysical properties of ceramide, specifically its ability to promote lateral segregation of immiscible Cer-rich and Cer-poor domains (Busto *et al.*, 2009; Sot *et al.*, 2006). Busto and coworkers showed, using DSC experiments, that addition of pCer to pSM bilayers resulted in the appearance of an asymmetric shoulder at higher temperatures on the pSM transition, which became a single high-temperature (over 65 ºC) asymmetric peak above 30% pCer (Busto *et al.*, 2009). The effect of 10% and 30% addition of Pentaene Cer to pSM bilayers was completely different though (Figure 3.14, Table 3.1). The peak did become asymmetric with the appearance of a small shoulder, suggesting that Pentaene Cer does not mix well with pSM either (Figure 3.14). However, instead of increasing the T_m of the pSM endotherm, Pentaene Cer slightly decreased it, probably due to a small disordering effect of the polyunsaturation (Figure 3.14, Table 3.1). Furthermore, confocal microscopy on pSM GUV with 10% and 30% Pentaene Cer showed no lateral segregation of highly ordered domains as observed with Rho-PE (Figure 3.15), in accordance with the lack of ordering effect of DSC results.

Table 3.1. Thermodynamic parameters of DSC endotherms of pSM liposomes with up to 30% Pentaene Cer. Averages ± SD are shown.

Bilayer composition	**ΔH (cal/mol)**	**T_m (ºC)**	**$\Delta T_{1/2}$ (ºC)**
pSM	8,600 ± 830	39.7 ± 0.3	1.6 ± 0.2
pSM:Pentaene Cer (9:1)	7,900 ± 260	37.3 ± 0.3	4.8 ± 0.4
pSM:Pentaene Cer (7:3)	6,100 ± 750	35.3 ± 0.2	7.5 ± 0.4

ΔH: transition enthalpy change.

$\Delta T_{1/2}$: transition width at half-height

Finally, Pentaene Cer was used as a membrane probe in GUV studies of lateral domain segregation, as previously done with Pentaene I. However, even 15 mol% of Pentaene Cer was not enough to obtain a good fluorescence signal (Figure 3.16), making this probe unsuitable for microscopy purposes.

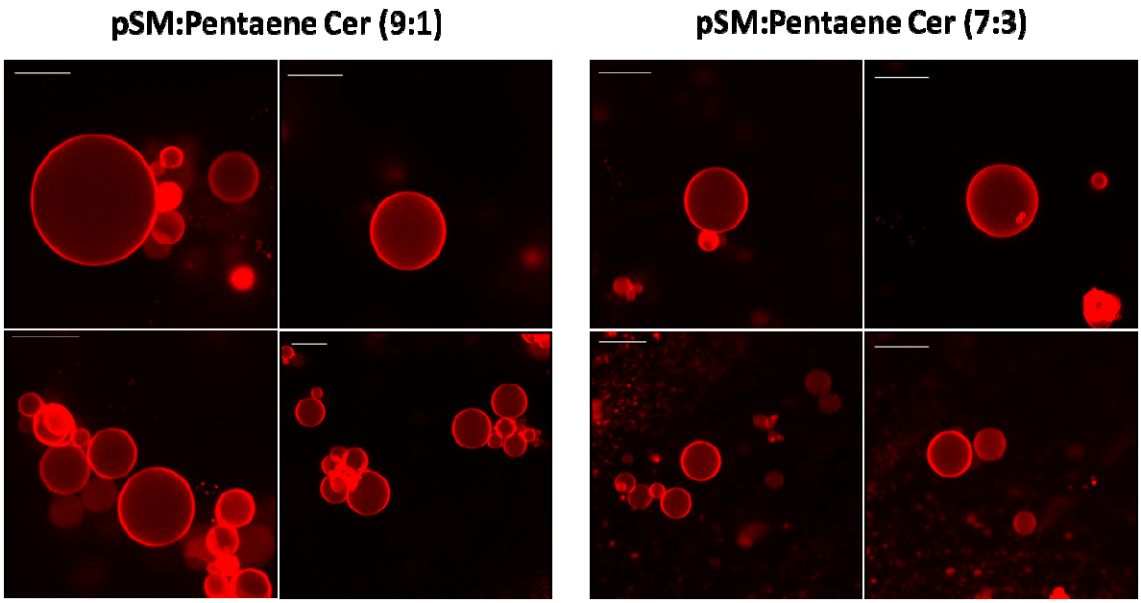

Figure 3.15. Confocal microscopy of GUV composed of pSM + 10% (left panels) or 30% Pentaene Cer (right panels), labeled with 0.3% Rho-PE. The fluorescence corresponds to Rho-PE. Scale bar = 10 µm.

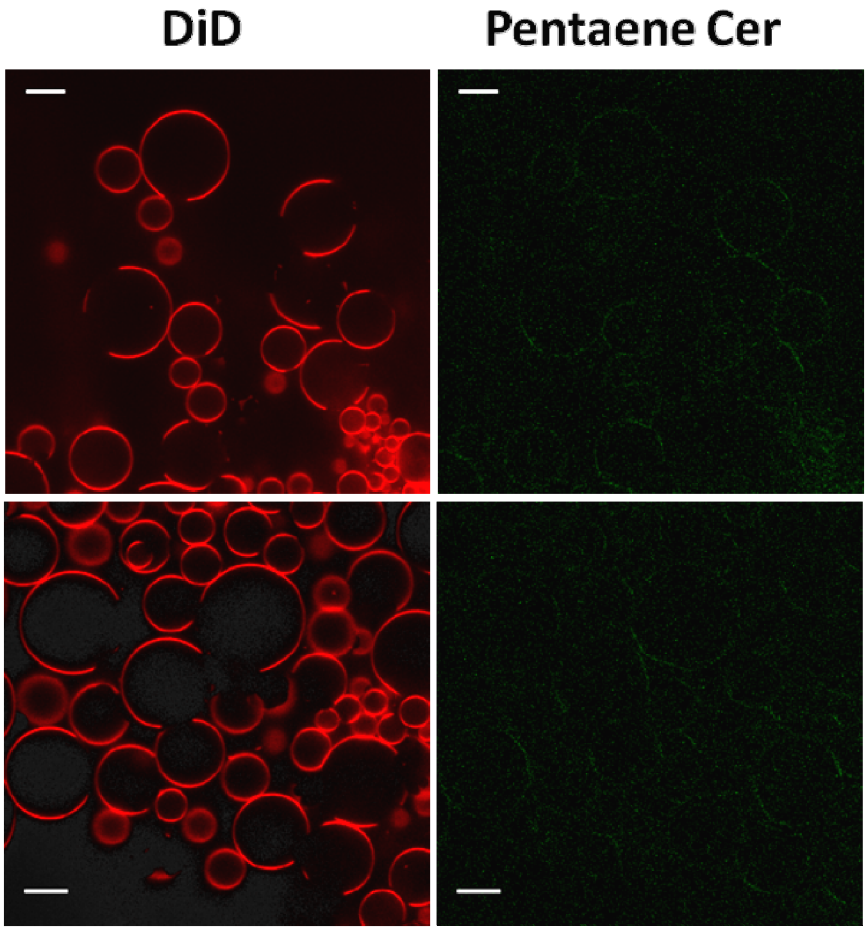

Figure 3.16. Confocal/multiphoton microscopy of GUV composed of DOPC:pSM:Chol (2:1:1) containing DID and 15% Pentaene Cer. Scale bar = 10 µm.

3.4 Discussion

Fluorescence arising from natural polyene systems has been known for decades. Sklar and coworkers identified a naturally occurring fluorescent fatty acid with a conjugated system of four double bonds, parinaric acid (Sklar *et al.*, 1975), that has found important applications in the physical chemistry of lipids (Castanho *et al.*, 1996; Nyholm *et al.*, 2011). More recently Souto and coworkers synthesized conjugated pentaenoic acids by a Wittig olefination reaction (Souto *et al.*, 1994), and then Kuerschner and coworkers included a pentaene fatty acid into a membrane lipid, sphingomyelin, that could be incorporated into cells (Kuerschner *et al.*, 2005). Following this line of experimental research, this chapter describes the biophysical properties of four novel pentaene lipids that can be of use in the study of cell membrane properties.

The three GABA-pentaenes (Pentaene I, Penta5dox and Penta16dox) are structural analogues of palmitoylceramide, with two differences, namely the lack of sphingosine C1(CH_2OH) and the oxo instead of a hydroxyl group in C3. The overall effect is a decrease in the polarity of the headgroup. Moreover two of the novel lipids (Penta5dox and Penta16dox) contain a doxyl radical in the *N*-acyl chain. The radical is intended to quench the pentaene fluorescence when in close proximity to the sphingosine chain (Green *et al.*, 1973). The fourth molecule is a palmitoylceramide molecule with five conjugated double bonds in the sphingosine moiety, more challenging to synthesize but probably closer to the natural ceramide in terms of its biophysical properties.

Polar lipids spontaneously organize in bilayers because of their amphipathic character, while strictly non-polar lipids tend to occupy the bilayer hydrophobic matrix. The three GABA-pentaenes, despite the low polarity of their headgroup, are expected to orientate similarly to ceramide with their polar moieties at the lipid-water interface. This is supported by the DSC data (Figure 3.9) that show a loss of the pre-transition and a moderate widening of the DPPC main transition in the presence of 15 mol % Pentaene I. This is the sort of effect found when DPPC is mixed with unsaturated phospholipids at 10-20 mol % concentrations (Aresta-Branco *et al.*, 2011), while nonpolar lipids that locate between the monolayers without a preferred orientation have a much smaller effect on the DSC thermograms (Aranda and Gomez-Fernandez, 1986). Also in favor of

an orientation normal to the membrane plane is the detection of gel-fluid phase transitions by Penta16dox (Figure 3.12). Doxyl quenching of the pentaene fluorescence requires the sphingosine and acyl chains of the molecule to be very close to each other, and this would be achieved most easily through a phospholipid-like orientation in the bilayer.

An important property of any membrane probe is its distribution among the various lamellar phases (gel, liquid-ordered, liquid-disordered) that can make it more or less useful in physico-chemical studies of lipid mixtures. Most bulky lipid substituents, e.g. Bodipy-lipids, NBD-lipids, etc. tend to partition preferentially into the liquid-disordered phases (Korlach *et al.*, 1999; McConnell *et al.*, 1984). Parinaric acid is known to partition into gel phases, though. The DSC data (Figure 3.9) suggest that Pentaene I partitions preferentially in fluid over gel phases, since it causes a decrease in the gel-fluid transition temperature of DPPC. However, it rather distributes along the whole extension of the bilayer, albeit staining the different domains with different intensities (Figures 3.10, 3.11). Indeed, Pentaene I appears to emit more intensely in liquid-ordered and gel domains than in liquid-disordered and fluid domains, respectively (Figures 3.10, 3.11). Furthermore, in mixtures containing natural ceramide, Pentaene I partitions into both the ceramide-rich and -poor domains (Figure 3.11). This is at variance with the case of NBD-ceramide, containing a bulky fluorescent moiety in the *N*-acyl chain, which cannot partition into domains enriched in natural ceramide (Sot *et al.*, 2008).

The fact that Pentaene I labels gel domains can be particularly useful in view of the putative presence of gel microdomains in live cell membranes (Aresta-Branco *et al.*, 2011; Busto *et al.*, 2014). The two-tailed overall structure of Pentaene I is more similar to that of a membrane lipid than that of parinaric acid, and this is an additional advantage to mimic the behavior of cell lipids. Nevertheless, the structure of Pentaene I is still markedly different from that of ceramide. Therefore, the promising results obtained with the GABA-pentaenes encouraged the synthesis of the pentaenic ceramide probe, in the hope of obtaining a fluorescent ceramide with a behavior close to the natural lipid. However, despite the structural similarities, Pentaene Cer behaved very differently as compared to natural ceramide. Indeed, DSC experiments showed a disordering effect on pSM (Figure 3.14), similar to that seen for Pentaene I on DPPC (Figure 3.9). This is probably due to the polyunsaturation of the sphingoid base that

drastically disrupts the ordering effect of ceramide. As expected by these results, Pentaene Cer was not able to segregate laterally into highly ordered domains as ceramide does in GUV experiments (Figure 3.15). Yet, having a polar headgroup identical to that of ceramide and taking into account the results with Pentaene I, Pentaene Cer could still be a good ceramide fluorescent marker. Multiphoton microscopy, however, revealed that the fluorescent signal of this probe is too low for it to be considered as a suitable tool in such experiments.

Chapter 4:

GEL TERNARY LIPID PHASES COMPOSED OF CHOLESTEROL, CERAMIDE AND A SATURATED PHOSPHOLIPID

Chapter 4: GEL TERNARY LIPID PHASES COMPOSED OF CHOLESTEROL, CERAMIDE AND A SATURATED PHOSPHOLIPID

4.1 Introduction

When the "fluid mosaic" model was proposed by Singer and Nicolson to explain the structure and dynamics of biological membranes, lipids where described to form a homogeneous lipid bilayer in which proteins would be embedded (Singer and Nicolson, 1972). However, decades of experimentation in the field of membranes have produced a great body of evidence that supports the presence of lateral heterogeneities and the formation of micro- and/or nanodomains in cell membranes (Eggeling *et al.*, 2009; Goni, 2014). Sphingolipids, considered as important bioactive molecules in relevant cellular processes such as cell proliferation, signal transduction and apoptosis (Carreira *et al.*, 2015; Hannun and Obeid, 2008), are well known lateral segregation inducers.

The most common sphingolipid in plasma membrane, sphingomyelin (SM), can interact via hydrogen bonding with other lipids, specifically cholesterol (Chol) and ceramide (Garcia-Arribas *et al.*, 2016; Slotte, 2016). When SM interacts with cholesterol they laterally segregate into liquid-ordered (L_o) domains (Veiga *et al.*, 2001), which may be related to membrane rafts (Lingwood and Simons, 2010). Additionally, SM can also interact with the simple sphingolipid ceramide to form highly ordered gel-like domains (Busto *et al.*, 2009; Sot *et al.*, 2006). These ceramide-enriched domains could then act as membrane platforms clustering receptor molecules and mediating signal transduction processes (Cremesti *et al.*, 2001; Zhang *et al.*, 2009). Ceramide levels in resting membranes are very low, yet they can significantly increase under cellular stress conditions via SM cleavage by sphingomyelinases (Cremesti *et al.*, 2002). Therefore, sphingomyelinase activity on SM- and Chol-rich domains present in plasma membranes would give rise to platforms enriched in sphingomyelin, cholesterol and ceramide. In this regard, Megha and London made the important observation that ceramide was able to displace cholesterol from L_o raft-like structures, a result that was confirmed by further studies using a wide range of techniques (Alanko *et al.*, 2005; Chiantia *et al.*, 2006; Megha and London, 2004; Nyholm *et al.*, 2010; Sot *et al.*, 2008).

Interestingly, ceramide-enriched domain formation is in turn modulated by the amount of cholesterol in the bilayer (Silva *et al.*, 2007; Silva *et al.*, 2009), even in the absence of SM (Castro et al., 2009). This suggested a possible direct interaction between cholesterol and ceramide. In line with this hypothesis, these two lipids have been recently shown to interact with each other in palmitoylsphingomyelin (pSM) or dipalmitoylphosphatidylcholine (DPPC) bilayers without a disordered phase, resulting in the formation of a homogenous ternary phase with unique properties (Busto *et al.*, 2014; Busto *et al.*, 2010; Garcia-Arribas *et al.*, 2015).

This work intends to confirm the aforementioned results and further characterize bilayers composed of ternary mixtures including a saturated phospholipid (pSM or DPPC), cholesterol and palmitoylceramide (pCer), using *trans*-parinaric acid (tPA) and diphenylhexatriene (DPH) fluorescence to study membrane order and thermostability of the ordered bilayers. Additionally, DSC experiments with decreasing proportions of Chol and pCer in the bilayer have also been performed in order to investigate the role that their combined amount in the bilayer and the Chol/pCer ratio may have in their interaction. The results from fluorescence spectroscopy fully agree with previous studies supporting the formation of a homogenous gel ternary phase with intermediate properties between Chol-rich L_o and pCer-rich gel-like phases. Furthermore, the DSC data show how the interaction or displacement between Chol and pCer depends on the bilayer concentration of the former, rather than on the ratio between both lipids.

4.2 Materials and Methods

Materials

Dipalmitoylphosphatidylcholine (DPPC), palmitoylsphingomyelin (pSM), palmitoylceramide (pCer) and cholesterol (Chol) were purchased from Avanti Polar Lipids (Alabaster, AL). Diphenylhexatriene (DPH) was from Molecular Probes (Eugene, OR). Colloidal silica (Ludox) was supplied by Sigma (St. Louis, MO). *Trans*-parinaric acid (tPA) was kindly provided by Prof. J. Peter Slotte (Åbo Akademi University, Turku, Finland). Due to its labile nature this fluorophore was stored dried in a N_2 atmosphere at -80ºC. Stock solutions were prepared by dissolving pure lipids in powder or DPH in chloroform/methanol (2:1 v/v) and stored at -20 ºC. Stocks of tPA

were dissolved in methanol and used within a week. The buffer solution was 150 mM NaCl, 1 mM EDTA, 20 mM PIPES, pH 7.4.

Liposome preparation

Multilamellar vesicles (MLV) were prepared by mixing the desired lipids and fluorophores and evaporating the solvent under a stream of nitrogen. The sample was then kept under high vacuum for 90 min to remove any remaining solvent. The resulting lipid film was hydrated by addition of the buffer solution preheated at 70º C, followed by vigorous vortex mixing. The samples were finally sonicated for 10 min in a bath sonicator at the same temperature in order to homogenize them.

Time-resolved fluorescence of tPA

Time-resolved measurements of tPA fluorescence were performed as follows. MLV with the desired lipid composition were prepared at 0.2 mM plus 1 mol% tPA and incubated at the desired temperature before performing the measurements. tPA intensity decays were measured in a Fluoromax-3 spectrofluorometer with a time-correlated single-photon counting (TCSPC) accessory (Horiba Jobin Yvon, Edison, NY) connected to a water bath for temperature control and under continuous stirring. The samples were excited with a pulsed 289 nm LED and the emission was recorded at 430 nm. The emission slit was adjusted so that the count rate was always 0.6-0.3% (0.6-0.3 photons detected per 100 excitation pulses). The instrument response function was measured for each sample at each temperature at an emission of 289 nm using a scattering solution of colloidal silica. Data were analyzed with the DAS6 software using the nonlinear least squares analysis method (Lakowicz, 2006c) and the intensity decays measured were fitted to a bi-exponential decay model:

$$\mathbf{I(t) = \alpha_1 \exp(-t/\tau_1) + \alpha_2 \exp(-t/\tau_2)} \qquad \text{[Eq. 4.1]}$$

where τ_1 and τ_2 are the lifetime components and α_1 and α_2 their respective pre-exponential factors. When $\sum\alpha_i$ is normalized to unity, α_1 and α_2 represent the fractional amplitude of their corresponding lifetimes. Since the radiative decay rate of tPA is independent of the environment, the fractional amplitudes can be considered proportional to the mole fraction of tPA exhibiting the corresponding lifetime (Wolber and Hudson, 1981).

In experiments where the temperature was increased, coexistence of gel and fluid domains should appear when the samples were heated at around their transition temperature, a three-exponential decay being the most appropriate model for those cases. However, there were no clear and objective parameters in the data to decide at which temperature the decay model should be changed, the results for some samples being significantly different depending on the temperature range where the three-exponential model had been used. Therefore, bi-exponential decays were used in all cases to avoid introducing a judgment bias in the analysis of the results. It has to be noted, however, that changes in the results according to the model used would not affect the conclusions drawn.

Fluorescence anisotropy

Anisotropy measurements were carried out with MLV at 0.1 mM plus 1 mol% tPA or DPH using a QuantaMaster 40 spectrofluorometer (Photon Technology International, Lawrenceville, NJ) and under continuous stirring. Samples were equilibrated for 5 min at the desired temperature before the anisotropy measurements. tPA was excited at 305 nm and its emission recovered at 410 nm, while DPH was excited at 360 nm and its emission recovered at 430 nm. The anisotropy was calculated by the instrument software (PTI FelixGX) from an average of measurements for each experimental point, automatically correcting for the G factor, which was measured for every sample at each temperature.

Differential scanning calorimetry (DSC)

All measurements were performed in a VP-DSC high-sensitivity scanning microcalorimeter (MicroCal, Northampton, MA). MLV to a final concentration of 1 mM were prepared as described above with a slightly different hydration step: instead of adding the buffer solution at once, increasing amounts of the solution were added, helping the dispersion by stirring with a glass rod. Then the vesicles were homogenized by forcing the sample 50-100 times between two syringes through a narrow tube (0.5 mm internal diameter, 10 cm long) at a temperature above the transition temperature of the lipid mixture.

Both the samples and buffer solutions were fully degassed before loading into the appropriate cell. Eight heating scans were performed for each sample at 45 ºC/h. The final lipid concentration, determined by a lipid phosphorus assay, and data from the last scans were used to obtain normalized thermograms. The data were processed using the software ORIGIN (MicroCal) provided with the calorimeter.

4.3 Results

Time-resolved fluorescence of tPA

tPA is a fluorescent lipid highly informative of the molecular order and lateral heterogeneity of bilayers. tPA is well known to show two lifetimes in isotropic solvents and in bilayers in either fluid or gel state (de Almeida *et al.*, 2002; Ruggiero and Hudson, 1989; Wolber and Hudson, 1981), while at least three lifetimes have been described in complex bilayers with coexistence of different domains (Artetxe *et al.*, 2013; Castro *et al.*, 2009; de Almeida *et al.*, 2002; Maula *et al.*, 2012) or bilayers of a single lipid near their transition temperature (Ruggiero and Hudson, 1989). The main advantage of this fluorescent probe is its high preference towards gel domains that, even at very low fractions, will give rise to a fingerprinting long-lifetime component above 30 ns (Castro *et al.*, 2007; Castro *et al.*, 2009; Maula *et al.*, 2012; Silva *et al.*, 2007), thus becoming highly useful in studies using ceramide.

First, as an initial characterization of the probe behavior, tPA fluorescent decays were analyzed in MLV of different compositions. As previously described, tPA showed a bi-exponential decay with two short lifetimes below 10 ns in a fluid POPC bilayer (Figure 4.1). The presence of liquid-ordered (L_o) domains in POPC:pSM:Chol (60:30:10) liposomes gave rise to a new long lifetime component (Figure 4.1). However, this new lifetime did not reach the 30 ns threshold of gel phases, as it happened with POPC:pCer (85:15) and POPC:pSM:pCer:Chol (60:15:15:10) liposomes exhibiting highly rigid gel domain segregation (Figure 4.1). All these results agree well with previously published data from other laboratories (Castro *et al.*, 2009; Maula *et al.*, 2012).

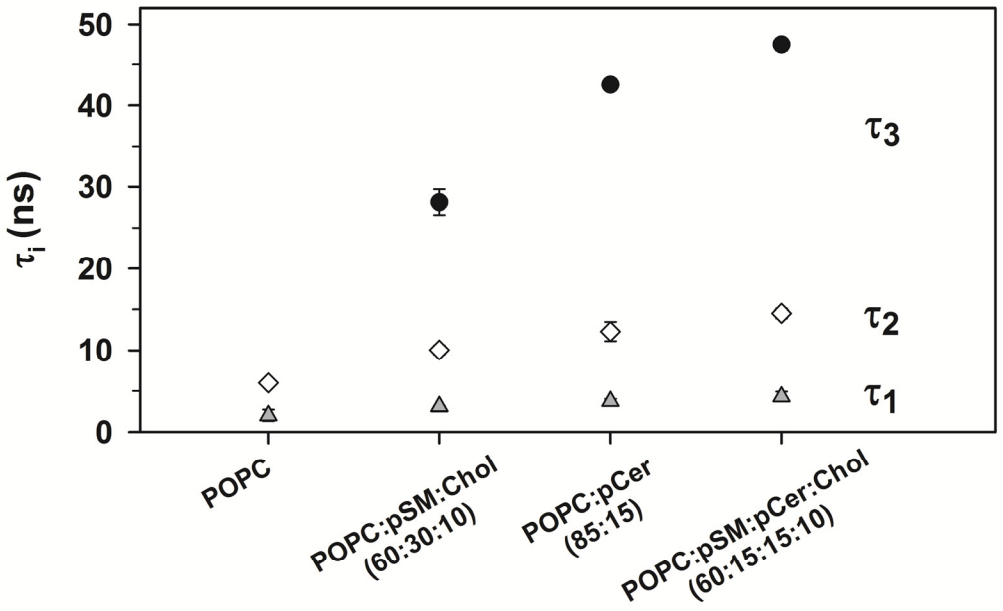

Figure 4.1. tPA lifetimes in liposomes of different composition at room temperature. Triangles: τ_1, shortest lifetime. Diamonds: τ_2, intermediate lifetime. Circles, τ_3, longest lifetime. Values shown are averages of three separate experiments ± SD.

Then, the effect of cholesterol and/or pCer incorporation into DPPC or pSM bilayers was studied. In bilayers of pure pSM or DPPC, tPA showed a bi-exponential intensity decay with a long lifetime component of 45-50 ns and a shorter lifetime around 15 ns (Figure 4.2), an expected result for a bilayer in a homogeneous gel phase (de Almeida *et al.*, 2002; Wolber and Hudson, 1981). Addition of cholesterol led to a decrease in the longest lifetime component and its fractional amplitude as described earlier (Wolber and Hudson, 1981), while addition of pCer resulted in an increase in the longest lifetime component (Figure 4.2), probably due to the ordering effect of the latter lipid. Both binary mixtures still exhibited a bi-exponential decay, in accordance with studies supporting the presence of a single phase in bilayers with that composition: a L_o phase in the case of cholesterol-containing bilayers (Busto *et al.*, 2010) and a highly rigid gel-like phase in the case of membranes with ceramide (Busto *et al.*, 2009).

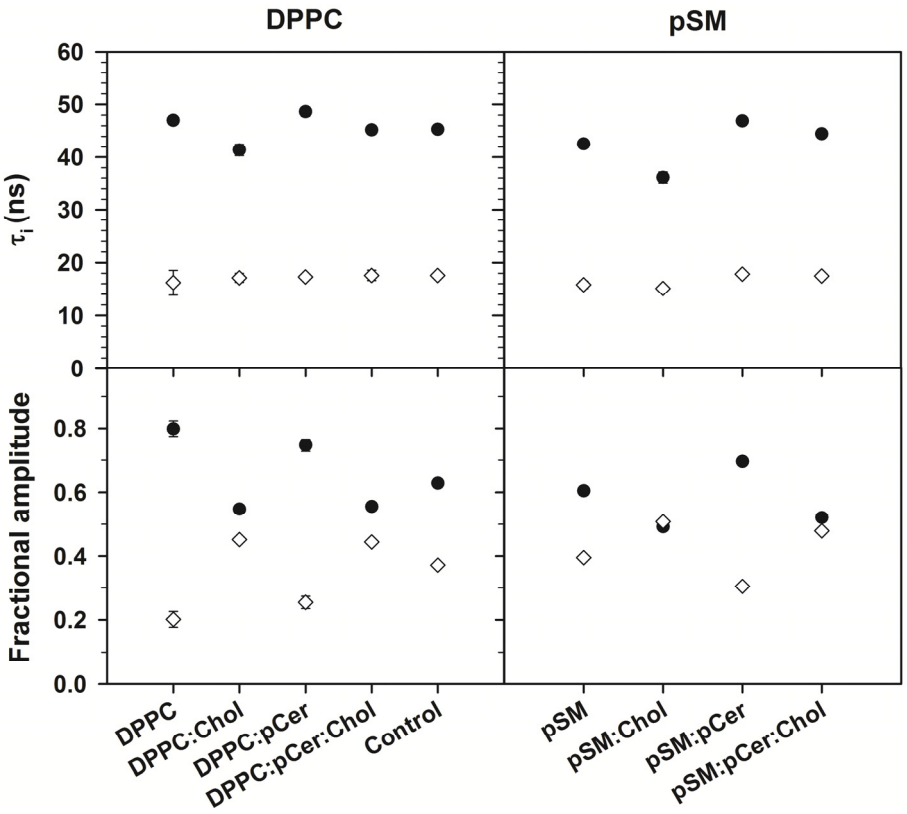

Figure 4.2. Effect of Chol and/or pCer incorporation into pSM or DPPC bilayers at room temperature. tPA intensity decays were fitted to obtain two lifetime components (top panels, filled circles and empty diamonds). The bottom panels show the fractional amplitudes corresponding to the long lifetime (filled circles) and the short lifetime (empty diamonds). The binary mixtures were 7:3 (mol ratio) and the ternary mixtures were 7:3:3. The control was a mixture of equal amounts of liposomes of both DPPC binary mixtures (DPPC:Chol 7:3 and DPPC:pCer 7:3). Values shown are averages of three separate experiments ± SD, but for the control (a single experiment).

The longest lifetime component of the ternary mixtures containing both Chol and pCer showed an intermediate value as compared to those of the binary mixtures, although the fractional amplitude was more similar to that of the Chol-containing binary mixtures (Figure 4.2). Similarly to the other compositions, the ternary mixture also showed a bi-exponential intensity decay. However, when a control sample containing a mixture of equal amounts of DPPC:Chol and DPPC:pCer liposomes was studied, the recovered intensity decay was still well adjusted to a bi-exponential decay. Therefore, the intensity decay of tPA seemed to be unable to distinguish between different ordered domains, so that the result obtained was just an average of the longest lifetimes of such domains and of their corresponding fractional amplitudes. It must be noted, however, that while the longest lifetimes of the control and the corresponding ternary mixture were identical, that was not the case for their fractional amplitudes (Figure 4.2).

In order to obtain further information about the system under study, the intensity decay of tPA was measured at increasing temperatures. As temperature was increased, the longest lifetime component decreased (Figure 4.3). Both pure pSM and DPPC bilayers showed a sharp decrease of the longest lifetime to < 10 ns at 45 ºC, when both bilayers become fluid (Figure 4.3, squares). Binary mixtures with pCer showed a nearly linear decrease of the longest lifetime with a drop below 10 ns at 70 ºC (Figure 4.3, triangles). This is in good agreement with thermograms obtained through calorimetry studies (Busto *et al.*, 2009) where the gel-fluid transition is completed around that temperature. Binary mixtures with Chol exhibited a different trend with no sudden drop but a change of slope when reaching the range of short lifetimes (<10 ns) at 50-55ºC (Figure 4.3, circles).

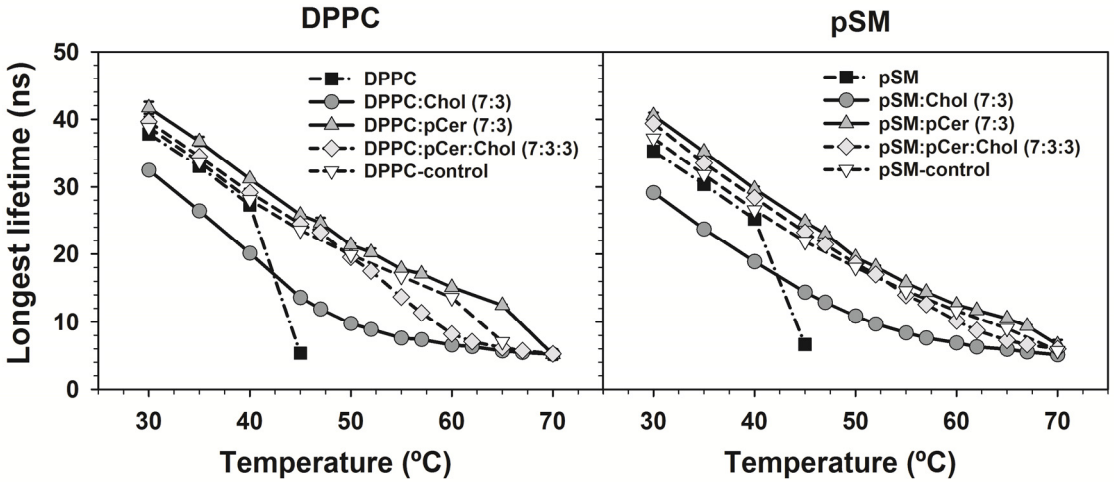

Figure 4.3. Decrease of the tPA longest lifetime with increasing temperature. The controls were a mixture of equal amounts of liposomes of both binary mixtures with DPPC (DPPC:Chol 7:3 and DPPC:pCer 7:3) and pSM (pSM:Chol 7:3 and pSM:pCer 7:3). Values shown are averages of three separate experiments ± SD, but for the controls (a single experiment).

When the ternary mixtures were studied, an intermediate behavior was observed both with DPPC and with pSM: the longest lifetime values were more similar to those of the binary mixtures with pCer, the trend of the decrease resembled more that of the Chol-containing mixtures and the region of the short lifetimes was reached at an intermediate temperature of 60-65 ºC (Figure 4.3, diamonds). Additionally, a mixture of liposomes of the binary mixtures was used as a control for the coexistence of Chol- and pCer-enriched domains. These controls showed a similar behavior to that of the binary mixtures with pCer (Figure 4.3, inverted triangles) (see Discussion).

Furthermore, the evolution of the fractional amplitude of the longest lifetime component with increasing temperature was also observed (Figure 4.4). This fractional amplitude is informative of the ordered (rigid) phase present in the bilayer (Wolber and Hudson, 1981) so it can be used to detect the melting behavior of that phase as temperature is increased (Ruggiero and Hudson, 1989). Indeed, DPPC and pSM bilayers showed sharp decreases above the temperatures corresponding to the pre-transition of DPPC and the main gel-fluid transition of both lipids (Figure 4.4, A). Binary mixtures with pCer (Figure 4.4, B) also showed a melting profile in good agreement with calorimetric studies of the same samples (Busto *et al.*, 2009).

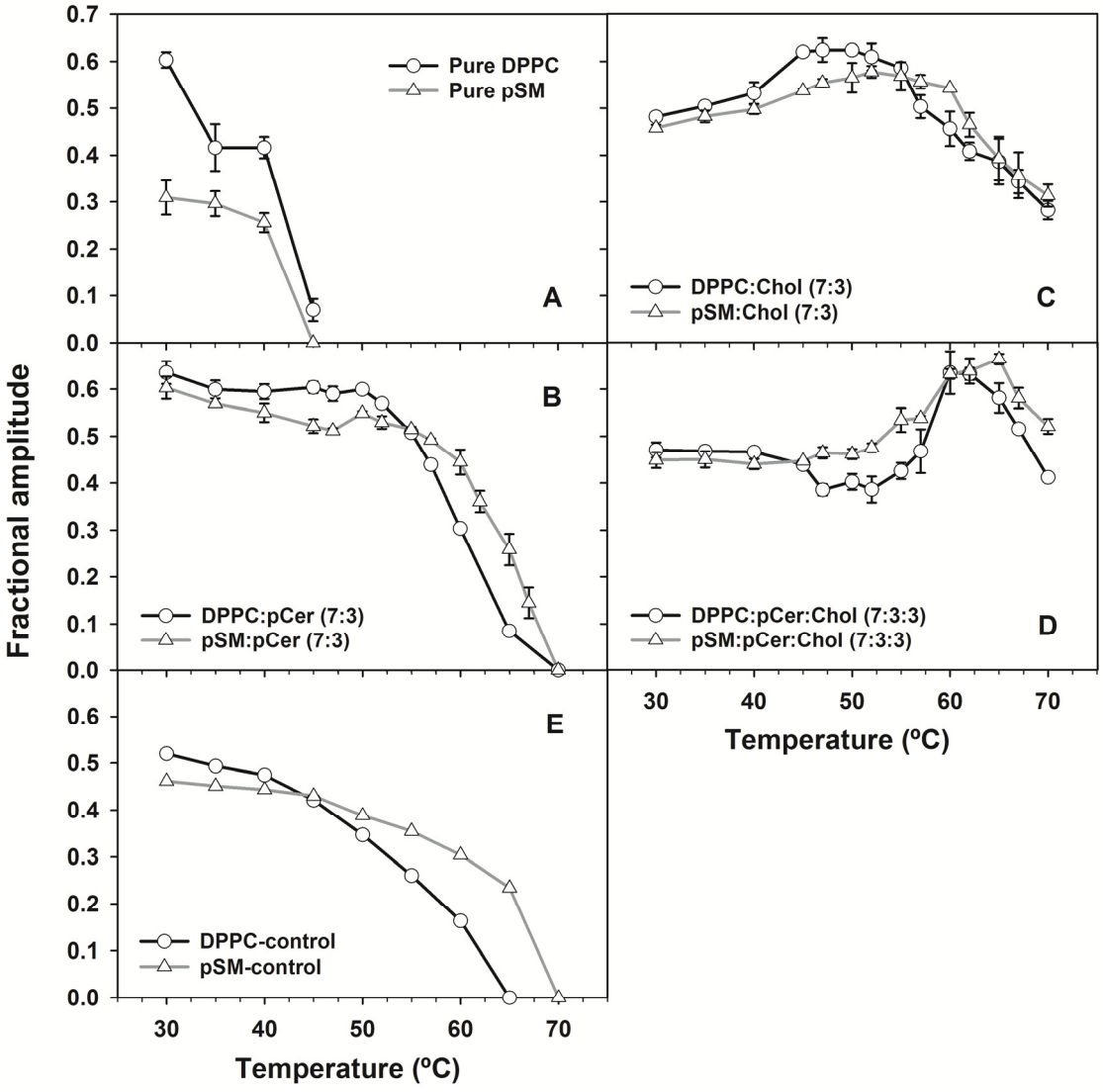

Figure 4.4. Evolution of the fractional amplitude of the longest lifetime component with increasing temperature. The controls were a mixture of equal amounts of liposomes of both binary mixtures with DPPC (DPPC:Chol 7:3 and DPPC:pCer 7:3) and pSM (pSM:Chol 7:3 and pSM:pCer 7:3). Values shown are averages of three separate experiments ± SD, but for the controls (a single experiment).

In the case of the binary mixtures with Chol however, a typical melting profile was not observed: the fractional amplitude first increased gradually and did not start to decrease until reaching the temperature corresponding to the short lifetime range, i.e. > 50-55 ºC (Figure 4.4, C). A similar result was exhibited by the ternary mixtures, again the fractional amplitude decreasing only when the short lifetime range was reached, above 60-65 ºC (Figure 4.4, D). Finally, the controls did show a typical melting profile resembling that of the binary mixtures with pCer (Figure 4.4, E). In all cases, the fractional amplitude of the longest lifetime started to decrease at a slightly lower temperature in DPPC-containing bilayers as compared to bilayers composed of pSM (Figure 4.4).

DPH and tPA anisotropy

Samples with the above compositions where then studied using DPH anisotropy as an additional tool for measuring bilayer order (Figure 4.5). Both DPPC and pSM liposomes showed high anisotropy values below their gel-fluid transition temperature, typical of bilayers in the gel phase, while low anisotropy values were recorded above their T_m, indicative of fluid bilayers (Figure 4.5A, B, squares). In the binary mixtures with pCer, the anisotropy profile shows a clear melting profile similar to that obtained with the amplitudes of tPA lifetimes (Figure 4.5A, B, triangles). At low temperatures the anisotropy keeps unchanged at a value similar to pure DPPC or pSM; the anisotropy then starts to drop at ~45 °C for DPPC:pCer and at ~55 °C for pSM:pCer until the bilayer seems to become fluid (similar anisotropies to pure DPPC and pSM in fluid state) at around 70 °C, similarly to what was seen with tPA lifetimes (Figure 4.4, B). In the binary mixtures with Chol, the anisotropy values started slightly below that of pure bilayers but decreased slowly and remained significantly higher than those of pure bilayers or binary mixtures with pCer at high temperatures. (Figure 4.5A, B, circles).

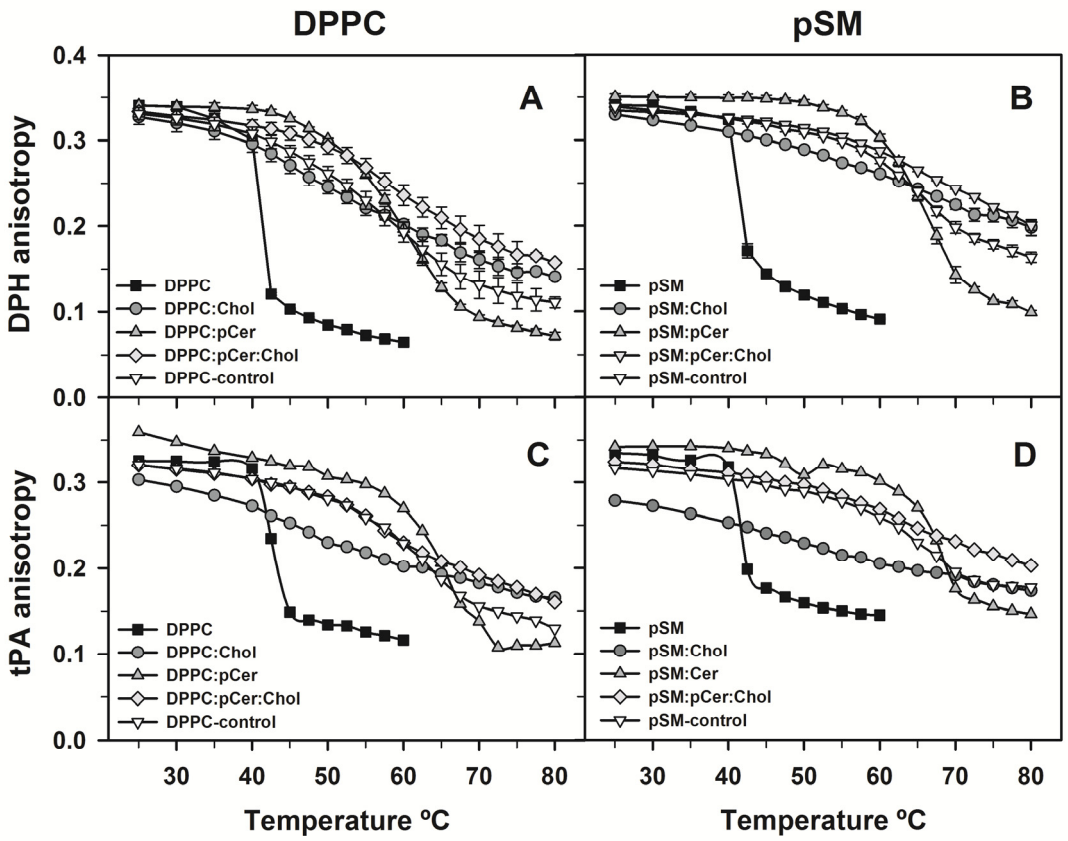

Figure 4.5. Fluorescence anisotropy of DPH (A, B) and tPA (C, D) as a function of temperature in MLV of varying compositions. The binary mixtures were 7:3 and the ternary mixtures were 7:3:3. The controls were a mixture of equal amounts of liposomes of both binary mixtures with DPPC (DPPC:Chol 7:3 and DPPC:pCer 7:3) and pSM (pSM:Chol 7:3 and pSM:pCer 7:3). Values shown for top panels are averages of three separate experiments ± SD. Values shown for bottom panels are from a single experiment.

Interestingly, the anisotropy of the ternary mixture has at 25 ºC a value intermediate between those of the binary mixtures with Chol and pCer and then slowly decreases without a clear melting profile but more similar to the decrease seen for Chol-containing binary mixtures (Figure 4.5A, B, diamonds), as observed for tPA lifetimes (Figure 4.4). Again, the anisotropy at high temperatures is kept at higher values than those of typical disordered bilayers. The anisotropy values of the controls are at all temperatures between those of the binary mixtures with Chol and pCer, even converging at ~60-65 °C (Figure 4.5A, B inverted triangles). This is an expected result for a mixture of equal amounts of liposomes of both binary mixtures. The profile is also significantly different from that of the ternary mixture. The results are quite similar for both DPPC- and pSM-containing bilayers, the only noticeable difference being again a slightly higher thermostability of ordered bilayers containing pSM as compared to those with DPPC (Figure 4.5A, B), as also seen with tPA lifetimes (Figure 4.4).

DPH and tPA can be considered as complementary probes in studies with bilayers containing pCer, since the former fluorophore is excluded from pCer-rich domains whereas the latter presents a high preference for such domains (Castro *et al.*, 2007; Silva *et al.*, 2007). Therefore, fluorescence anisotropy of tPA was also measured in the same lipid mixtures to confirm the results obtained with DPH (Figure 4.5C, D). Overall, the results with tPA anisotropy resemble those of DPH, the main differences being: lower anisotropy values for binary mixtures with Chol, higher values for pure bilayers and binary bilayers with pCer in the fluid phase, and higher thermostability of the ordered phase of DPPC:pCer bilayers (Figure 4.5), all of them probably due to the higher affinity of this probe to gel and pCer-rich domains.

Differential scanning calorimetry

The presence of a homogenous gel ternary phase in bilayers is probably highly dependent on the lipid proportions. In order to explore this hypothesis, pSM:pCer:Chol ternary bilayers with decreasing pCer and Chol amounts at a constant 1:1 ratio were studied by DSC (Figure 4.6, Table 4.1). The ternary mixture at 54:23:23 proportion showed a symmetric endotherm centered at 60 ºC (Figure 4.6, Table 4.1), as previously reported (Busto *et al.*, 2010). Decreasing pCer and Chol resulted in a noticeable increase in the overall transition enthalpy and a slight decrease in the transition temperature (Figure 4.6, Table 4.1). Additionally, the peak became clearly asymmetric, as confirmed upon deconvolution of the endotherms: while the endotherm of the ternary mixture at 54:23:23 proportion showed a single component, two were obtained for the samples at 60:20:20 proportion and a third small component appeared at 66:17:17, which became more noticeable in 70:15:15 samples (Figure 4.6). The endotherm for the latter sample was similar to that obtained in previous DSC studies of the pSM:pCer:Chol mixture at low Chol proportion (Busto *et al.*, 2010).

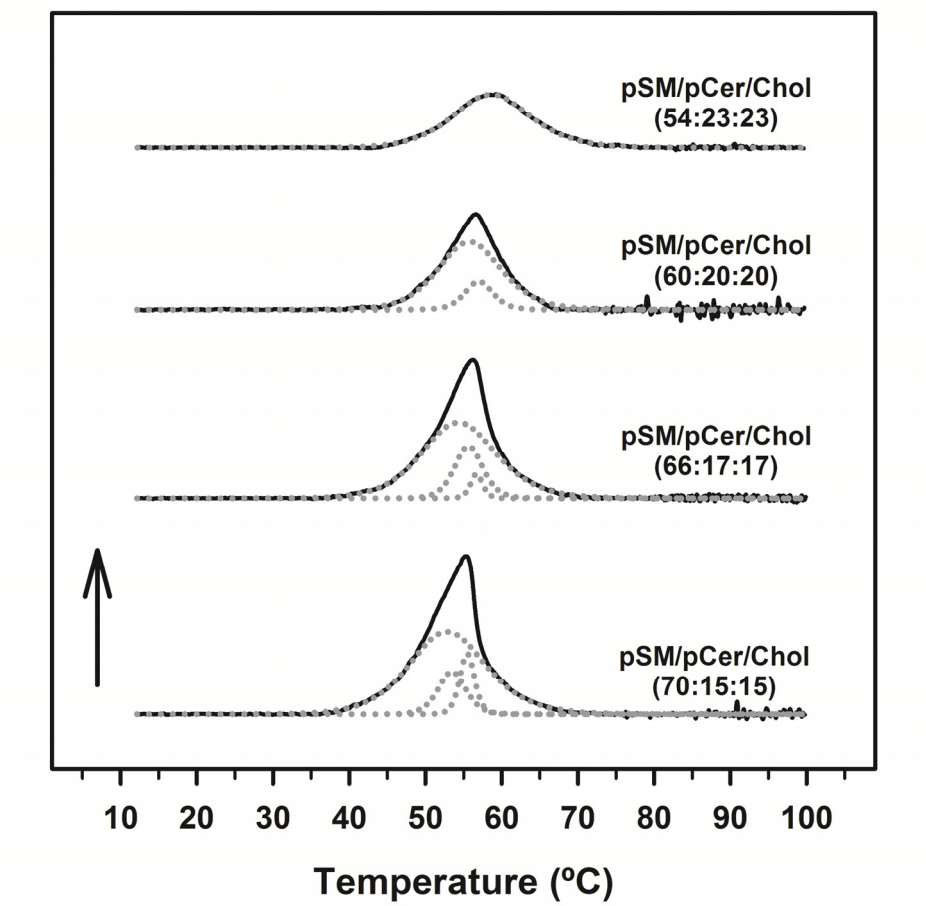

Figure 4.6. DSC of aqueous dispersions of pSM:pCer:Chol at different mol proportions. Dotted lines represent peak fitted endotherms. The arrow corresponds to 0.5 kcal/mol/ºC.

Table 4.1. Thermodynamic parameters of DSC endotherms of pSM:pCer:Chol liposomes at different mol proportions. Averages ± SD are shown.

Bilayer composition	**ΔH (cal/mol)**	**T_m (ºC)**	**$\Delta T_{1/2}$ (ºC)**
pSM:pCer:Chol (54:23:23)	2800 ± 210	59.0 ± 0.5	11.5 ± 0.4
pSM:pCer:Chol (60:20:20)	3260 ± 70	56.7 ± 0.1	7.2 ± 1.0
pSM:pCer:Chol (66:17:17)	4900 ± 190	56.2 ± 0.1	6.9 ± 0.3
pSM:pCer:Chol (70:15:15)	5500 ± 200	55.3 ± 0.1	7.3 ± 0.5

ΔH: transition enthalpy change.

$\Delta T_{1/2}$: transition width at half-height

4.4 Discussion

Previous studies have shown that in the absence of a fluid phase both Chol and pCer appear to coexist together with saturated lipids in a homogeneous gel ternary phase (Busto *et al.*, 2014; Busto *et al.*, 2010; Garcia-Arribas *et al.*, 2015). These studies made use of a wide range of techniques such as DSC, confocal microscopy, X ray diffraction and atomic force microscopy (AFM). In this work, fluorescence spectroscopy techniques were used as complementary tools to extend the previously obtained results. Specifically, the fluorescent probes tPA and DPH have been used as reporters of membrane order to compare the properties of DPPC or pSM bilayers containing Chol and/or pCer in an attempt to gain further insight into the behavior of bilayers with a saturated lipid and both Chol and pCer in the absence of a fluid disordered phase.

When the intensity decay of tPA was measured at room temperature, the ternary mixture showed a combination of characteristics from the binary ones (Figure 4.2). However, the technique did not seem sensitive enough to distinguish the coexistence of different kinds of ordered phases, so measurements were carried out as the temperature was increased. In these experiments, the ternary mixture showed again a combination of characteristics from the binary mixtures (Figure 4.3, Figure 4.4).

Such a behavior could be a consequence of the coexistence of pCer- and Chol-enriched domains, rather than arising from the presence of a single ternary phase. Due to the characteristics of the experiment, however, if there is a coexistence of lipid domains with significantly different longest lifetime values (as it happens with pCer- and Chol-enriched domains) the behavior observed should correspond to the phase with the longest lifetimes. This is because the technique lacks the sensitivity to resolve the four individual lifetimes, thus a long and an intermediate lifetime are obtained with different contributions from each of the present four ones. According to this, the long lifetime obtained should mainly correspond to the longest among the four lifetimes, while the contribution from the other long lifetime would be divided between the long and intermediate lifetimes obtained. Indeed, when controls with a mixture of both binary mixtures were analyzed, the results were similar to those with the pCer-containing binary mixtures and clearly different compared to those of the ternary mixtures (Figure 4.2, Figure 4.3, Figure 4.4).

DPH and tPA anisotropy experiments further confirmed the intermediate behavior of ternary mixtures as compared to that of the binary mixtures with pCer and Chol (Figure 4.5). The controls, as expected, showed an averaged anisotropy value between those of binary mixtures while ternary mixtures exhibited a unique behavior, again allowing us to exclude the possibility of coexistence of binary domains in such bilayers (Figure 4.5). Therefore, the results obtained with both tPA and DPH allow us to conclude that in the absence of a disordered phase both Chol and pCer can coexist in a ternary phase with the ordered lipid, in good agreement with previous work on the same system (Busto *et al.*, 2014; Busto *et al.*, 2010; Garcia-Arribas *et al.*, 2015). This ternary phase displays unique properties with both lipids probably contributing to its characteristics. First, it shows a high molecular order (as seen by the long lifetimes and high anisotropy), possibly due to the ordering effect of pCer. Its behavior when temperature is increased, however, seems to be governed by the effect of Chol: no clear melting of the ordered phase into a fluid one is observed, just a slow decrease in bilayer order occurs. Additionally, as it happens with the liquid-ordered phase in binary mixtures with Chol, the ternary phase does not seem to become completely disordered even at high temperatures. Interestingly, the effect of pCer may also be seen in the higher thermostability of the ternary phase. Furthermore, the behavior and properties of the ternary phase do not seem to be dependent on the ordered phospholipid used, since both bilayers with DPPC and bilayers with pSM gave similar results, as previously seen (Busto *et al.*, 2014; Garcia-Arribas *et al.*, 2015).

The relative proportions of pCer and Chol are important for both lipids to interact together with pSM to form an homogeneous ternary phase (Busto *et al.*, 2010). DSC experiments show that when pCer + Chol presence in ternary bilayers is lowered while keeping their 1:1 ratio, the peak of the endotherm becomes asymmetric and its enthalpy is increased (Figure 4.6, Table 4.1), suggesting association of pCer with pSM to form highly ordered domains, as it happens when cholesterol is not present (Busto *et al.*, 2009). From these and previous results in ternary bilayers with low and high cholesterol content (Busto *et al.*, 2010), it can be concluded that the ability of Chol to displace pCer from its interaction with pSM depends more strongly on the overall cholesterol proportion in the bilayer rather than on the Chol/pCer ratio.

Figure 4.7 shows a partial ternary pSM:pCer:Chol phase diagram with the distribution of the ternary samples from this work together with data from previous studies. The ternary lipid bilayers studied here by DSC (Figure 4.7, circles) lie between ternary samples that were shown to have pCer-enriched domain segregation (Figure 4.7, triangles up) and ternary samples with a homogeneous phase (Figure 4.7, triangles down). According to DSC data, the boundary between domain coexistence and the presence of a homogenous phase should lie between the 66:17:17 and 60:20:20 compositional points. In order to further characterize the effect of Chol and Cer proportions on the properties of ternary bilayers, further studies using confocal microscopy on GUV and AFM on supported bilayers are planned to be performed.

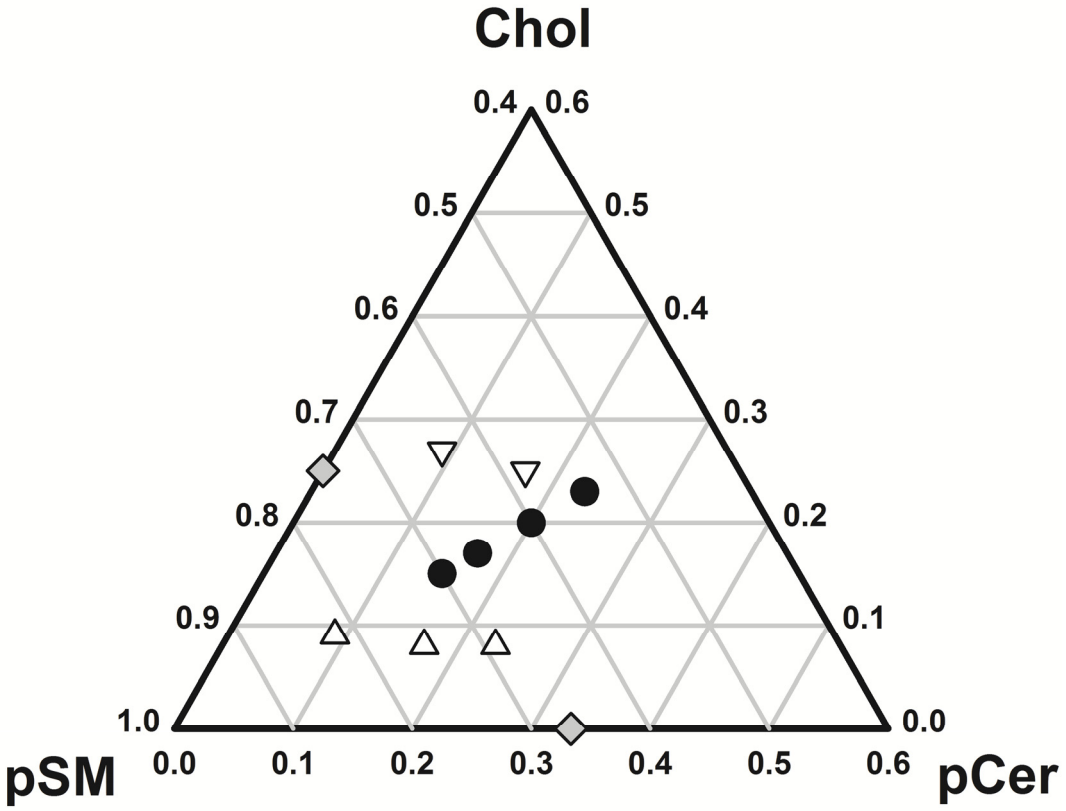

Figure 4.7. Partial ternary pSM:pCer:Chol phase diagram. Circles correspond to the ternary samples used in DSC experiments in this work. Triangles correspond to ternary samples of a previous study showing pCer-enriched domain segregation (triangles up) and a single homogenous phase (triangles down) (Busto *et al.*, 2010). Diamonds correspond to the approximate compositional points of Chol and pCer in pSM:Chol and pSM:pCer binary mixtures, i.e. the starting point of a single L_o and pCer-enriched gel-like phase, respectively (Busto *et al.*, 2009; Busto *et al.*, 2010).

Chapter 5:

DOES CERAMIDE FORM CHANNELS? THE CERAMIDE-INDUCED MEMBRANE PERMEABILIZATION MECHANISM

Chapter 5: DOES CERAMIDE FORM CHANNELS? THE CERAMIDE-INDUCED MEMBRANE PERMEABILIZATION MECHANISM

5.1 Introduction

Sphingolipids are bioactive lipids present in biological membranes and involved as metabolic signals in several cellular processes such as cell proliferation, signal transduction or apoptosis (Carreira *et al.*, 2015; Goni *et al.*, 2014; Hannun and Obeid, 2008). Among them, ceramide has been studied in great detail. Although ceramide levels in resting membranes are very low, they can significantly increase under cellular stress conditions or upon several stimuli (such as death receptor ligands, cytokines or ionizing radiation) and act as second messengers in different intracellular response pathways (Hannun, 1996; Kolesnick *et al.*, 2000). Ceramides also exhibit unique structural features that allow them to alter the biophysical properties of membranes, promoting lateral domain segregation, facilitating the formation of non-lamellar phases and inducing membrane negative curvature (Castro *et al.*, 2014; Goni *et al.*, 2014).

An important property of ceramides, which could be related to their biological function, is their ability to induce membrane permeabilization. The ability of ceramide to permeabilize lipid membranes was assessed in early studies (Montes *et al.*, 2002; Ruiz-Arguello *et al.*, 1996; Siskind and Colombini, 2000), but the mechanism behind the process is still debated. This is important, since it could be directly related to the ability of ceramide to induce permeabilization of mitochondria to cytochrome c during apoptosis (Di Paola *et al.*, 2000). Determining the permeabilization mechanism of ceramide could therefore help us to clarify the still debated role of this lipid in programmed cell death.

The work by Montes and coworkers led us to propose that membrane permeabilization occurs due to bilayer restructuring and destabilization induced by ceramide, as well as to the packing defects formed at the boundaries of ceramide-enriched domains (Goni *et al.*, 2014; Montes *et al.*, 2002). However, studies by Siskind, Colombini and coworkers propose that ceramide-induced membrane permeabilization occurs through the formation of large, structured and stable ceramide-channels, specific

of the mitochondrial outer membrane, which would induce apoptosis by direct permeabilization of the mitochondria to cytochrome c (Anishkin *et al.*, 2006; Colombini, 2016; Samanta *et al.*, 2011; Siskind and Colombini, 2000; Siskind *et al.*, 2003; Siskind *et al.*, 2002). This topic is highly controversial, mainly due to the large amount of energy that formation of those highly ordered structures would require .

In order to shed some light on this issue, an improved membrane leakage assay based on time-resolved analysis of calcein fluorescence that allows determination of the leakage mechanism (Patel *et al.*, 2009) has been used in this work. When assaying membrane permeabilization through leakage assays on liposomes, partial efflux could result from either only some vesicles releasing all their contents (all-or-none leakage) or from all the vesicles releasing part of their contents (graded leakage). The presence of ceramide channels in the liposomes would undoubtedly cause an all-or-none leakage, while a graded leakage would be more consistent with our view of permeabilization due to destabilization of membranes by ceramide-induced lateral domain segregation, or localized phenomena of non-lamellar phase formation.

This study shows that ceramide-induced leakage from SM- and Chol-rich liposomes follows a graded mechanism rather than an all-or-none one, while no leakage is observed in lipid bilayers with low amounts of those two lipids, or bilayers that mimic the composition of the mitochondrial outer membrane. Thus, these results raise serious doubts about the ability of ceramide to produce stable channels.

5.2 Materials and Methods

Materials

Egg phosphatidylcholine (ePC) and egg phosphatidylethanolamine (ePE) were purchased from Lipid Products (South Nutfield, UK). Liver phosphatidylinositol (PI), dioleoylphosphatidylserine (DOPS), cardiolipin (CL), egg sphingomyelin (eSM), egg ceramide (eCer), acetylceramide (C2-Cer), cholesterol (Chol) and the lipophilic fluorescent probe 18:1 phosphatidylethanolamine-N-(lissamine rhodamine B sulfonyl) (Rho-PE) were from Avanti Polar Lipids (Alabaster, AL). 8-aminonaphtalene-1,3,6-trisulfonic acid (ANTS), and *p*-xylene-bis-pyridinium bromide (DPX) were supplied by Molecular Probes (Eugene, OR). The hydrophilic fluorescent probe Atto 488 was purchased from Atto TEC (Siegen-Weidenau, Germany).

Sphingomyelinase (SMase) from *Bacillus cereus*, calcein, Sephacryl 500-HR, EDTA, casein and fatty acid-free bovine serum albumin (BSA) were supplied by Sigma (St. Louis, MO). PD-10 desalting columns were from GE Healthcare (Little Chalfont, UK). Stock solutions of lipids were prepared by dissolving pure lipids in chloroform/methanol (2:1 v/v) and stored at -20 °C.

Liposome preparation

Lipid vesicles for calcein release studies were prepared by mixing the desired lipids and evaporating the solvent under a stream of nitrogen. The resulting lipid film was then kept under high vacuum for 90 min in order to ensure complete removal of any residual solvent. The sample was hydrated in calcein-containing buffer at 55 °C, followed by vigorous vortex mixing. SMase requires Ca^{2+} and Mg^{2+} for optimal catalytic activity under our conditions, so a cation-containing buffer was used in experiments with eSM:ePE:Chol (2:1:1 by mol) liposomes (unless otherwise stated): HEPES 10 mM, calcein 70 mM, NaCl 30 mM, $CaCl_2$ 10 mM, $MgCl_2$ 2 mM, pH 7.4. Experiments with other vesicle compositions were carried out with a buffer lacking cations: HEPES 10 mM, calcein 70 mM, NaCl 30 mM, pH 7.4. After hydration, large unilamellar vesicles (LUV) were prepared by subjecting the sample to 10 freeze/thaw cycles, followed by extrusion through disposable polypropylene filters 0.1-μm pore diameter (Anotop 10 Whatman, Germany) with 2-ml plastic syringes. Calcein-loaded vesicles were finally separated from unencapsulated dye by gel filtration in a 1 × 30 cm column packed with Sephacryl HR-500, eluting with an isosmotic calcein-free buffer.

Lipid vesicles for ANTS/DPX studies were prepared by a slightly different method: the lipid film was hydrated with an ANTS- and DPX-containing buffer (HEPES 10 mM, ANTS 20 mM, DPX 70 mM, NaCl 30 mM, $CaCl_2$ 10 mM, $MgCl_2$ 2 mM, pH 7.4); extrusion was performed using 0.1-μm pore diameter polycarbonate filters and vesicles were separated from unencapsulated ANTS and DPX by gel filtration in a PD-10 desalting column containing Sephadex G-25 resin and eluting with an isosmotic ANTS- and DPX-free buffer.

Vesicle size was checked by quasi-elastic light scattering using a Malvern Zeta-Sizer 4 spectrometer (Malvern Instruments, Worcestershire, UK). Lipid concentration was determined by phosphate analysis (Bartlett, 1959).

Aqueous content release assays

Vesicle content release was primarily assessed using a method based on calcein fluorescence lifetime measurements (Patel *et al.*, 2009). In experiments with externally added ceramide, aliquots of calcein-loaded vesicles at 30 µM (lipid concentration) were incubated at 37 °C with 2.5%, 5%, 7.5% and 10% egg ceramide or C2 ceramide. Due to the slow kinetics of vesicle leakage induced by externally added ceramide (Montes *et al.*, 2002), incubation was carried out for 6 h. C2-Cer or eCer were added dissolved in DMSO. In experiments with SMase, aliquots of calcein-loaded vesicles 30 µM in lipid were incubated at 37 °C with 0.16 U/ml SMase for 5 min. In an alternative approach, a low enzyme concentration (0.6 U/l) was used in order to obtain a longer temporal resolution and 12 mM EDTA was added to stop the reaction at different times. SMase was used diluted in calcein-free buffer, with 0.1% (w/v) BSA to stabilize the enzyme (Urbina *et al.*, 2009). In each experiment, a spontaneous efflux control with no permeabilizer and a 100% efflux control with 0.1% Triton-X-100 were also analyzed.

Fluorescence decays were measured using a FluoroMax-3 spectrofluorometer equipped with a time-correlated single photon counting (TCSPC) system (Horiba Jobin Yvon, Edison, NY) (excitation 467 nm, and emission 515 nm). Data analysis was performed using DAS 6 software (Horiba Jobin Yvon). The curve for free calcein (100% efflux control) follows a mono-exponential behavior, with a lifetime around 4 ns (τ_F). The decay curves for the liposome samples were fitted to the following bi-exponential model:

$$I(t) = \alpha_F \exp(-t/\tau_F) + \alpha_E \exp(-t/\tau_E) \quad \text{[Eq. 5.1]}$$

where τ_F and τ_E are the lifetime components corresponding to free calcein and entrapped calcein respectively, and α_F and α_E their respective pre-exponential factors. τ_F was fixed at the value obtained with the 100% efflux control. $\sum\alpha_i$ was normalized to unity so that α_F and α_E represented the fractional amplitude of their corresponding lifetimes. The efflux value (E) was determined according to equation 5.2 below (Patel *et al.*, 2009), where α_{F0} is the pre-exponential factor of free calcein in a spontaneous efflux control without permeabilizer and Q_{stat} is the static quenching factor.

$$E = \frac{(\alpha_F - \alpha_{F0})}{(\alpha_F - \alpha_{F0} + Q_{stat}\alpha_E)} \quad \text{[Eq. 5.2]}$$

In the absence of any permeabilizer, the decay shows a dominant α_E with a τ_E around 0.4 ns, corresponding to fully entrapped calcein, and a weak α_{F0} corresponding to spontaneous dye release. When permeabilization occurs, the efflux increase can be followed as a decrease in α_E and a concomitant increase in α_F. Furthermore, partial unloading of vesicles leads to an increase in the τ_E value, so the leakage mechanism can be determined by the correlation between the measured efflux and τ_E (Figure 5.1), as described in Patel *et al.* (2009). When all-or-none leakage occurs, only some of the vesicles are leaky and release all their content (not contributing to τ_E), while the rest remain intact and fully loaded with calcein (τ_E = 0.4 ns). Therefore, the degree of efflux changes but τ_E does not (Figure 5.1, dotted line). In graded leakage all the vesicles release part of their contents, becoming partially unloaded (τ_E > 0.4 ns). In this case, τ_E should increase along with the efflux (Figure 5.1, dashed line).

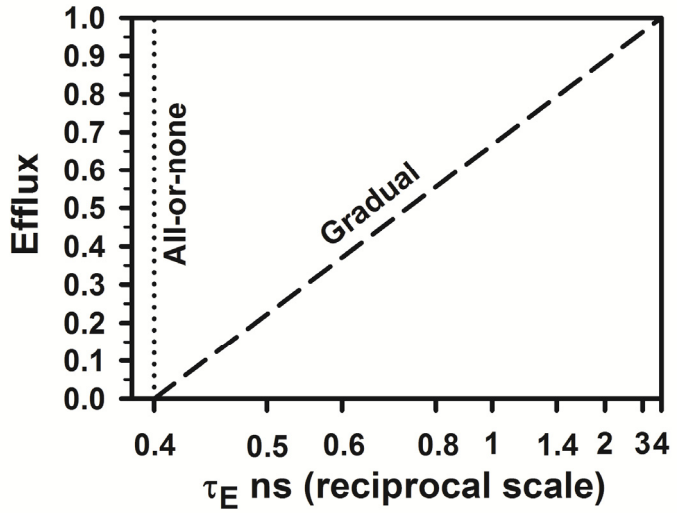

Figure 5.1. Expected correlation between calcein efflux and lifetime of entrapped dye (τ_E) for ideal all-or-none (dotted line) and gradual (dashed line) leakage mechanisms.

Additionally, the ability of EDTA to stop SMase reaction was assayed using the ANTS/DPX system (Ellens *et al.*, 1985). The fluorescence of 0.3 mM LUV entrapping both ANTS and DPX was monitored using a QuantaMaster 40 spectrofluorometer (Photon Technology International, Lawrenceville, NJ) (λ_{ex} = 355 nm, λ_{em} = 520 nm). After a 5 min baseline, 6 U/l SMase was added. 12 mM EDTA was then added at different times during the reaction to stop the content release. All these measurements were performed under continuous stirring and at a constant temperature of 37 ºC.

GUV permeabilization assay

Giant unilamellar vesicles (GUV) were produced by electroformation. 10 µg lipid mixture with 0.2% Rho-PE dissolved in chloroform was spread on the platinum wires of the electroformation chamber and allowed to dry. The platinum wires were immersed in 300 mM sucrose and electroformation was performed for 2 h at 1.5 V and 10 Hz, followed by 1 h at 2 Hz to detach the vesicles. Atto 488 was mixed with buffer (HEPES 10 mM, NaCl 150 mM, pH 7.4) in LabTec chambers (Thermo Fisher Scientific) previously blocked with casein, to a final probe concentration of 0.2 µM. Afterwards, 70 µl of the GUV suspension were added to a final volume of 300 µl.

1 µM C2-Cer or eCer (approximately 10 mol% of final lipid concentration) dissolved in DMSO, or DMSO alone as a negative control were added to the GUV in the visualization chamber. Imaging was performed at different time points during incubation at 37 °C over 6 h. The samples were imaged using a LSM710 confocal microscope with a C-Apochromat × 40 NA. 1.2 water immersion objective (Zeiss, Jena, Germany), with excitation laserlines at 488 and 561 nm. A spectral beam guide was used to separate emitted fluorescence. Images were processed automatically with a homemade analysis software (Hermann *et al.*, 2014) detecting the filling degree of each GUV. At least a hundred GUV were analyzed per experiment. The degree of GUV filling was calculated following equation 5.3, where F_t^{in} and F_t^{out} are the average fluorescence inside and outside a GUV at time t, and F_0 is the background fluorescence:

$$\% \text{ GUV filling} = [(F_t^{in} - F_0) / (F_t^{out} - F_0)] \times 100 \qquad \text{[Eq. 5.3]}$$

5.3 Results

First, the mechanism of ceramide-induced leakage was studied by *in situ* ceramide generation using the enzyme SMase. Calcein-loaded LUV composed of eSM:ePE:Chol (2:1:1 by mol) were treated with 0.16 U/ml SMase and after 5 min incubation at 37 ºC a high efflux (around 85%) was observed (Table 5.1), similarly to a previous study using an ANTS/DPX release assay (Ruiz-Arguello *et al.*, 1996). A noticeable increase of τ_E was observed from 0.41 ns to 1.14 ns (Table 5.1), clearly indicative of a gradual leakage mechanism. However, experimental points at intermediate efflux values could be not obtained using this experimental setup. Therefore, an alternative approach was used.

Table 5.1. Calcein time-resolved fluorescence after addition of SMase to calcein-loaded eSM:ePE:Chol (2:1:1) and 5 min incubation at 37 ºC. Average values ± SD are shown.

Sample	τ_F (ns)	α_F	τ_E (ns)	α_E	Efflux (%)
Control (no SMase)	3.91 ± 0.02	0.14 ± 0.03	0.41 ± 0.03	0.86 ± 0.03	0
0.16 U/ml SMase	3.90 ± 0.02	0.88 ± 0.03	1.14 ± 0.18	0.12 ± 0.03	86.7 ± 2.9

τ: lifetime corresponding to free calcein (τ_F) or entrapped calcein (τ_E)

α: pre-exponential factor corresponding to free calcein (α_F) or entrapped calcein (α_E)

SMase activity is dependent on Ca^{2+} and Mg^{2+}, thus addition of the chelating agent EDTA should be able to stop the SMase reaction. Indeed, no efflux could be detected in the presence of 12 mM EDTA (Figure 5.2A). In order to extend the reaction time and facilitate the acquisition of intermediate points, a lower SMase concentration was also used (0.6 U/l). Figure 5.2B shows, using an ANTS/DPX leakage assay, the slower leakage kinetics resulting from diluted SMase, as well as the ability of EDTA to stop the SMase reaction. This approach can thus be used to measure content release at different times along the efflux curve.

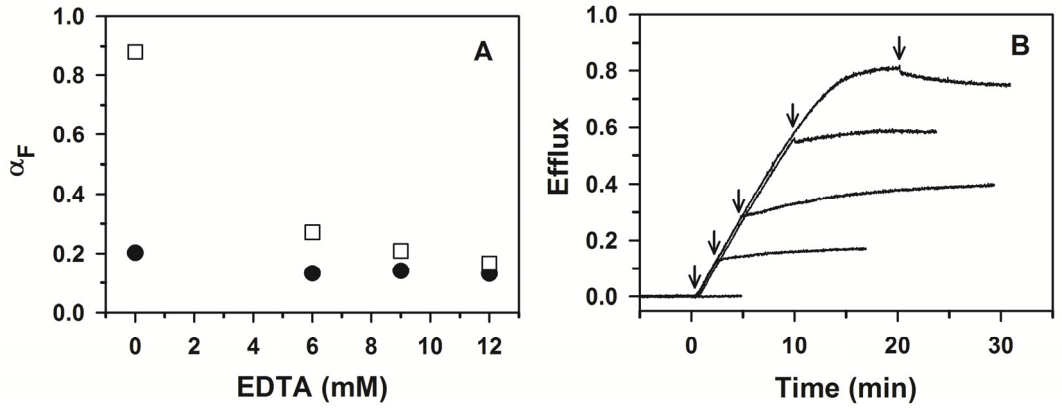

Figure 5.2. Inhibition of SMase activity on eSM:ePE:Chol (2:1:1) liposomes by EDTA. (A) Calcein release inhibition by different concentrations of EDTA on liposomes treated with 0.16 U/ml SMase (squares) or control liposomes without SMase (circles) after 5 min incubation at 37 ºC. α_F: pre-exponential factor corresponding to free dye. (B) Stopping SMase reaction with addition of 12 mM EDTA to ANTS/DPX-loaded eSM:ePE:Chol (2:1:1) vesicles treated with 6 U/l SMase at 37 ºC. SMase was added at time = 0 min. Arrows show the time points when 12 mM EDTA was added to the samples.

Using this alternative approach, calcein-loaded LUV were treated with 0.6 U/l SMase and the resulting calcein efflux was measured after stopping the reaction at different time points with EDTA (Figure 5.3A). The efflux curve obtained was nearly identical to that seen with the ANTS/DPX leakage assay (Figure 5.2B). τ_E increased up to 2 ns (Figure 5.3B), again a clear indication of a gradual permeabilization mechanism.

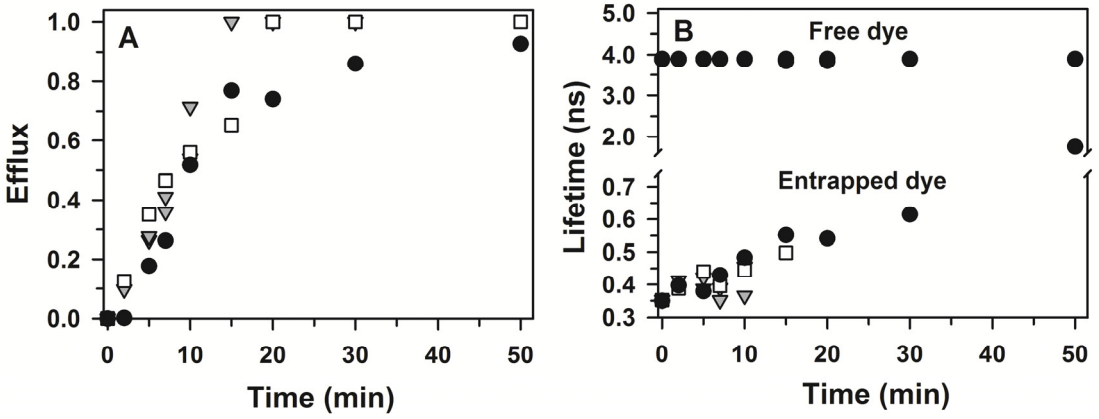

Figure 5.3. Calcein leakage induced by *in situ* ceramide generation on eSM:ePE:Chol (2:1:1) LUV by SMase action (0.6 U/l) at 37 ºC. The results from three independent experiments are shown using different symbols. (A) Calcein efflux as a function of SMase reaction time. (B) Lifetime of free and entrapped calcein as a function of SMase reaction time.

However, when analyzing experimental points corresponding to intermediate efflux values, during the first 7 minutes of the reaction (efflux < 50%) τ_E values remained virtually unchanged (0.35-0.45 ns) and only started to increase above 50% efflux. Therefore, the data was further analyzed by correlating the measured efflux values with their corresponding τ_E (Figure 5.4), as described by Patel *et al.* (2009). The results obtained with high SMase concentration show a correlation very close to what would be expected for an ideal gradual mechanism (Figure 5.4A). The data from intermediate efflux values obtained with the alternative approach, however, shows a correlation that lies between an ideal gradual mechanism and an all-or-none mechanism (Figure 5.4B).

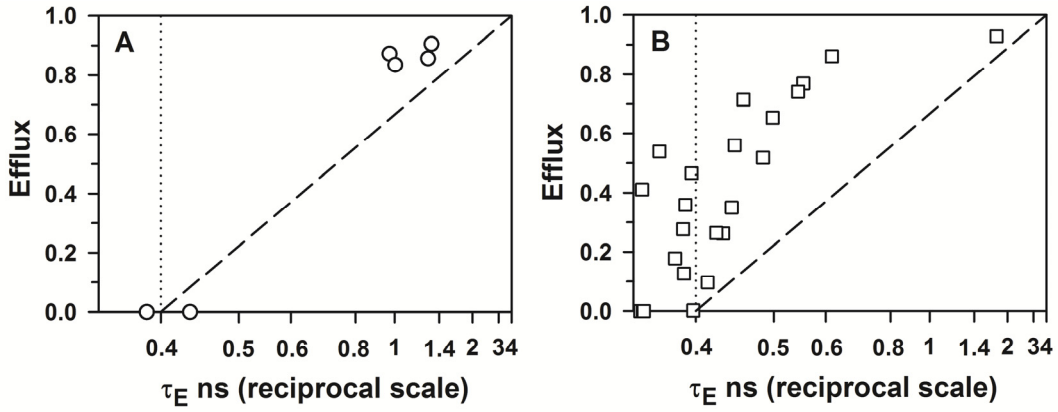

Figure 5.4. Correlation of calcein efflux with the lifetime of entrapped dye induced by SMase treatment of eSM:ePE:Chol (2:1:1) liposomes at 37 ºC. (A) 0.16 U/ml SMase treatment after 5 min incubation at 37 ºC. (B) 0.6 U/l SMase treatment at 37 ºC, stopped with EDTA at different time points along the reaction. The dashed line corresponds to an ideal graded leakage mechanism and the dotted line corresponds to an ideal all-or-none leakage mechanism.

Next, the leakage mechanism was studied with ceramide added to pre-formed liposomes (Figure 5.5). When egg ceramide was added to eSM:ePE:Chol (2:1:1) LUV, a slow release occurred (Montes *et al.*, 2002) with a clear ceramide concentration dependency, reaching around 45% efflux for 10% ceramide (Figure 5.5A). τ_E showed a gradual increase with increasing ceramide concentration, indicative of a gradual leakage mechanism (Figure 5.5B). Indeed, the correlation between calcein efflux and τ_E shows a behavior very close to that expected for a graded leakage mechanism (Figure 5.5C). In contrast, no significant efflux was observed when C2 ceramide was added, (Figure 5.5A) in agreement with our previous data (Montes *et al.*, 2002).

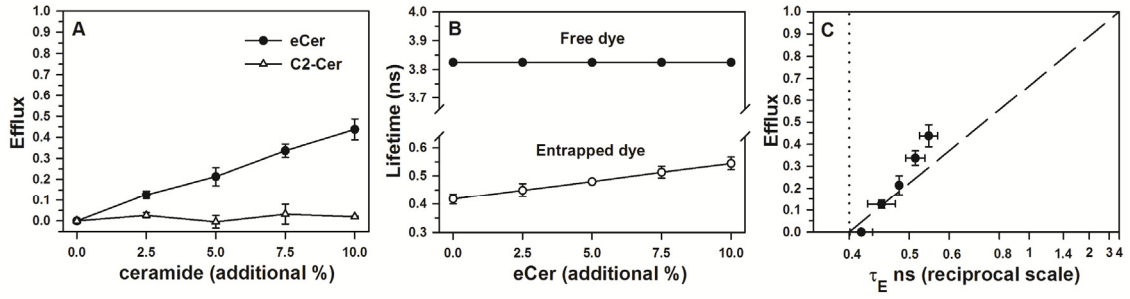

Figure 5.5. Calcein leakage induced by external addition of ceramide to eSM:ePE:Chol (2:1:1) LUV after 6h incubation at 37 ºC. Average values from three separate experiments ± SD are shown. (A) Calcein efflux as a function of ceramide concentration. (B) Increase of entrapped dye lifetime with increasing egg ceramide concentration. (C) Correlation of calcein efflux induced by egg ceramide with the lifetime of entrapped dye. The dashed line corresponds to an ideal graded leakage mechanism and the dotted line corresponds to an ideal all-or-none leakage mechanism.

As previously described, SMase requires Ca^{2+} and Mg^{2+} for optimal activity. However, the presence of these cations may affect membrane stability and thus membrane permeability. In order to determine the effect of cations on ceramide-induced permeabilization, egg ceramide was added to eSM:ePE:Chol (2:1:1) LUV generated in a cation-free buffer (Figure 5.6). The efflux value with 10% additional egg ceramide was half that observed for liposomes generated in a cation-containing buffer (Figure 5.6A). Therefore, cations seem to have a strong effect on membrane stability. However, the permeabilization mechanism remained similar to that shown by the previous experiments in the presence of cations (Figure 5.6B).

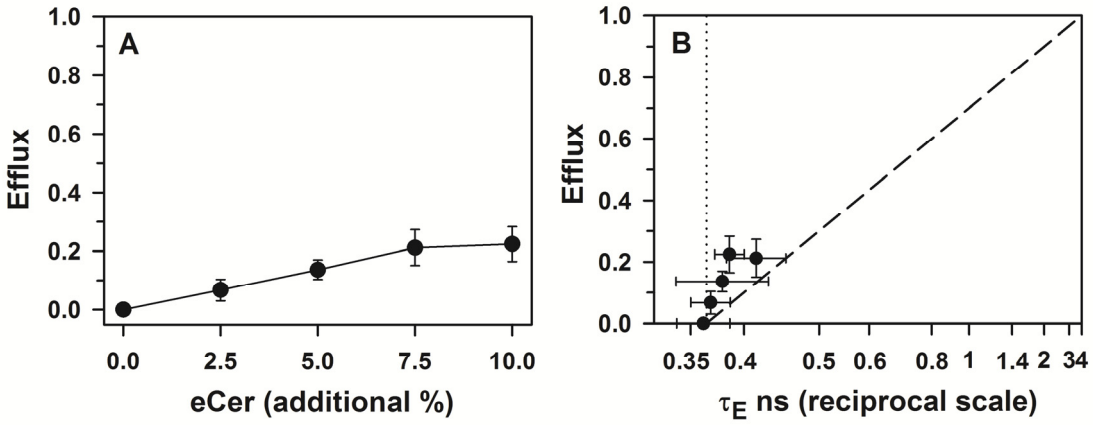

Figure 5.6. Calcein leakage induced by external addition of egg ceramide to eSM:ePE:Chol (2:1:1) LUV generated in a cation-free buffer after 6h incubation at 37 ºC. Average values from three separate experiments ± SD are shown. (A) Calcein efflux as a function of egg ceramide concentration. (B) Correlation of calcein efflux induced by egg ceramide with the lifetime of entrapped dye. The dashed line corresponds to an ideal graded leakage mechanism and the dotted line corresponds to an ideal all-or-none leakage mechanism.

Finally, the effect of membrane composition was assessed on calcein leakage by performing the experiments with externally added ceramide (egg ceramide or C2 ceramide) in LUV composed of either eSM:ePE:Chol (2:1:1) + 30% mol ePC (i.e. eSM:ePC:ePE:Chol 38:24:19:19 mol ratio) or a lipid mixture mimicking the mitochondrial outer membrane (MOM) (ePC:ePE:PI:DOPS:CL, 46:25:11:10:8 w/w) (Figure 5.7). In neither case was there a measurable efflux.

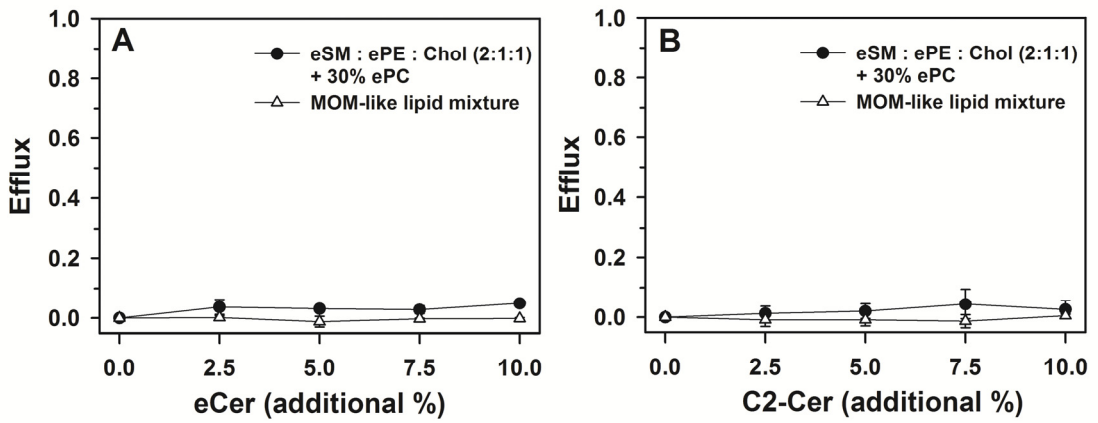

Figure 5.7. Calcein leakage induced by external addition of (A) egg ceramide or (B) C_2-ceramide to LUV composed of either eSM:ePE:Chol (2:1:1) + 30% ePC (i.e. eSM:ePC:ePE:Chol 38:24:19:19 mol ratio) or a MOM-like lipid mixture (ePC:ePE:PI:DOPS:CL, 46:25:11:10:8 w/w) after 6 h incubation at 37 ºC. Average values from three separate experiments ± SD are shown.

These results were confirmed by using a permeabilization assay with giant unilamellar vesicles and confocal microscopy. Ceramide was externally added to GUV composed of either eSM:ePE:Chol (2:1:1) + 30% ePC or the MOM-like lipid mixture and the permeabilization degree of the vesicles was measured as a function of incubation time (Figure 5.8). As observed with LUV, no significant permeabilization was detected, regardless of the ceramide or bilayer composition used. GUV of eSM:ePE:Chol (2:1:1) composition could not be used for this assay due to their high spontaneous permeability.

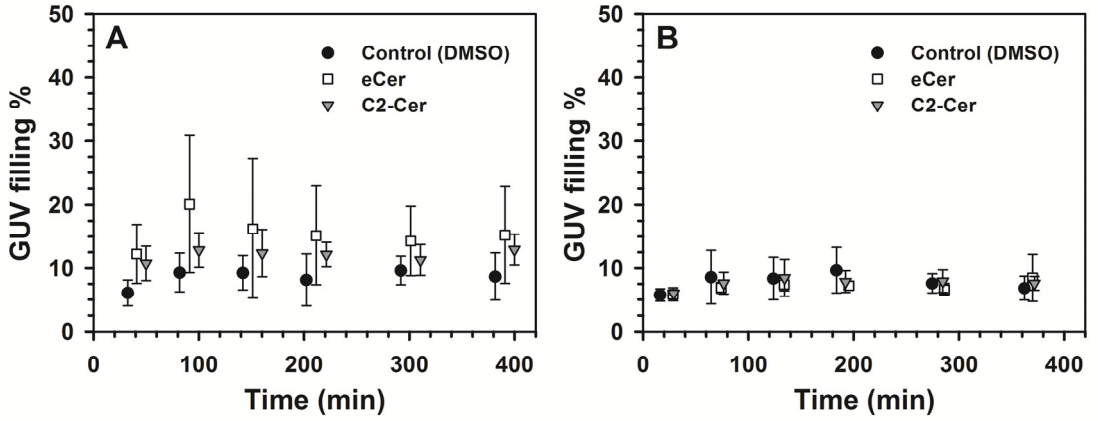

Figure 5.8. GUV permeabilization induced by external addition of 1 μM ceramide (approximately 10 mol% of final lipid concentration) to GUV composed of (A) eSM:ePE:Chol (2:1:1) + 30% ePC (i.e. eSM:ePC:ePE:Chol 38:24:19:19 mol ratio) or (B) the MOM-like lipid mixture (ePC:ePE:PI:DOPS:CL, 46:25:11:10:8 w/w) at 37 ºC. Average values from at least three separate experiments ± SD are shown.

5.4 Discussion

Time-resolved analysis of calcein leakage has been used as a tool to determine the mechanism behind ceramide-induced membrane permeabilization. *In situ* ceramide generation by SMase clearly showed a gradual leakage, characterized by the long τ_E values at high efflux (Table 5.1, Figure 5.3, Figure 5.4). Moreover, when external egg ceramide was used, the results again were very close to those expected for an ideal gradual mechanism (Figure 5.5). These findings clearly speak against the presence of large and stable channels in the membrane (Colombini, 2016), which could only cause all-or-none leakage.

Note that the results obtained in the SMase experiments under conditions of low efflux agreed better with an all-or-none mechanism (Figure 5.3, Figure 5.4). When considering the whole time range of the reaction this suggests a mixed leakage mechanism taking place (Figure 5.4): some vesicles would burst or release all their contents at once, thereby increasing the measured efflux but not the τ_E, while the rest would release their contents gradually. However, these all-or-none observations can hardly be attributed to channel formation since, if channels were formed at low ceramide concentrations in the vesicles, it would be difficult to explain that at higher ceramide concentrations (longer times of enzyme activity) channels would disassemble and graded release would occur. A simpler explanation would be that, due to vesicle heterogeneity, some more sensitive vesicles would break down at the beginning of the reaction, following the mechanism described for red blood cells enriched in ceramide (Montes *et al.*, 2008).

Another interesting result is that C2 ceramide did not elicit any vesicle permeabilization in our system (Figure 5.5A), as seen previously (Montes *et al.*, 2002). This ceramide, which has clearly different biophysical properties than the more physiological long-chain ceramides (Sot *et al.*, 2005a; Sot *et al.*, 2005b), has been extensively used in the studies proposing the ceramide channel hypothesis (Anishkin *et al.*, 2006; Siskind and Colombini, 2000; Siskind *et al.*, 2003; Siskind *et al.*, 2002, 2006). Since C2 ceramide cannot elicit any membrane permeabilization in our system, it seems dubious that it forms membrane channels as claimed in the above publications.

The discordance between the results from this work and those by Siskind, Colombini and coworkers may arise from the different techniques used. The ceramide channel hypothesis lies primarily on electrophysiology observations on planar membranes (Siskind and Colombini, 2000; Siskind et al., 2003), while our results come from solute release experiments with fluorescent dyes using large unilamellar vesicles. Electrophysiology observations are much more sensitive than leakage experiments, which could explain why permeabilization is detected with the former method but not with the latter. However, this would not support the conclusion that ceramide channels are being formed in the lipid bilayer.

Differences in membrane composition could also be responsible for the discrepancies in the results. Indeed, one of the studies supporting the ceramide channel hypothesis failed to see any channel formation in erythrocyte plasma membranes, concluding that ceramide channels are specific to mitochondrial membranes, probably due to differences in membrane composition (Siskind *et al.*, 2006). Our SM- and Chol-rich membranes can be regarded as more similar to plasma membranes than to mitochondrial ones, so the results with SM:PE:Chol (2:1:1) vesicles could go along with their suggestion that ceramide may behave differently in plasma membranes and only form ceramide channels in mitochondrial membranes. However, when we tested other membrane composition, both by adding 30% PC and even by using a lipid mixture mimicking the mitochondrial outer membrane, no significant permeabilization was detected with permeabilization experiments neither with LUV (Figure 5.7), nor with GUV (Figure 5.8).

Additionally, the studies in which ceramide channels were proposed primarily used asolectin, a raw lipid extract from soybean that cannot be considered as a good model of the mitochondrial membrane. This lipid mixture exhibits a high spontaneous permeability at 37 ºC, the temperature at which our experiments were conducted, so its usefulness in permeability studies may also be debatable (Montes et al., 2002). Another lipid present in the membranes of such studies is diphytanoylphosphatidylcholine (DPhPC), a phospholipid with branched acyl chains which shows clearly different biophysical properties than the commonly found linear-chain phospholipids, including a marked difference in permeability to non-electrolytes (Balleza *et al.*, 2014; Tristram-Nagle *et al.*, 2010). The use of these membranes may again not be adequate to support the conclusion of ceramide channel formation in mitochondria.

The ceramide channel hypothesis has also been supported by molecular dynamics simulations (Anishkin *et al.*, 2006). However, the simulations in this study only showed that, once formed, a ceramide channel could be kept stable within a bilayer. They did not show how such a structure could be formed, which is probably the main point of controversy, and the most critical one to be addressed.

Finally, an electron microscopy study claimed to have visualized the ceramide channels in liposomes (Samanta *et al.*, 2011). However, we believe that the results of the microscopy are not conclusive by themselves. The staining method that was used can only give accurate information of the surface, so the dark circles seen could be deep invaginations of the membrane caused by ceramide. They could also be artifacts produced by the treatment with osmium tetroxide and uranyl acetate affecting the vesicles differently depending on the presence or absence of ceramide. Cryomicroscopy should be a more suitable technique since the vesicles maintain their spherical shape instead of being deformed because of dehydration and no staining is needed. Additionally, the lipid concentration and therefore the lipid/ceramide ratio of vesicles observed by electron microscopy is nowhere stated on the publication, preventing reproduction of those experiments. Interestingly, the time range for ceramide channel growth shown on Figure 7A of the aforementioned article is nearly as long as the duration of our SMase reactions at low concentration. This suggests that the all-or-none behavior seen for low efflux values on such experiments (Figure 5.4B) should not correspond with the presence of ceramide channels.

Chapter 6:

EFFECTS OF CERAMIDE ON MEMBRANE INTEGRITY

Chapter 6: EFFECTS OF CERAMIDE ON MEMBRANE INTEGRITY.

6.1 Introduction

The main function of cell membranes is to act as a semipermeable barrier that separates two compartments from each other while allowing selective exchange of substances between them. However, membranes can loss their integrity due to several factors. Exposition to physical factors such as ultrasounds or electric fields, for example, can induce pore formation in the lipid bilayer (Kotnik *et al.*, 2015). Membrane poration can also be induced by several proteins and peptides (Gilbert, 2016). Additionally, some bioactive lipids such as sphingosine and ceramide have been shown to disrupt the permeability barrier of the lipid bilayer (Jimenez-Rojo *et al.*, 2014c; Ruiz-Arguello *et al.*, 1996).

Ceramide is an important bioactive lipid involved as a second messenger in several cellular processes such as stress responses (Carreira *et al.*, 2015; Gomez-Munoz *et al.*, 2016; Hannun and Obeid, 2008). This sphingolipid has the ability to markedly alter the biophysical properties of the lipid bilayer, which may be the underlying mechanism for its cellular action (Castro *et al.*, 2014; Goni *et al.*, 2014). For instance, ceramide has been shown to induce membrane permeabilization (Montes *et al.*, 2002; Ruiz-Arguello *et al.*, 1996; Siskind and Colombini, 2000), which could be directly related to the ability of ceramide to induce permeabilization of mitochondria to cytochrome c (Di Paola *et al.*, 2000). The mechanism behind this ceramide-induced permeabilization is still under debate, though. The work described in chapter 5 attempts to shed some light on this issue. However, many questions are yet to be answered.

The ceramide channel hypothesis proposes that ceramide molecules can interact with each other to form highly organized channels permeating the membrane (Colombini, 2013). However, the formation of such structure would require a huge amount of energy, especially when the geometry of ceramide and its tendency to induce negative curvature in the lipid bilayer is taken into account. Determination of the mechanical properties of ceramide could therefore be useful to assess the energy barrier that ceramide channel formation would need to overcome.

An interesting property of lipid bilayers in relation to membrane poration is the edge tension. This value describes the energy penalty of the lipid reorganization occurring at the edge of a transient pore in order to avoid exposure of the hydrophobic acyl chains to water (Boal, 2002). Therefore, the effect of ceramide on the edge tension may provide further insight into the ability of this lipid to disrupt membrane integrity.

Additionally, it is well known that the biophysical properties of ceramide depend highly on its structure. For instance, ceramides have been shown to display different behavior depending on the length and unsaturation degree of both their sphingoid base (Fabrias *et al.*, 2012; Maula *et al.*, 2012) and their acyl chain (Chiantia *et al.*, 2007; Jimenez-Rojo *et al.*, 2014a; Megha *et al.*, 2007; Pinto *et al.*, 2011; Sot *et al.*, 2005a; Sot *et al.*, 2005b). Quite recently a novel category of bioactive sphingolipids was described to be synthesized in mammalian cells and animals (Zitomer *et al.*, 2009), sphingoid bases without the 1-hydroxy group giving rise to 1-deoxyceramides (Figure 6.1), which show interesting biophysical properties (Jimenez-Rojo *et al.*, 2014b).

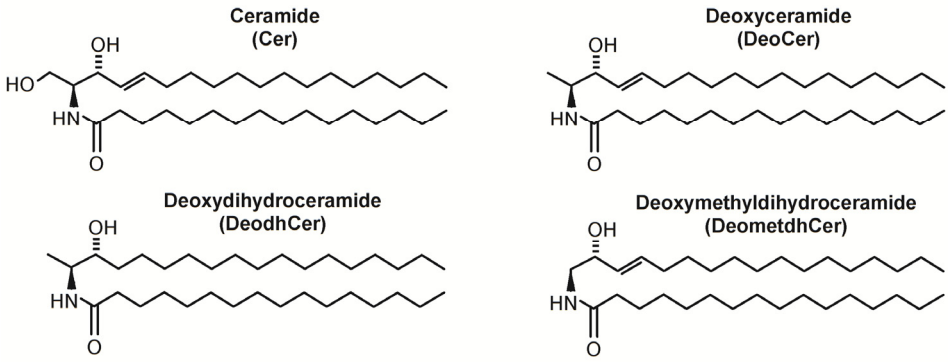

Figure 6.1. Structure of the ceramides studied in this work.

In this chapter we intend to further assess the effect of ceramide on membrane integrity and permeabilization using two different approaches. Edge tension measurements of ceramide-containing giant vesicles were carried out using an electroporation assay. The results showed no effect of ceramide on the edge tension; however, the experimental setup allowed only a small amount of ceramide to be present in the liposomes. Additionally, the ability of different acyl chain length ceramides and deoxyceramides to permeabilize membranes was studied using an ANTS/DPX leakage assay. The results showed little effect of the acyl chain length, but a significant decrease in the membrane permeabilization was observed for all the deoxyceramides.

6.2 Materials and Methods

Materials

Palmitoyloleoylphosphatidylcholine (POPC), dipalmitoylglycerol (DPG), egg sphingomyelin (eSM), egg phosphatidylethanolamine (ePE), cholesterol (Chol), and all the different ceramides and deoxyceramides were from Avanti Polar Lipids (Alabaster, AL). 8-aminonaphtalene-1,3,6-trisulfonic acid (ANTS), and *p*-xylene-bis-pyridinium bromide (DPX) were supplied by Molecular Probes (Eugene, OR). PD-10 desalting columns were from GE Healthcare (Little Chalfont, UK).

GUV preparation

GUV for electroporation experiments were prepared using the electroformation procedure as previously described (Portet and Dimova, 2010). Stocks of the lipid mixtures under study were prepared from pure lipid stocks to a final concentration of 4 mM in chloroform. 10 µl of the desired stock solution were deposited on the conducting sides of glass slides coated with indium tin oxide (ITO), which were then kept under high vacuum for 30 minutes at 55 ºC in order to remove any residual solvent. The ITO-glasses were then assembled into a chamber, spaced by a 2 mm-thick PTFE frame, and equilibrated at 55 ºC. The chamber was filled with a sucrose solution (240 mM sucrose, 1 mM HEPES, pH 7) previously equilibrated at the same temperature as the chamber. The ITO-glasses were then connected to a generator via copper stripes and a sinusoidal voltage of 25 mV peak-to-peak was applied at 10 Hz. The voltage was increased in 100 mV steps every 5 min until a value of 1225 mV was reached. After 2 h, the frequency was decreased to 5 Hz for 30 min so the vesicles detached from the glasses.

Electroporation

Electroporation was performed using a homemade chamber constructed from a glass coverslip (Figure 2.13). Two parallel copper strips were stuck on the glass coverslip 0.5 cm apart and heated parafilm was used to create a cavity between the copper strips. This cavity was filled with 72 µl glucose buffer (255 mM glucose, 1 mM HEPES, 1 mM NaCl, pH 7) and 8 µl GUV solution. The osmolarity of the glucose buffer was previously adjusted to that of the GUV solution. Finally, a smaller cover glass was placed on top of the chamber.

The chamber was mounted under an inverted microscope (Axiovert 135, Zeiss, Göttingen, Germany) equipped with a 20 x Ph2 objective and connected to a βtech pulse generator GHT-Bi500 (βtech, l'Union, France). Electric pulses of 5 ms duration and 50-70 kV/m amplitude were applied directly under the microscope while phase-contrast images of vesicles were collected at an acquisition speed of 5000 frames/s (fps) with a fast digital camera (HG-100K, Redlake, San Diego, CA). Illumination during routine observations was performed with a halogen lamp, while a mercury lamp (HBOW/2) was used for image acquisition.

Image analysis

First, using Image J (National Institutes of Health, Bethesda, MD) the vesicle radii, *R*, were manually measured and the raw vesicle images were transformed into binary images with the membrane represented by the nonzero pixel. Then the pore radii, *r*, were determined via custom algorithms, as previously published (Portet and Dimova, 2010). $R^2 \ln(r)$ was plotted as a function of time *t*, and the linear region of the curve was fitted to an equation with an expression of the form $y = at + b$ (Portet and Dimova, 2010):

$$R^2 \ln(r) = -\frac{2\gamma}{3\pi\eta}t + C \qquad \text{[Eq. 6.1]}$$

where γ is the edge tension, η is the viscosity of the aqueous medium (1.133×10^{-3} Pa·s for the glucose solution) and *C* is a time-independent constant that varies for each experiment. The edge tension can thus be calculated from the slope of the linear fit, *a*, according to the relation $\gamma = -(3/2)\pi\eta a$. Equation 6.1 is solved assuming constant *R*, so in order to avoid effects caused by changes in vesicle radius, which usually happen before the linear stage of the curve (Portet and Dimova, 2010), *R* was measured at the end of this stage.

LUV preparation

Lipid vesicles for membrane permeability studies were prepared by mixing the desired lipids and evaporating the solvent under a stream of nitrogen. The resulting lipid film was then kept under high vacuum for 90 min in order to ensure complete removal of any residual solvent. The sample was hydrated in an ANTS- and DPX-containing buffer (HEPES 10 mM, ANTS 20 mM, DPX 70 mM, NaCl 30 mM, pH 7.4), followed

by vigorous vortex mixing. After hydration, large unilamellar vesicles (LUV) were prepared by subjecting the sample to 10 freeze/thaw cycles, followed by extrusion through 0.1-μm pore diameter polycarbonate filters. Unencapsulated ANTS and DPX were finally removed by gel filtration in a PD-10 desalting column containing Sephadex G-25 resin, eluting with an isosmotic ANTS- and DPX-free buffer. Vesicle size was checked by quasi-elastic light scattering using a Malvern Zeta-Sizer 4 spectrometer (Malvern Instruments, Worcestershire, UK). Lipid concentration was determined by phosphate analysis (Bartlett, 1959).

Aqueous content release assay

The ability of ceramides to induce membrane permeabilization was assayed using the ANTS/DPX system (Ellens *et al.*, 1985). 0.3 mM LUV entrapping both ANTS and DPX were incubated with 10 additional mol% ceramide or deoxyceramide (dissolved in DMSO) for 6 h at 37 ºC. ANTS fluorescence was monitored using a QuantaMaster 40 spectrofluorometer (Photon Technology International, Lawrenceville, NJ) (λ_{ex} = 355 nm, λ_{em} = 520 nm) under continuous stirring and at a temperature of 37 ºC. 100% efflux was determined after addition of 0.1% Triton-X-100 to the vesicles. In all experiments a negative control with only DMSO addition was also measured and used to correct for basal permeabilization.

6.3 Results

Edge tension measurements

In this study, the edge tension of vesicles of different composition was measured using the electroporation methodology described by Portet and Dimova (2010). A GUV solution was observed under phase-contrast microscopy while the vesicles were subjected to a single electric pulse that caused formation of a macropore. The process of pore formation and closure was then recorded using fast digital imaging (Figure 6.2A). Vesicle radii, R, and pore radii, r, were determined from the recorded images and pore dynamics was described in terms of the evolution of the porated zone, characterized as $R^2 \ln(r)$, as a function of time (Figure 6.2B). The edge tension of the vesicles could then be determined from the slope of the linear region of the curve as described in the Material and Methods section.

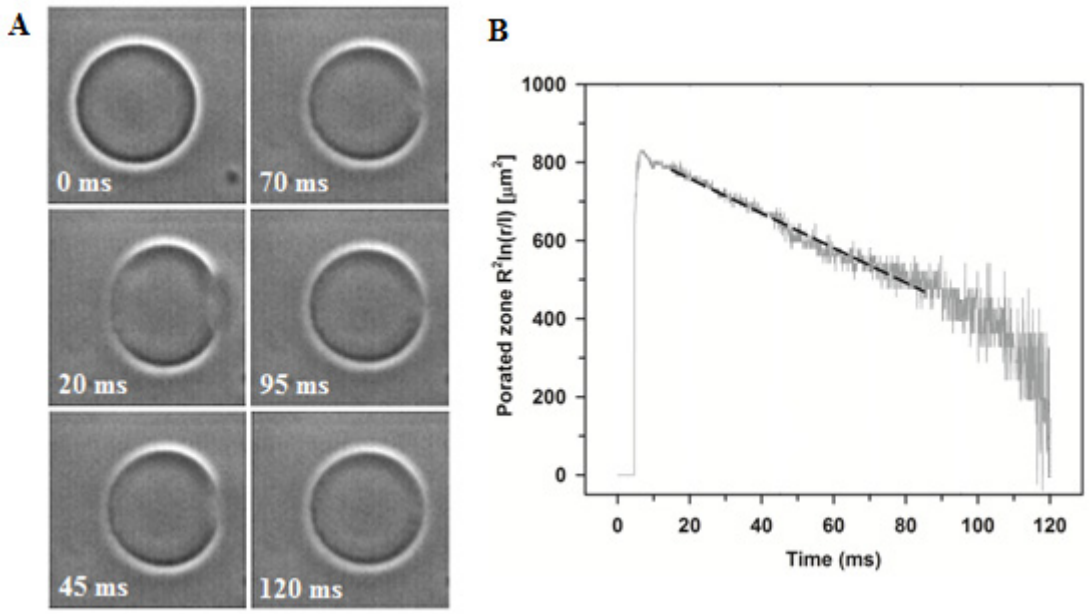

Figure 6.2. Imaging and analysis of a POPC vesicle with a radius of 18.3 µm subjected to an electric pulse of 5 ms duration and 60 kV/m amplitude (applied at time = 0). (A) Time sequence of raw images. (B) Evolution of the porated area as a function of time. l = 1 µm was introduced to avoid plotting a dimensional value in the logarithmic term. The solid line corresponds to the experimental data and the dashed line corresponds to the linear fit.

Table 6.1 and Figure 6.3 show the edge tension values determined for pure DOPC and POPC liposomes, as well as for POPC liposomes containing either egg ceramide (eCer) or dipalmitoylglycerol (DPG). Pure DOPC and POPC bilayers showed similar edge tension values: 35.7 pN and 33.3 pN respectively (Table 6.1, Figure 6.3). POPC liposomes with up to 3 mol% egg ceramide were then studied, but the presence of eCer did not elicit any change in the measured edge tension (Table 6.1, Figure 6.3). Finally, POPC liposomes with 10 mol% DPG, the glycerophospholipid analogue of palmitoylceramide (the main lipid species of eCer), were analyzed. Again, no change in the edge tension could be observed (Table 6.1, Figure 6.3).

Table 6.1. Edge tension values for GUV of different membrane composition. Averages ± SE are shown.

Bilayer composition	Edge tension (pN)	n (vesicle number)
DOPC	35.7 ± 3.0	29
POPC	33.3 ± 1.3	61
POPC:eCer (99:1)	33.2 ± 1.4	40
POPC:eCer (98:2)	33.9 ± 1.4	56
POPC:eCer (97:3)	33.8 ± 1.7	19
POPC:DPG (90:10)	34.1 ± 1.8	12

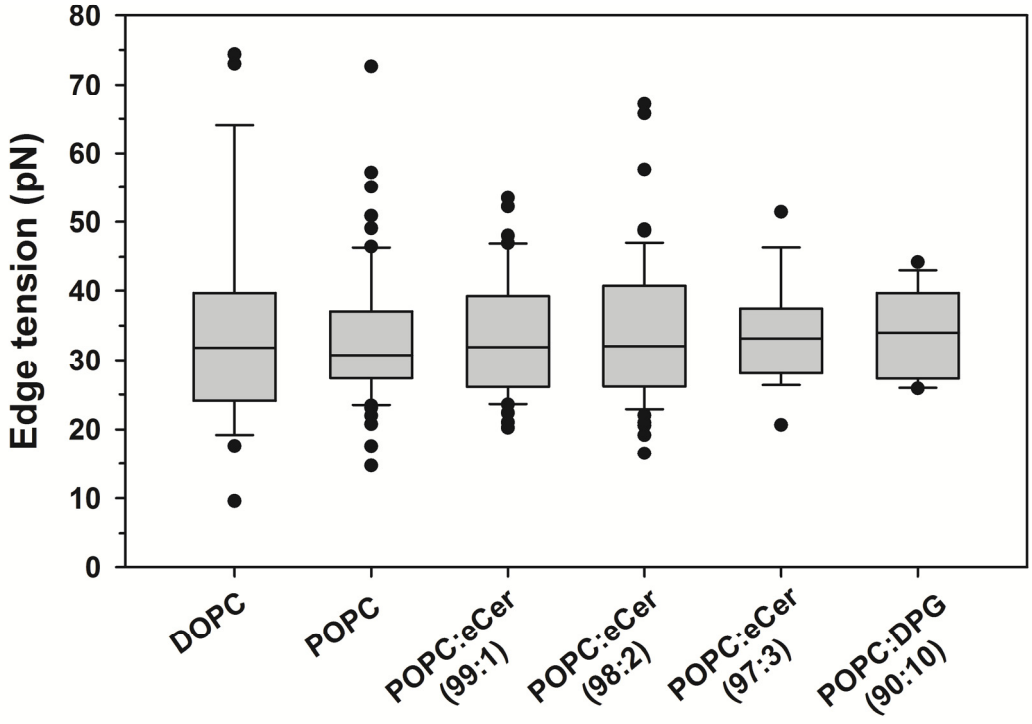

Figure 6.3. Box plot of experimental edge tension values for GUV of different membrane composition. Whiskers correspond to the 10th and 90th percentiles, and circles correspond to outlier values.

Ceramide-induced permeabilization

Next, the ability of different acyl chain ceramides and deoxyceramides to permeabilize lipid bilayers was assessed using the ANTS/DPX aqueous content release assay in eSM:ePE:Chol (2:1:1 by mol) vesicles. Figure 6.4 shows the content efflux induced by external addition of 10 mol% C16 ceramide and C16 deoxymethyldihydroceramide as a function of time. C16-Cer caused a slow release of aqueous contents (Montes *et al.*, 2002), reaching after 6h an efflux value around 20% (Figure 6.4), similar to the value obtained in chapter 5 for 10 mol% egg ceramide addition with the calcein release assay in the absence of cations (Figure 5.6A). C16-DeometdhCer, on the contrary, hardly elicited any efflux (Figure 6.4).

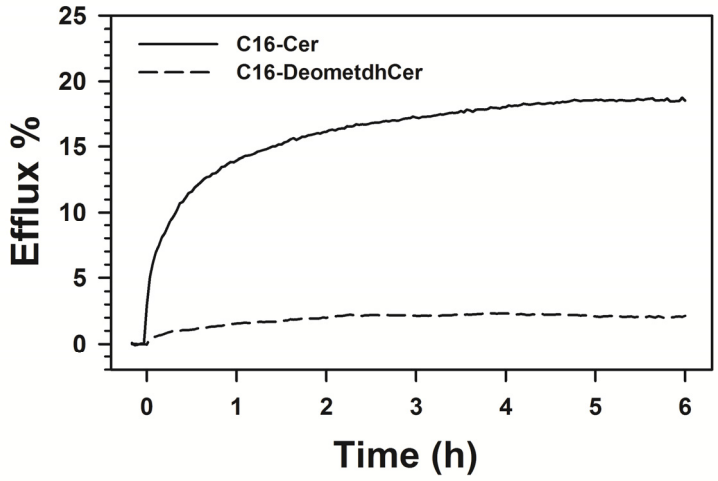

Figure 6.4. Time course of content efflux induced by external addition of 10 mol% C16-Cer (solid line) and C16-DeometdhCer (dashed line) to eSM:ePE:Chol (2:1:1) LUV at 37 ºC. The curves were corrected using a sample to which only DMSO was added as a baseline.

Figure 6.5 summarizes the permeabilization results obtained for ceramides and deoxyceramides of C16:0, C24:1 and C12:0 acyl chain after 6 h incubation. All the deoxyceramides showed a marked decrease in their permeabilization ability as compared to the corresponding ceramides (Figure 6.5), suggesting an important role for the polar headgroup of these sphingolipids in their ability to induce membrane permeabilization. The acyl chain, on the contrary, seemed not to significantly affect the ceramide-induced permeabilization (Figure 6.5).

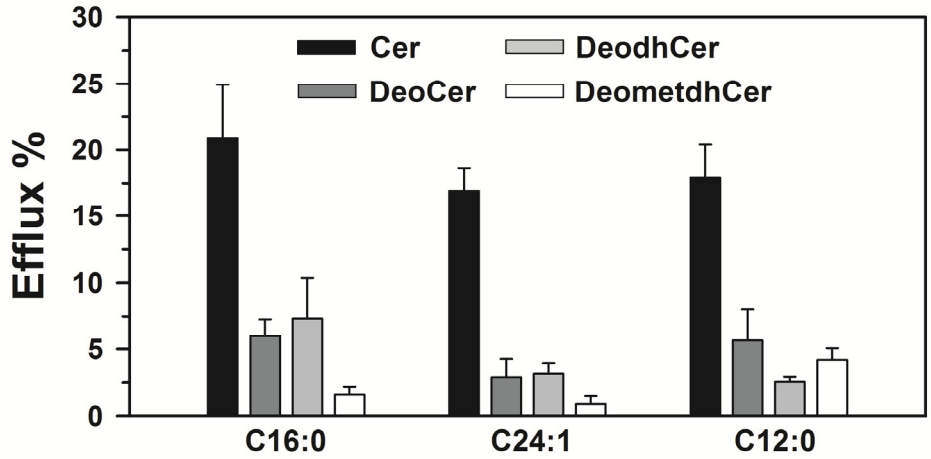

Figure 6.5. Vesicle content efflux induced by external addition of 10 mol% of different acyl chain ceramides and deoxyceramides to eSM:ePE:Chol (2:1:1) LUV after 6h incubation at 37 ºC. The values were corrected using a sample where only DMSO was added as a control of basal efflux.

6.4 Discussion

Edge tension studies

Maintaining membrane integrity is crucial for a correct cell function. However, several factors can perturb the membrane and even induce formation of pores. Electrical fields, ultrasounds and toxins are some examples of such pore-forming factors. When a pore is formed the hydrophobic core of the membrane is exposed to water, thus the lipids will reorganize in order to shield their acyl chains from unfavorable interaction with water molecules. The energy penalty for this process is described by the edge tension value (Boal, 2002). The edge tension value of a lipid bilayer depends on its composition (Portet and Dimova, 2010), the geometry and properties of different lipids penalizing or favoring lipid rearrangement at the pore edge, thus determining the stability of the pores and the ability of the membrane to reseal after pore formation. These data may be important in studies on membrane permeabilization.

Ceramide is a membrane-permeabilizing lipid molecule with a cone geometry that facilitates non-lamellar phase formation in lipid bilayers . It has also been proposed that this lipid could organize into stable channels that porate the lipid bilayer (Colombini, 2013). Thus, ceramide would be expected to have a big impact on the edge tension of membranes. However, no effect was seen on POPC bilayers up to a 3 mol% (Table 6.1, Figure 6.3). This unexpected lack of effect may be a result of the low ceramide amount used in the experiment, since the methodology used in this work did not allow for higher ceramide concentration as the bilayers are required to be completely fluid (Knorr *et al.*, 2010) and over 4 mol% ceramide already induces gel-like domains (Castro *et al.*, 2007). With 10 mol% DPG, a glycerophospholipid analogue of ceramide, the edge tension still remained unaltered (Table 6.1, Figure 6.3).

Portet and Dimova showed significant effects of both cholesterol and PE on the edge tension of DOPC bilayers (Portet and Dimova, 2010). However, the amount of these lipids in the aforementioned study was at least five times the one used in this work for ceramide. Therefore, the absence of a noticeable effect for ceramide shown in this work may be due to the methodology not being sensitive enough to work with such low lipid amounts.

Additionally, the edge tension values obtained here for DOPC and POPC, 35.7 and 33.3 pN respectively, significantly differ from those published by Portet and Dimova for DOPC and egg PC, 27.7 and 14.2 pN respectively (Portet and Dimova, 2010). This fact, together with the high variability observed for the edge tension values (Figure 6.3) may indicate that the methodology here employed had not been sufficiently optimized, thus raising doubts about the validity of the results.

Interestingly, Portet and Dimova showed that cholesterol and PE, both of them lipids with similar cone geometry, had contrary effects on the edge tension value of DOPC bilayers: cholesterol increased the edge tension, while PE reduced it (Portet and Dimova, 2010). This suggests that the geometry of a lipid alone cannot explain the effect of that lipid on the edge tension, so its properties and interactions with the rest of the bilayer lipids should also be considered. Thus, the lack of effect observed for ceramide and DPG should not be too readily discarded as an experimental artifact.

Permeability measurements

The structure of ceramide is probably of high importance for its function (Goni *et al.*, 2014). Indeed, the lack of the sphingosine double bond has been shown to alter the ceramide behavior (Fabrias *et al.*, 2012), including changes in its membrane permeabilization ability (Hernandez-Tiedra *et al.*, 2016; Siskind and Colombini, 2000). A recent study showed how a novel category of ceramides, 1-deoxyceramides, exhibited highly different biophysical properties than their canonical ceramide counterparts (Jimenez-Rojo *et al.*, 2014b). In this chapter we further confirm that observation showing that all the deoxyceramides studied here present almost no permeabilization effect, in contrast to ceramides (Figure 6.5).

The main structural difference of deoxyceramides is that they lack the hydroxyl group that constitutes the small polar headgroup of canonical ceramides (Figure 6.1). Therefore, deoxyceramides become even more hydrophobic and less amphipathic than ceramides. This should have several implications, from a lower miscibility with bilayer lipids to possible alterations in the orientation of the molecule in the bilayer, probably being more deeply buried in the hydrophobic core. The lack of hydroxyl group can also reduce the ability of ceramide to interact with other lipids via hydrogen bonding (Garcia-Arribas *et al.*, 2016; Slotte, 2016).

Since the mechanism of ceramide-induced membrane permeabilization is still poorly understood, the lack of permeabilization effect of deoxyceramides cannot be readily explained yet. For instance, the lower miscibility and (probably) higher tendency to laterally segregate of deoxyceramides could be expected to result in an increased permeabilization via defects between domain interfaces. However, the high hydrophobicity of these lipids could well result in their aggregation and lack of inclusion into the lipid bilayer. The low amphipathicity could also result in these lipids positioning themselves far from the interface of the bilayer, thus not affecting membrane curvature as much as ceramides.

As it was shown by Jimenez-Rojo and coworkers, deoxyceramides present unique biophysical properties that often do not follow recognizable patterns and can be difficult to explain (Jimenez-Rojo *et al.*, 2014b). In this chapter it has been shown that deoxyceramides present a reduced ability to permeabilize lipid membranes. However, we cannot give a solid explanation for that behavior yet. Further studies on the mechanism of ceramide-induced membrane permeabilization and on the biophysical properties of deoxyceramides will be needed in order to fill the missing gaps and further understand the precise effect of ceramide structure on its behavior and function.

Chapter 7:

OVERVIEW AND CONCLUSIONS

Capítulo 7:

RESUMEN Y CONCLUSIONES

Chapter 7: OVERVIEW AND CONCLUSIONS

The present thesis was devoted to the study of the biophysical properties of ceramide, a bioactive sphingolipid with a relevant role in several cellular processes. The work has been carried out employing lipid vesicles as model membranes and using a variety of biophysical techniques, principally fluorescence spectroscopy and microscopy, in three main areas of research:

- The suitability of pentaene ceramide analogues as fluorescent membrane probes.
- The effect of ceramide and cholesterol incorporation on saturated phospholipid membranes.
- The effect of ceramides on membrane integrity and the ceramide-induced membrane permeabilization mechanism.

7.1 Pentaene ceramide analogues as fluorescent membrane probes

Membrane biophysical studies of ceramides have commonly benefited from the use of fluorescence techniques, both spectroscopy and microscopy. These techniques are versatile, sensitive and powerful, but they require suitable fluorescent probes. Membrane probes are supposed to mimic the behavior of natural lipids. Hydrophobic molecules such as DPH or DiI and fluorescently labeled lipids such as Rhodamine-PE or NBD-ceramide are commonly used in membrane studies. However, most of these membrane probes show noticeably different structures and/or properties as compared to the natural lipids.

Polyene lipids, lipids with several conjugated double bonds in their acyl chains, represent a fluorescent system that is rather similar to natural lipids. Chapter 3 intends to assess the suitability of several pentaene ceramide analogues as useful membrane probes in biophysical studies. The probes studied were: a GABA-derived pentaene probe with a structure resembling that of ceramide (Pentaene I), two similar GABA-pentaene probes containing a doxyl radical in their acyl chain at positions 5 or 16 (Penta5dox and Penta16dox) and a pentaenic ceramide (Pentaene Cer).

First, the quantum yields of the GABA-pentaenes were analyzed, examining their excitation and emission spectra in different solvents, in lipid vesicles of different composition and at different concentrations. Interestingly, the recovered spectra on lipid vesicles of different composition showed that the quenching effect of the doxyl group of Penta5dox and Penta16dox on the pentaene fluorescence emission is highly dependent on the fluidity of the lipid bilayer, a behavior consistent with the degree of packing of the bilayer influencing the proximity of the doxyl radical to the polyene system and thus the extent of fluorescence quenching. Penta16dox fluorescence was shown to be able to even detect the gel-fluid transition of DPPC bilayers.

Confocal microscopy was used to examine the behavior of the GABA-pentaenes on giant vesicles with lateral domain segregation. Most membrane fluorophores favorably partition into the most fluid domains; Pentaene I, on the contrary, preferentially stains liquid-ordered and gel domains over liquid-disordered and fluid ones. This fluorescent probe could even partition into ceramide-rich domains, which almost no other fluorescent probe can. Due to this behavior Pentaene I seems a particularly useful membrane probe in studies on gel microdomains in cell membranes.

The main limitation of GABA-pentaene fluorophores is that their structure, although similar to that of natural ceramides, still differs noticeably. However, when the pentaenic ceramide was studied, it also showed a different behavior as compared to natural ceramide. Therefore, the pentaene moiety alone seems to be able to disrupt the natural lipid properties. Nevertheless, although displaying a different behavior than ceramide, the pentaene ceramide analogues described in this work have been shown to be useful probes in membrane biophysical studies using fluorescence techniques.

7.2 Ceramide and cholesterol in saturated phospholipid membranes

Ceramide levels in a resting cell are very low, but can be rapidly increased upon specific signals. One of the pathways for this fast ceramide production is the hydrolysis of sphingomyelin. Ceramide has been shown to interact with sphingomyelin and induce lateral segregation of highly ordered rigid domains. However, sphingomyelin can also interact with cholesterol, which is highly present in plasma membranes, inducing the formation of liquid-ordered domains. Therefore, sphingomyelinase activity would give rise to platforms enriched in sphingomyelin, cholesterol and ceramide.

Initially, several studies showed that ceramide can displace cholesterol from its interaction with sphingomyelin. However, cholesterol was also shown to be able to modulate ceramide-rich domain formation. Recently, it has been suggested that ceramide and cholesterol may interact with each other in a saturated phospholipid bilayer without a disordered phase to form a homogeneous ternary phase with unique properties. Chapter 4 intends to confirm this observation and to further characterize the effect of ceramide and cholesterol incorporation on pSM or DPPC bilayers, using tPA time-resolved fluorescence and DPH anisotropy to study membrane order and the thermostability of the ordered bilayers.

The results obtained from the fluorescence spectroscopy techniques fully agree with previous studies supporting the formation of a homogeneous gel ternary phase. This phase displays unique properties with both ceramide and cholesterol probably contributing to its characteristics: it shows a high molecular order and thermostability, possibly due to the ordering effect of ceramide; yet no clear phase transition is observed and the ternary phase does not seem to become completely disordered even at high temperatures, probably due to the effect of cholesterol.

Additionally, DSC experiments were carried out with decreasing proportions of cholesterol and ceramide in the bilayer in order to determine the role that their combined amount in the bilayer and their ratio may have in their interaction. The results showed that their interaction depends mainly on the cholesterol bilayer concentration, rather than on the ratio between both lipids.

7.3 The ceramide-induced membrane permeabilization mechanism

An important property of ceramides, which could be related to their biological function in the cellular stress response, is their ability to induce membrane permeabilization. The mechanism behind the process is still not well understood though. Our hypothesis proposes that membrane permeabilization occurs due to bilayer restructuring and destabilization induced by ceramide, as well as to the packing defects formed at the boundaries of ceramide-enriched domains. However, studies by Siskind, Colombini and coworkers propose that ceramide-induced membrane permeabilization occurs through the formation of large, structured and stable ceramide-channels which would induce apoptosis by direct permeabilization of the mitochondria to cytochrome c.

Chapter 5 tries to shed some light into this topic, using an improved membrane leakage assay based on time-resolved fluorescence of calcein that allows determination of the leakage mechanism. When assaying membrane permeabilization through leakage assays on liposomes, partial efflux could result from either only some vesicles releasing all their contents (all-or-none leakage) or from all the vesicles releasing part of their contents (graded leakage). The presence of ceramide channels in the liposomes would undoubtedly cause an all-or-none leakage, while a graded leakage would be more consistent with the view of permeabilization due to destabilization of membranes by ceramide-induced lateral domain segregation, or localized phenomena of non-lamellar phase formation.

First, using sphingomyelin- and cholesterol-rich liposomes, *in situ* ceramide generation by action of sphingomyelinase was shown to cause a fast aqueous content release with a mixed leakage mechanism. This was probably due to the leakage being primarily graded but with some more sensitive vesicles breaking down at the beginning of the reaction, following a mechanism already described for red blood cells enriched in ceramide. Moreover, membrane permeabilization by external addition of egg ceramide showed a clear gradual leakage mechanism taking place. These results speak against the presence of large and stable channels in the membrane which could only cause an all-or-none leakage.

Interestingly, a short-chain ceramide which has been extensively used in several studies proposing the ceramide channel hypothesis, C2 ceramide, did not elicit any vesicle permeabilization in our system. Therefore, it seems dubious that this ceramide, which has clearly different biophysical properties than the more physiological long-chain ceramides, can form membrane channels as claimed in those studies.

The ceramide channel hypothesis proposes these channels to be specific of the mitochondrial outer membrane, and the sphingomyelin- and cholesterol-rich liposomes can be regarded as more similar to plasma membranes than to mitochondrial ones, so experiments changing the membrane composition by adding 30% PC or even using a lipid mixture mimicking the mitochondrial outer membrane were carried out. However, no significant permeabilization was seen neither with leakage experiments in LUV, nor with GUV permeabilization experiments. Again, these results speak against the formation of channels in the membrane.

The discordance between the results obtained from this work and those obtained by Siskind, Colombini and coworkers may arise from the different techniques used. Differences in the membrane composition may also been important, especially since the studies that propose the formation of ceramide channel use membranes that may not be considered adequate due to their low biological relevance and high spontaneous permeability. Furthermore, studies supporting the ceramide channel hypothesis by molecular dynamics simulations and electron microscopy may be considered not conclusive.

7.4 Effects of ceramide on membrane integrity

The main function of cell membranes is to act as a semipermeable barrier that separates two compartments. However, membranes can loss their integrity due to several factors, including some bioactive lipids such as ceramide. Chapter 5 has allowed gaining further insight on the ceramide-induced membrane permeabilization mechanism. However, many questions are yet to be answered. Therefore, chapter 6 describes further studies on the ability of ceramide to affect membrane integrity.

First, the effect of ceramide on the bilayer edge tension was explored. This is a mechanical property of the lipid bilayer that describes the energy penalty for the lipid reorganization that takes places upon the formation of a pore, when the lipids on the pore edge have to shield their hydrophobic acyl chains from unfavorable interactions with water. Therefore, the edge tension determines the ability of the membrane to reseal after loss of its integrity and can be highly informative in studies dealing with membrane permeabilization. In the case of ceramide, it may be especially interesting taking into account the hypothesis of ceramide channel formation. Due to the cone geometry and the unique biophysical properties of the ceramide, this lipid should be expected to significantly alter the membrane edge tension. However, no effect was observed on the edge tension of POPC bilayers with up to 3 mol% ceramide or 10 mol% DPG (a glycerophospholipid analogue of ceramide). This lack of effect could be due to the low amount of ceramide present in the bilayer, limited by the experimental setup. However, it is important to take into account that the relationship between the lipid properties and its effect on the edge tension are not easy to predict.

In a separate series of studies, the membrane-permeabilizing ability of a recently described novel ceramide species, 1-deoxyceramides, was studied using different acyl chain ceramides and deoxyceramides. While little differences were observed for different acyl chains, deoxyceramides induced a significantly lower permeability than their canonical counterpart ceramides. Therefore, the hydroxyl group that constitutes the polar head of ceramide seems to be a highly important structural feature for the ceramide ability to permeabilize membranes.

7.5 Conclusions

The main conclusions of this work include:

1) Pentaene lipids can be useful probes in membrane biophysical studies using fluorescence spectroscopy and microscopy.

2) Ternary mixtures including a saturated phospholipid (pSM or DPPC), cholesterol (Chol) and palmitoylceramide (pCer) show a single homogenous ordered phase displaying intermediate properties between Chol-enriched liquid-ordered and the pCer-enriched gel-like bilayers.

3) In the above ternary mixtures, the ability of Chol to restrict pCer interaction with pSM and pCer-enriched domain segregation depends more strongly on the overall cholesterol content of the bilayer rather than on the Chol/pCer ratio.

4) Cer-induced leakage in SM- and Chol-rich liposomes follows primarily a graded leakage mechanism, while no leakage is induced by ceramide in lipid bilayers with low amounts of those two lipids, or in bilayers that mimic the composition of the mitochondrial outer membrane. Under our condition ceramide does not appear to form channels across the bilayer.

Capítulo 7: RESUMEN Y CONCLUSIONES

La presente tesis se ha centrado en el estudio de las propiedades biofísicas de la ceramida, un esfingolípido bioactivo que muestra un rol relevante en varios procesos celulares. El trabajo se ha llevado a cabo empleando vesículas lipídicas como membranas modelo y valiéndose de diversas técnicas biofísicas, principalmente espectroscopía y microscopía de fluorescencia, en tres áreas principales:

- La idoneidad de análogos pentaénicos de ceramida como sondas fluorescentes de membrana.

- El efecto de la incorporación de ceramida y colesterol en membranas de fosfolípidos saturados.

- El efecto de las ceramidas en la integridad de la membrana y el mecanismo de permeabilización de membranas inducido por ceramida.

7.1 Análogos pentaénicos de ceramida como sondas fluorescentes de membrana.

Los estudios de biofísica de membranas sobre la ceramida se han beneficiado frecuentemente del uso de técnicas de fluorescencia, tanto espectroscópicas como microscópicas. Estas técnicas son versátiles, sensibles y potentes, pero requieren de sondas fluorescentes adecuadas. Las sondas de membrana deberían imitar el comportamiento de los lípidos naturales. Moléculas hidrofóbicas como el DPH o el DiI y lípidos marcados fluorescentemente como la Rodamina-PE o la NBD-ceramida son comúnmente usados en estudios de membrana. Sin embargo, la mayoría de estas sondas de membrana presentan estructuras y/o propiedades notoriamente diferentes a las de los lípidos naturales.

Los lípidos poliénicos, lípidos con varios enlaces dobles conjugados en sus cadenas acílicas, representan un sistema fluorescente bastante similar a los lípidos naturales. El Capítulo 3 trata de evaluar la idoneidad de varios análogos pentaénicos de la ceramida como sondas de membrana útiles para estudios biofísicos.

Las sondas estudiadas fueron: una sonda pentaénica derivada del GABA con una estructura parecida a la de la ceramida (Pentaene I), dos sondas GABA-pentaenos con un radical doxilo en su cadena acílica en las posiciones 5 o 16 (Penta5dox y Penta16dox) y una ceramida pentaénica (Pentaene Cer).

Primero se analizaron los rendimientos cuánticos de los GABA-pentaenos, y luego se llevó a cabo el análisis de sus espectros de excitación y emisión en diferentes disolventes, en vesículas lipídicas de diferente composición y a diferentes concentraciones. Los espectros obtenidos en vesículas lipídicas de diferente composición demostraron que el efecto atenuador del grupo doxilo de las sondas Penta5dox y Penta16dox sobre la emisión fluorescente del pentaeno es altamente dependiente de la fluidez de la bicapa lipídica, un comportamiento consistente con que el grado de empaquetamiento de la bicapa influencie la proximidad del radical doxilo con el sistema polieno y de esta manera el grado de atenuación de la fluorescencia. Debido a esto, la fluorescencia de la sonda Penta16dox demostró la capacidad de detectar la transición gel-fluido de bicapas de DPPC.

A continuación se examinó el comportamiento de los GABA-pentaenos en vesículas gigantes con segregación lateral de dominios mediante microscopía confocal. La mayoría de fluoróforos particiona favorablemente en los dominios más fluidos; la sonda Pentaene I, por el contrario, marca preferencialmente los dominios líquido-ordenado y gel sobre los dominios líquido-desordenado y fluidos. Esta sonda fluorescente puede incluso entrar en dominios ricos en ceramida, algo que casi ninguna otra sonda puede hacer. Este comportamiento hace de Pentaene I una sonda particularmente útil en estudios de microdominios gel en membranas celulares.

La principal limitación de los GABA-pentaenos es que su estructura, aunque similar a la de las ceramidas naturales, posee diferencias importantes. Sin embargo, cuando se estudió una ceramida pentaénica, su comportamiento seguía difiriendo del observado para la ceramida natural. Por ello, el sistema pentaénico parece ser capaz por sí sólo de perturbar las propiedades de la ceramida. De todas maneras, aún presentando un comportamiento diferente a las ceramidas naturales, los análogos pentaénicos descritos en este trabajo han demostrado ser sondas de gran utilidad en estudios biofísicos que empleen técnicas de fluorescencia.

7.2 Ceramida y colesterol en membranas de fosfolípidos saturados

Los niveles de ceramida en la célula son muy bajos en condiciones de reposo, pero pueden verse rápidamente elevados por la acción de señales específicas. Una de las secuencias metabólicas encargadas de esta rápida producción de ceramida es la hidrólisis de la esfingomielina. Se ha demostrado que la ceramida puede interactuar con la esfingomielina para inducir la segregación lateral de dominios rígidos y altamente ordenados. Sin embargo, la esfingomielina es capaz también de interactuar con el colesterol, presente en gran cantidad en las membranas plasmáticas, induciendo la formación de dominios líquido-ordenado. Por lo tanto, la actividad esfingomielinasa daría lugar a plataformas enriquecidas en esfingomielina, colesterol y ceramida.

Inicialmente, varios estudios mostraron cómo la ceramida puede desplazar al colesterol de su interacción con la esfingomielina. Sin embargo, también se demostró que el colesterol puede regular la formación de dominios ricos en ceramida. Recientemente se ha sugerido que la ceramida y el colesterol podrían interactuar entre ellos en una bicapa de fosfolípidos saturados sin una fase desordenada para formar una fase ternaria homogénea con propiedades únicas. El Capítulo 4 trata de confirmar esta observación y de caracterizar más a fondo el efecto de la incorporación de la ceramida y el colesterol en bicapas de esfingomielina o DPPC, empleando los tiempos de vida del tPA y la anisotropía del DPH para estudiar el orden de la membrana y la estabilidad térmica de las bicapas ordenadas. Los resultados obtenidos mediante estas técnicas fluorescentes coinciden completamente con los estudios previos respaldando la formación de una fase ternaria homogénea. Esta fase muestra propiedades únicas reguladas probablemente tanto por la ceramida como por el colesterol: demuestra un alto orden y estabilidad térmica, probablemente como consecuencia del efecto de la ceramida; pero aún así no se observa una transición de fases clara y la fase ternaria no parece desordenarse por completo incluso a altas temperaturas, probablemente por efecto del colesterol.

Por otra parte se llevaron a cabo experimentos con DSC en bicapas con proporciones decrecientes de colesterol y ceramida para determinar el rol que su cantidad combinada en la bicapa y su relación molar pueden tener sobre su interacción. Los resultados muestran que la interacción entre la ceramida y el colesterol depende no tanto de su relación molar como de la concentración de colesterol en la bicapa.

7.3 El mecanismo de permeabilización de membranas inducido por la ceramida.

Una propiedad importante de las ceramidas, que podría estar relacionada con su función biológica en la respuesta celular al estrés, es su habilidad para inducir la permeabilización de las membranas. No obstante, el mecanismo subyacente a este proceso todavía se desconoce. Nuestra hipótesis propone que la permeabilización de la membrana ocurre debido a la reestructuración y desestabilización de la bicapa inducida por la ceramida, así como debido a los defectos de empaquetamiento en los límites de los dominios enriquecidos en ceramida. Sin embargo, estudios de Sikind, Colombini y colaboradores proponen que la permeabilización de membrana inducida por ceramida ocurre a través de la formación de canales de ceramida estructurados, estables y de gran tamaño, los cuales podrían inducir la apoptosis de manera directa mediante la permeabilización de la mitocondria y la liberación del citocromo c.

El capítulo 5 trata de aclarar esta incógnita, empleando para ello un ensayo de liberación basado en los tiempos de vida de la calceína, que permite la determinación del mecanismo de liberación. En los ensayos de liberación con liposomas empleados para estudiar la permeabilización de membrana, la liberación parcial puede producirse debido a que algunas vesículas liberan todo su contenido (liberación todo-o-nada) o a través de una liberación parcial de todas las vesículas (liberación gradual). La presencia de canales de ceramida en la membrana causaría sin duda alguna una liberación todo-o-nada, mientras que la liberación gradual sería más consistente con la hipótesis de la permeabilización debido a la desestabilización de las membranas por la segregación lateral de dominios de ceramida o por la formación localizada de fases no lamelares.

Primero, usando liposomas ricos en esfingomielina y colesterol, se observó que la generación *in situ* de ceramida a través de la acción de la esfingomielinasa produce una rápida liberación de contenidos siguiendo un mecanismo de liberación mixto. Esto es probablemente debido a una liberación principalmente gradual, pero con algunas vesículas más sensibles rompiéndose al comienzo de la reacción, siguiendo un mecanismo similar al previamente descrito para eritrocitos enriquecidos en ceramida. Además, la permeabilización de la membrana por la adición de ceramida de huevo demostró una clara liberación gradual. Estos resultados no admiten la presencia de canales en la membrana, que solamente podrían causar una liberación todo-o-nada.

Varios de los estudios que proponen la hipótesis de los canales de ceramida han usado de forma habitual una ceramida de cadena corta, la ceramida C2, la cual no fue capaz de provocar la permeabilización de vesículas en nuestro sistema. Por lo tanto, parece poco probable que esta ceramida, con propiedades biofísicas claramente diferentes a las de las ceramidas de cadena larga, puedan formar canales en las membranas tal y como se ha afirmado en dichos estudios.

La hipótesis de los canales de ceramida propone que estos canales son específicos de la membrana mitocondrial externa, por lo que dado que los liposomas ricos en esfingomielina y colesterol son más similares a la membrana plasmática que a la mitocondrial, se realizaron experimentos cambiando la composición de las membranas añadiendo un 30% de PC o incluso empleando liposomas con la composición lipídica de la membrana mitocondrial externa. Sin embargo, no se observó una permeabilización significativa en experimentos de liberación en LUV ni en experimentos de permeabilización en GUV. Una vez más, los resultados son contrarios a la hipótesis de la formación de canales de ceramida en la membrana.

Las discrepancias entre los resultados de este trabajo y los obtenidos por Siskind, Colombini y colaboradores podrían ser debidos a las diferentes técnicas empleadas. Las diferencias en la composición de las membranas podrían ser también importantes, especialmente dado que los estudios que proponen la formación de canales de ceramida usan membranas que podrían no ser consideradas como adecuadas, dada su poca relevancia biológica y su alta permeabilidad espontánea. Además, los estudios en favor de la hipótesis de los canales de ceramida empleando simulaciones y microscopía electrónica pueden ser considerados como no concluyentes.

7.4 Efectos de la ceramida sobre la integridad de la membrana

La función principal de las membranas celulares es crear una barrera semipermeable que separa dos compartimentos. Sin embargo, las membranas pueden perder su integridad debido a diversos factores, entre los que se incluyen algunos lípidos bioactivos como la ceramida. El capítulo 5 ha permitido profundizar en el mecanismo de la permeabilización de la membrana inducida por ceramida. Sin embargo, todavía quedan muchas cuestiones sin aclarar. Por lo tanto, el capítulo 6 continúa con los estudios sobre la habilidad de la ceramida para afectar la integridad de la membrana.

Primero se exploró el efecto de la ceramida en la tensión de borde de la bicapa. Esta es una propiedad mecánica de la bicapa lipídica que describe la penalización energética para la reorganización lipídica que tiene lugar tras la formación de un poro, cuando los lípidos en el borde del poro tienen que proteger sus cadenas hidrofóbicas del contacto desfavorable con el agua. Por lo tanto, la tensión de borde determina la habilidad de la membrana para sellarse tras haber perdido su integridad y puede ser altamente informativa en estudios sobre permeabilización de membranas.

El caso de la ceramida puede ser especialmente interesante si se tiene en cuenta la hipótesis de la formación de canales de ceramida. Debido a la geometría de cono de la ceramida y a sus propiedades biofísicas singulares, sería esperable que este lípido afectara de manera significativa a la tensión de borde de la membrana. Sin embargo, no se observó ningún efecto en la tensión de borde de bicapas de POPC ni con 3 mol% de ceramida ni con 10 mol% de DPG (un glicerofosfolípido análogo de la ceramida). Esta ausencia de efecto podría ser debida a la pequeña cantidad de ceramida presente en la bicapa, una limitación de la técnica experimental. No obstante, es importante tener en cuenta que la relación entre las propiedades de un lípido y su efecto sobre la tensión de borde no es fácil de predecir.

En una serie separada de experimentos, se estudió la habilidad permeabilizadora de las 1-deoxiceramidas, un nuevo tipo de ceramida recientemente descrito empleando ceramidas y deoxiceramidas con diferentes cadenas acílicas. Mientras que las diferentes cadenas acílicas no mostraron apenas diferencias en su efecto, las deoxiceramidas provocaron una permeabilidad significativamente menor que la de sus correspondientes ceramidas. Por lo tanto, el grupo hidroxilo que constituye la cabeza polar de la ceramida parece ser una característica estructural de gran importancia para la habilidad de la ceramida para permeabilizar membranas.

7.5 Conclusiones

Las principales conclusiones de este trabajo incluyen:

1) Los lípidos pentaenos pueden ser sondas útiles para su uso en estudios biofísicos de membrana empleando espectroscopía y microscopía de fluorescencia.

2) Mezclas ternarias compuestas por un fosfolípidos saturado (pSM o DPPC), colesterol (Chol) y palmitoilceramida (pCer) muestran una única fase ordenada homogénea que exhibe propiedades intermedias entre las de bicapas liquido-ordenadas enriquecidas en colesterol y las de bicapas similares a gel enriquecidas en pCer.

3) En las mezclas ternarias anteriores, la habilidad del colesterol para restringir la interacción de la pCer con la pSM y la segregación de dominios enriquecidos en pCer depende más del contenido total de colesterol en la bicapa que de la relación molar Chol/pCer.

4) La liberación inducida por ceramida en liposomas ricos en SM y Chol presenta principalmente un mecanismo gradual, mientras que la ceramida no induce liberación en bicapas lipídicas con baja cantidad de dichos dos lípidos, o en bicapas que imitan la composición lipídica de la membrana mitocondrial externa. En nuestras condiciones la ceramida no parece generar canales a través de la bicapa.

REFERENCES

REFERENCES

Alanko, S.M., Halling, K.K., Maunula, S., Slotte, J.P., and Ramstedt, B. (2005). Displacement of sterols from sterol/sphingomyelin domains in fluid bilayer membranes by competing molecules. *Biochim Biophys Acta* 1715: 111-121.

Angelova, M.I., and Dimitrov, D.S. (1986). Liposome electroformation. *Faraday Discussions of the Chemical Society* 81: 303.

Anishkin, A., Sukharev, S., and Colombini, M. (2006). Searching for the molecular arrangement of transmembrane ceramide channels. *Biophys J* 90: 2414-2426.

Aranda, F.J., and Gomez-Fernandez, J.C. (1986). Fluorescence probe studies of the interaction of ubiquinone-10 and ubiquinol-10 with phosphatidylcholine bilayers. *Biochem Int* 12: 137-143.

Aresta-Branco, F., Cordeiro, A.M., Marinho, H.S., Cyrne, L., Antunes, F., and de Almeida, R.F. (2011). Gel domains in the plasma membrane of Saccharomyces cerevisiae: highly ordered, ergosterol-free, and sphingolipid-enriched lipid rafts. *J Biol Chem* 286: 5043-5054.

Artetxe, I., Sergelius, C., Kurita, M., Yamaguchi, S., Katsumura, S., Slotte, J.P., and Maula, T. (2013). Effects of sphingomyelin headgroup size on interactions with ceramide. *Biophys J* 104: 604-612.

Bagatolli, L.A. (2006). To see or not to see: lateral organization of biological membranes and fluorescence microscopy. *Biochim Biophys Acta* 1758: 1541-1556.

Bakht, O., Delgado, J., Amat-Guerri, F., Acuna, A.U., and London, E. (2007). The phenyltetraene lysophospholipid analog PTE-ET-18-OMe as a fluorescent anisotropy probe of liquid ordered membrane domains (lipid rafts) and ceramide-rich membrane domains. *Biochim Biophys Acta* 1768: 2213-2221.

Balleza, D., Garcia-Arribas, A.B., Sot, J., Ruiz-Mirazo, K., and Goni, F.M. (2014). Ether- versus ester-linked phospholipid bilayers containing either linear or branched apolar chains. *Biophys J* 107: 1364-1374.

Bangham, A.D., and Horne, R.W. (1964). Negative Staining of Phospholipids and Their Structural Modification by Surface-Active Agents as Observed in the Electron Microscope. *J Mol Biol* 8: 660-668.

Bartlett, G.R. (1959). Phosphorus assay in column chromatography. *J Biol Chem* 234: 466-468.

Basanez, G., Ruiz-Arguello, M.B., Alonso, A., Goni, F.M., Karlsson, G., and Edwards, K. (1997). Morphological changes induced by phospholipase C and by sphingomyelinase on large unilamellar vesicles: a cryo-transmission electron microscopy study of liposome fusion. *Biophys J* 72: 2630-2637.

Baumgart, T., Hunt, G., Farkas, E.R., Webb, W.W., and Feigenson, G.W. (2007). Fluorescence probe partitioning between Lo/Ld phases in lipid membranes. *Biochim Biophys Acta* 1768: 2182-2194.

Benson, A.A. (1966). On the orientation of lipids in chloroplast and cell membranes. *J Am Oil Chem Soc* 43: 265-270.

Bertea, M., Rutti, M.F., Othman, A., Marti-Jaun, J., Hersberger, M., von Eckardstein, A., and Hornemann, T. (2010). Deoxysphingoid bases as plasma markers in diabetes mellitus. *Lipids Health Dis* 9: 84.

Bjorkbom, A., Rog, T., Kaszuba, K., Kurita, M., Yamaguchi, S., Lonnfors, M., Nyholm, T.K., Vattulainen, I., Katsumura, S., and Slotte, J.P. (2010). Effect of sphingomyelin headgroup size on molecular properties and interactions with cholesterol. *Biophys J* 99: 3300-3308.

Boal, D. (2002). Biomembranes. In Mechanics of the cell (Cambridge: Cambridge University Press), pp. 268-274.

Böttcher, C.J.F., Van gent, C.M., and Pries, C. (1961). A rapid and sensitive sub-micro phosphorus determination. *Analytica Chimica Acta* 24: 203-204.

Brash, A.R. (2001). Arachidonic acid as a bioactive molecule. *J Clin Invest* 107: 1339-1345.

Brouwer, A.M. (2011). Standards for photoluminescence quantum yield measurements in solution (IUPAC Technical Report). *Pure and Applied Chemistry* 83: 2213-2228.

Brown, D.A., and London, E. (1998). Structure and origin of ordered lipid domains in biological membranes. *J Membr Biol* 164: 103-114.

Busto, J.V., Fanani, M.L., De Tullio, L., Sot, J., Maggio, B., Goni, F.M., and Alonso, A. (2009). Coexistence of immiscible mixtures of palmitoylsphingomyelin and palmitoylceramide in monolayers and bilayers. *Biophys J* 97: 2717-2726.

Busto, J.V., Garcia-Arribas, A.B., Sot, J., Torrecillas, A., Gomez-Fernandez, J.C., Goni, F.M., and Alonso, A. (2014). Lamellar gel (lbeta) phases of ternary lipid composition containing ceramide and cholesterol. *Biophys J* 106: 621-630.

Busto, J.V., Sot, J., Requejo-Isidro, J., Goni, F.M., and Alonso, A. (2010). Cholesterol displaces palmitoylceramide from its tight packing with palmitoylsphingomyelin in the absence of a liquid-disordered phase. *Biophys J* 99: 1119-1128.

Carreira, A.C., Ventura, A.E., Varela, A.R., and Silva, L.C. (2015). Tackling the biophysical properties of sphingolipids to decipher their biological roles. *Biol Chem* 396: 597-609.

Carrer, D.C., and Maggio, B. (1999). Phase behavior and molecular interactions in mixtures of ceramide with dipalmitoylphosphatidylcholine. *J Lipid Res* 40: 1978-1989.

Castanho, M., Prieto, M., and Acuna, A.U. (1996). The transverse location of the fluorescent probe trans-parinaric acid in lipid bilayers. *Biochim Biophys Acta* 1279: 164-168.

Castro, B.M., de Almeida, R.F., Silva, L.C., Fedorov, A., and Prieto, M. (2007). Formation of ceramide/sphingomyelin gel domains in the presence of an unsaturated phospholipid: a quantitative multiprobe approach. *Biophys J* 93: 1639-1650.

Castro, B.M., Prieto, M., and Silva, L.C. (2014). Ceramide: A simple sphingolipid with unique biophysical properties. *Prog Lipid Res* 54C: 53-67.

Castro, B.M., Silva, L.C., Fedorov, A., de Almeida, R.F., and Prieto, M. (2009). Cholesterol-rich fluid membranes solubilize ceramide domains: implications for the structure and dynamics of mammalian intracellular and plasma membranes. *J Biol Chem* 284: 22978-22987.

Catapano, E.R., Arriaga, L.R., Espinosa, G., Monroy, F., Langevin, D., and Lopez-Montero, I. (2011). Solid character of membrane ceramides: a surface rheology study of their mixtures with sphingomyelin. *Biophys J* 101: 2721-2730.

Colombini, M. (2013). Membrane channels formed by ceramide. *Handb Exp Pharmacol*: 109-126.

Colombini, M. (2016). Ceramide channels and mitochondrial outer membrane permeability. *J Bioenerg Biomembr*.

Contreras, F.X., Basanez, G., Alonso, A., Herrmann, A., and Goni, F.M. (2005). Asymmetric addition of ceramides but not dihydroceramides promotes transbilayer (flip-flop) lipid motion in membranes. *Biophys J* 88: 348-359.

Contreras, F.X., Villar, A.V., Alonso, A., Kolesnick, R.N., and Goni, F.M. (2003). Sphingomyelinase activity causes transbilayer lipid translocation in model and cell membranes. *J Biol Chem* 278: 37169-37174.

Cremesti, A., Paris, F., Grassme, H., Holler, N., Tschopp, J., Fuks, Z., Gulbins, E., and Kolesnick, R. (2001). Ceramide enables fas to cap and kill. *J Biol Chem* 276: 23954-23961.

Cremesti, A.E., Goni, F.M., and Kolesnick, R. (2002). Role of sphingomyelinase and ceramide in modulating rafts: do biophysical properties determine biologic outcome? *FEBS Lett* 531: 47-53.

Chiantia, S., Kahya, N., Ries, J., and Schwille, P. (2006). Effects of ceramide on liquid-ordered domains investigated by simultaneous AFM and FCS. *Biophys J* 90: 4500-4508.

Chiantia, S., Kahya, N., and Schwille, P. (2007). Raft domain reorganization driven by short- and long-chain ceramide: a combined AFM and FCS study. *Langmuir* 23: 7659-7665.

Danielli, J.F., and Davson, H. (1935). A contribution to the theory of permeability of thin films. *Journal of Cellular and Comparative Physiology* 5: 495-508.

Davis, P.J., Coolbear, K.P., and Keough, K.M. (1980). Differential scanning calorimetric studies of the thermotropic phase behavior of membranes composed of dipalmitoyllecithin and mixed-acid unsaturated lecithins. *Can J Biochem* 58: 851-858.

de Almeida, R.F., Fedorov, A., and Prieto, M. (2003). Sphingomyelin/phosphatidylcholine/cholesterol phase diagram: boundaries and composition of lipid rafts. *Biophys J* 85: 2406-2416.

de Almeida, R.F., Loura, L.M., Fedorov, A., and Prieto, M. (2002). Nonequilibrium phenomena in the phase separation of a two-component lipid bilayer. *Biophys J* 82: 823-834.

Di Paola, M., Cocco, T., and Lorusso, M. (2000). Ceramide interaction with the respiratory chain of heart mitochondria. *Biochemistry* 39: 6660-6668.

Eggeling, C., Ringemann, C., Medda, R., Schwarzmann, G., Sandhoff, K., Polyakova, S., Belov, V.N., Hein, B., von Middendorff, C., Schonle, A*., et al.* (2009). Direct observation of the nanoscale dynamics of membrane lipids in a living cell. *Nature* 457: 1159-1162.

Ellens, H., Bentz, J., and Szoka, F.C. (1985). H+- and Ca2+-induced fusion and destabilization of liposomes. *Biochemistry* 24: 3099-3106.

Engelman, D.M. (2005). Membranes are more mosaic than fluid. *Nature* 438: 578-580.

Fabrias, G., Munoz-Olaya, J., Cingolani, F., Signorelli, P., Casas, J., Gagliostro, V., and Ghidoni, R. (2012). Dihydroceramide desaturase and dihydrosphingolipids: debutant players in the sphingolipid arena. *Prog Lipid Res* 51: 82-94.

Fadok, V.A., Bratton, D.L., Frasch, S.C., Warner, M.L., and Henson, P.M. (1998). The role of phosphatidylserine in recognition of apoptotic cells by phagocytes. *Cell Death Differ* 5: 551-562.

Fanani, M.L., Hartel, S., Maggio, B., De Tullio, L., Jara, J., Olmos, F., and Oliveira, R.G. (2010). The action of sphingomyelinase in lipid monolayers as revealed by microscopic image analysis. *Biochim Biophys Acta* 1798: 1309-1323.

Fidorra, M., Heimburg, T., and Bagatolli, L.A. (2009). Direct visualization of the lateral structure of porcine brain cerebrosides/POPC mixtures in presence and absence of cholesterol. *Biophys J* 97: 142-154.

Fiske, C.H., and Subbarow, Y. (1925). The colorimetric determination of phosphorus. *Journal of Biological Chemistry* 66: 375-400.

Garcia-Arribas, A.B., Alonso, A., and Goni, F.M. (2016). Cholesterol interactions with ceramide and sphingomyelin. *Chem Phys Lipids* 199: 26-34.

Garcia-Arribas, A.B., Busto, J.V., Alonso, A., and Goni, F.M. (2015). Atomic force microscopy characterization of palmitoylceramide and cholesterol effects on phospholipid bilayers: a topographic and nanomechanical study. *Langmuir* 31: 3135-3145.

Gilbert, R.J. (2016). Protein-lipid interactions and non-lamellar lipidic structures in membrane pore formation and membrane fusion. *Biochim Biophys Acta* 1858: 487-499.

Gomez-Munoz, A., Presa, N., Gomez-Larrauri, A., Rivera, I.G., Trueba, M., and Ordonez, M. (2016). Control of inflammatory responses by ceramide, sphingosine 1-phosphate and ceramide 1-phosphate. *Prog Lipid Res* 61: 51-62.

Goni, F.M. (2014). The basic structure and dynamics of cell membranes: an update of the Singer-Nicolson model. *Biochim Biophys Acta* 1838: 1467-1476.

Goni, F.M., and Alonso, A. (1999). Structure and functional properties of diacylglycerols in membranes. *Prog Lipid Res* 38: 1-48.

Goni, F.M., Alonso, A., Bagatolli, L.A., Brown, R.E., Marsh, D., Prieto, M., and Thewalt, J.L. (2008). Phase diagrams of lipid mixtures relevant to the study of membrane rafts. *Biochim Biophys Acta* 1781: 665-684.

Goni, F.M., Sot, J., and Alonso, A. (2014). Biophysical properties of sphingosine, ceramides and other simple sphingolipids. *Biochem Soc Trans* 42: 1401-1408.

Gorter, E., and Grendel, F. (1925). On Bimolecular Layers of Lipoids on the Chromocytes of the Blood. *J Exp Med* 41: 439-443.

Green, J.A., Singer, L.A., and Parks, J.H. (1973). Fluorescence quenching by the stable free radical di-t-butylnitroxide. *The Journal of Chemical Physics* 58: 2690.

Halling, K.K., Ramstedt, B., Nystrom, J.H., Slotte, J.P., and Nyholm, T.K. (2008). Cholesterol interactions with fluid-phase phospholipids: effect on the lateral organization of the bilayer. *Biophys J* 95: 3861-3871.

Hannun, Y.A. (1996). Functions of ceramide in coordinating cellular responses to stress. *Science* 274: 1855-1859.

Hannun, Y.A., Loomis, C.R., Merrill, A.H., Jr., and Bell, R.M. (1986). Sphingosine inhibition of protein kinase C activity and of phorbol dibutyrate binding in vitro and in human platelets. *J Biol Chem* 261: 12604-12609.

Hannun, Y.A., and Obeid, L.M. (2008). Principles of bioactive lipid signalling: lessons from sphingolipids. *Nat Rev Mol Cell Biol* 9: 139-150.

Henry, B., Ziobro, R., Becker, K.A., Kolesnick, R., and Gulbins, E. (2013). Acid Sphingomyelinase. In Sphingolipids: Basic Science and Drug Development, E. Gulbins, and I. Petrache, eds. (Vienna: Springer Vienna), pp. 77-88.

Hermann, E., Bleicken, S., Subburaj, Y., and Garcia-Saez, A.J. (2014). Automated analysis of giant unilamellar vesicles using circular Hough transformation. *Bioinformatics*.

Hernandez-Tiedra, S., Fabrias, G., Davila, D., Salanueva, I.J., Casas, J., Montes, L.R., Anton, Z., Garcia-Taboada, E., Salazar-Roa, M., Lorente, M.*, et al.* (2016). Dihydroceramide accumulation mediates cytotoxic autophagy of cancer cells via autolysosome destabilization. *Autophagy* 12: 2213-2229.

Holzl, G., and Dormann, P. (2007). Structure and function of glycoglycerolipids in plants and bacteria. *Prog Lipid Res* 46: 225-243.

Huang, H.W., Goldberg, E.M., and Zidovetzki, R. (1996). Ceramide induces structural defects into phosphatidylcholine bilayers and activates phospholipase A2. *Biochem Biophys Res Commun* 220: 834-838.

Huang, J., and Feigenson, G.W. (1999). A microscopic interaction model of maximum solubility of cholesterol in lipid bilayers. *Biophys J* 76: 2142-2157.

Ipsen, J.H., Karlstrom, G., Mouritsen, O.G., Wennerstrom, H., and Zuckermann, M.J. (1987). Phase equilibria in the phosphatidylcholine-cholesterol system. *Biochim Biophys Acta* 905: 162-172.

Irvine, R.F. (2016). A short history of inositol lipids. *J Lipid Res* 57: 1987-1994.

Israelachvili, J.N., Marcelja, S., and Horn, R.G. (1980). Physical principles of membrane organization. *Q Rev Biophys* 13: 121-200.

Jacobi, J., Garcia-Barros, M., Rao, S., Rotolo, J.A., Thompson, C., Mizrachi, A., Feldman, R., Manova, K., Bielawska, A., Bielawska, J.*, et al.* (2016). Targeting acid sphingomyelinase with anti-angiogenic chemotherapy. *Cell Signal* 29: 52-61.

Jimenez-Rojo, N., Garcia-Arribas, A.B., Sot, J., Alonso, A., and Goni, F.M. (2014a). Lipid bilayers containing sphingomyelins and ceramides of varying N-acyl lengths: a glimpse into sphingolipid complexity. *Biochim Biophys Acta* 1838: 456-464.

Jimenez-Rojo, N., Sot, J., Busto, J.V., Shaw, W.A., Duan, J., Merrill, A.H., Jr., Alonso, A., and Goni, F.M. (2014b). Biophysical properties of novel 1-deoxy-(dihydro)ceramides occurring in mammalian cells. *Biophys J* 107: 2850-2859.

Jimenez-Rojo, N., Sot, J., Viguera, A.R., Collado, M.I., Torrecillas, A., Gomez-Fernandez, J.C., Goni, F.M., and Alonso, A. (2014c). Membrane permeabilization induced by sphingosine: effect of negatively charged lipids. *Biophys J* 106: 2577-2584.

Juhasz, J., Davis, J.H., and Sharom, F.J. (2010). Fluorescent probe partitioning in giant unilamellar vesicles of 'lipid raft' mixtures. *Biochem J* 430: 415-423.

Kleinzeller, A. (1998). Ernest Overtons contribution to the cell membrane concept: a centennial appreciation. *Am J Physiol Cell Physiol* 274: 13-23.

Knorr, R.L., Staykova, M., Gracia, R.S., and Dimova, R. (2010). Wrinkling and electroporation of giant vesicles in the gel phase. *Soft Matter* 6: 1990-1996.

Kolesnick, R.N. (1987). 1,2-Diacylglycerols but not phorbol esters stimulate sphingomyelin hydrolysis in GH3 pituitary cells. *J Biol Chem* 262: 16759-16762.

Kolesnick, R.N., Goni, F.M., and Alonso, A. (2000). Compartmentalization of ceramide signaling: physical foundations and biological effects. *J Cell Physiol* 184: 285-300.

Korlach, J., Schwille, P., Webb, W.W., and Feigenson, G.W. (1999). Characterization of lipid bilayer phases by confocal microscopy and fluorescence correlation spectroscopy. *Proc Natl Acad Sci U S A* 96: 8461-8466.

Kotnik, T., Frey, W., Sack, M., Haberl Meglic, S., Peterka, M., and Miklavcic, D. (2015). Electroporation-based applications in biotechnology. *Trends Biotechnol* 33: 480-488.

Kuerschner, L., Ejsing, C.S., Ekroos, K., Shevchenko, A., Anderson, K.I., and Thiele, C. (2005). Polyene-lipids: a new tool to image lipids. *Nat Methods* 2: 39-45.

Lakowicz, J.R. (2006a). Fluorescence Anisotropy. In Principles of Fluorescence Spectroscopy, J.R. Lakowicz, ed. (Boston, MA: Springer US), pp. 353-382.

Lakowicz, J.R. (2006b). Principles of Fluorescence Spectroscopy (Boston, MA: Springer US).

Lakowicz, J.R. (2006c). Time-Domain Lifetime Measurements. In Principles of Fluorescence Spectroscopy, J.R. Lakowicz, ed. (Boston, MA: Springer US), pp. 97-155.

Lete, M.G., Sot, J., Gil, D., Valle, M., Medina, M., Goni, F.M., and Alonso, A. (2015). Histones cause aggregation and fusion of lipid vesicles containing phosphatidylinositol-4-phosphate. *Biophys J* 108: 863-871.

Li, F., and Zhang, N. (2015). Ceramide: Therapeutic Potential in Combination Therapy for Cancer Treatment. *Curr Drug Metab* 17: 37-51.

Lichtenberg, D., Goni, F.M., and Heerklotz, H. (2005). Detergent-resistant membranes should not be identified with membrane rafts. *Trends Biochem Sci* 30: 430-436.

Lingwood, D., and Simons, K. (2010). Lipid rafts as a membrane-organizing principle. *Science* 327: 46-50.

Lonnfors, M., Doux, J.P., Killian, J.A., Nyholm, T.K., and Slotte, J.P. (2011). Sterols have higher affinity for sphingomyelin than for phosphatidylcholine bilayers even at equal acyl-chain order. *Biophys J* 100: 2633-2641.

Lopez-Montero, I., Rodriguez, N., Cribier, S., Pohl, A., Velez, M., and Devaux, P.F. (2005). Rapid transbilayer movement of ceramides in phospholipid vesicles and in human erythrocytes. *J Biol Chem* 280: 25811-25819.

Luckey, M. (2008). Membrane Structural Biology With Biochemical and Biophysical Foundations (New York: Cambridge University Press).

Luzzati, V. (1968). X-ray diffraction studies of lipid-water systems. In Biological Membranes, D. Chapman, ed. (London: Academic Press), pp. 71-123.

Mateo, C.R., Souto, A.A., Amat-Guerri, F., and Acuna, A.U. (1996). New fluorescent octadecapentaenoic acids as probes of lipid membranes and protein-lipid interactions. *Biophys J* 71: 2177-2191.

Maula, T., Artetxe, I., Grandell, P.M., and Slotte, J.P. (2012). Importance of the Sphingoid Base Length for the Membrane Properties of Ceramides. *Biophys J* 103: 1870-1879.

Mayer, L.D., Hope, M.J., and Cullis, P.R. (1986). Vesicles of variable sizes produced by a rapid extrusion procedure. *Biochim Biophys Acta* 858: 161-168.

McConnell, H.M., Tamm, L.K., and Weis, R.M. (1984). Periodic structures in lipid monolayer phase transitions. *Proc Natl Acad Sci U S A* 81: 3249-3253.

Megha, and London, E. (2004). Ceramide selectively displaces cholesterol from ordered lipid domains (rafts): implications for lipid raft structure and function. *J Biol Chem* 279: 9997-10004.

Megha, Sawatzki, P., Kolter, T., Bittman, R., and London, E. (2007). Effect of ceramide N-acyl chain and polar headgroup structure on the properties of ordered lipid domains (lipid rafts). *Biochim Biophys Acta* 1768: 2205-2212.

Mollinedo, F., and Gajate, C. (2006). Fas/CD95 death receptor and lipid rafts: new targets for apoptosis-directed cancer therapy. *Drug Resist Updat* 9: 51-73.

Montes, L.R., Alonso, A., Goni, F.M., and Bagatolli, L.A. (2007). Giant unilamellar vesicles electroformed from native membranes and organic lipid mixtures under physiological conditions. *Biophys J* 93: 3548-3554.

Montes, L.R., Lopez, D.J., Sot, J., Bagatolli, L.A., Stonehouse, M.J., Vasil, M.L., Wu, B.X., Hannun, Y.A., Goni, F.M., and Alonso, A. (2008). Ceramide-enriched membrane domains in red blood cells and the mechanism of sphingomyelinase-induced hot-cold hemolysis. *Biochemistry* 47: 11222-11230.

Montes, L.R., Ruiz-Arguello, M.B., Goni, F.M., and Alonso, A. (2002). Membrane restructuring via ceramide results in enhanced solute efflux. *J Biol Chem* 277: 11788-11794.

Morris, J.V., Mahaney, M.A., and Huber, J.R. (1976). Fluorescence quantum yield determinations. 9,10-Diphenylanthracene as a reference standard in different solvents. *The Journal of Physical Chemistry* 80: 969-974.

Mullen, T.D., Jenkins, R.W., Clarke, C.J., Bielawski, J., Hannun, Y.A., and Obeid, L.M. (2011). Ceramide synthase-dependent ceramide generation and programmed cell death: involvement of salvage pathway in regulating postmitochondrial events. *J Biol Chem* 286: 15929-15942.

Mullen, T.D., and Obeid, L.M. (2012). Ceramide and apoptosis: exploring the enigmatic connections between sphingolipid metabolism and programmed cell death. *Anticancer Agents Med Chem* 12: 340-363.

Nyholm, T.K., Grandell, P.M., Westerlund, B., and Slotte, J.P. (2010). Sterol affinity for bilayer membranes is affected by their ceramide content and the ceramide chain length. *Biochim Biophys Acta* 1798: 1008-1013.

Nyholm, T.K., Lindroos, D., Westerlund, B., and Slotte, J.P. (2011). Construction of a DOPC/PSM/cholesterol phase diagram based on the fluorescence properties of trans-parinaric acid. *Langmuir* 27: 8339-8350.

Obeid, L.M., Linardic, C.M., Karolak, L.A., and Hannun, Y.A. (1993). Programmed cell death induced by ceramide. *Science* 259: 1769-1771.

Patalag, L.J., and Werz, D.B. (2012). Fluorescent penta- and hexaene fatty acids by a Wittig-Horner/elimination strategy. *J Org Chem* 77: 5297-5304.

Patel, H., Tscheka, C., and Heerklotz, H. (2009). Characterizing vesicle leakage by fluorescence lifetime measurements. *Soft Matter* 5: 2849-5851.

Pinto, S.N., Fernandes, F., Fedorov, A., Futerman, A.H., Silva, L.C., and Prieto, M. (2013). A combined fluorescence spectroscopy, confocal and 2-photon microscopy approach to re-evaluate the properties of sphingolipid domains. *Biochim Biophys Acta* 1828: 2099-2110.

Pinto, S.N., Silva, L.C., Futerman, A.H., and Prieto, M. (2011). Effect of ceramide structure on membrane biophysical properties: the role of acyl chain length and unsaturation. *Biochim Biophys Acta* 1808: 2753-2760.

Portet, T., and Dimova, R. (2010). A new method for measuring edge tensions and stability of lipid bilayers: effect of membrane composition. *Biophys J* 99: 3264-3273.

Robertson, J.D. (1959). The ultrastructure of cell membranes and their derivatives. *Biochem Soc Symp* 16: 3-43.

Robertson, J.D. (1981). Membrane structure. *The Journal of Cell Biology* 91: 189s-204s.

Ruggiero, A., and Hudson, B. (1989). Critical density fluctuations in lipid bilayers detected by fluorescence lifetime heterogeneity. *Biophys J* 55: 1111-1124.

Ruiz-Arguello, M.B., Basanez, G., Goni, F.M., and Alonso, A. (1996). Different effects of enzyme-generated ceramides and diacylglycerols in phospholipid membrane fusion and leakage. *J Biol Chem* 271: 26616-26621.

Samanta, S., Stiban, J., Maugel, T.K., and Colombini, M. (2011). Visualization of ceramide channels by transmission electron microscopy. *Biochim Biophys Acta* 1808: 1196-1201.

Siddique, M.M., Li, Y., Chaurasia, B., Kaddai, V.A., and Summers, S.A. (2015). Dihydroceramides: From Bit Players to Lead Actors. *J Biol Chem* 290: 15371-15379.

Silva, L.C., de Almeida, R.F., Castro, B.M., Fedorov, A., and Prieto, M. (2007). Ceramide-domain formation and collapse in lipid rafts: membrane reorganization by an apoptotic lipid. *Biophys J* 92: 502-516.

Silva, L.C., Futerman, A.H., and Prieto, M. (2009). Lipid raft composition modulates sphingomyelinase activity and ceramide-induced membrane physical alterations. *Biophys J* 96: 3210-3222.

Simons, K., and Ikonen, E. (1997). Functional rafts in cell membranes. *Nature* 387: 569-572.

Singer, S.J., and Nicolson, G.L. (1972). The fluid mosaic model of the structure of cell membranes. *Science* 175: 720-731.

Siskind, L.J., and Colombini, M. (2000). The lipids C2- and C16-ceramide form large stable channels. Implications for apoptosis. *J Biol Chem* 275: 38640-38644.

Siskind, L.J., Davoody, A., Lewin, N., Marshall, S., and Colombini, M. (2003). Enlargement and contracture of C2-ceramide channels. *Biophys J* 85: 1560-1575.

Siskind, L.J., Kolesnick, R.N., and Colombini, M. (2002). Ceramide channels increase the permeability of the mitochondrial outer membrane to small proteins. *J Biol Chem* 277: 26796-26803.

Siskind, L.J., Kolesnick, R.N., and Colombini, M. (2006). Ceramide forms channels in mitochondrial outer membranes at physiologically relevant concentrations. *Mitochondrion* 6: 118-125.

Sklar, L.A., Hudson, B.S., and Simoni, R.D. (1975). Conjugated polyene fatty acids as membrane probes: preliminary characterization. *Proc Natl Acad Sci U S A* 72: 1649-1653.

Slotte, J.P. (2016). The importance of hydrogen bonding in sphingomyelin's membrane interactions with co-lipids. *Biochim Biophys Acta* 1858: 304-310.

Sot, J., Aranda, F.J., Collado, M.I., Goni, F.M., and Alonso, A. (2005a). Different effects of long- and short-chain ceramides on the gel-fluid and lamellar-hexagonal transitions of phospholipids: a calorimetric, NMR, and x-ray diffraction study. *Biophys J* 88: 3368-3380.

Sot, J., Bagatolli, L.A., Goni, F.M., and Alonso, A. (2006). Detergent-resistant, ceramide-enriched domains in sphingomyelin/ceramide bilayers. *Biophys J* 90: 903-914.

Sot, J., Goni, F.M., and Alonso, A. (2005b). Molecular associations and surface-active properties of short- and long-N-acyl chain ceramides. *Biochim Biophys Acta* 1711: 12-19.

Sot, J., Ibarguren, M., Busto, J.V., Montes, L.R., Goni, F.M., and Alonso, A. (2008). Cholesterol displacement by ceramide in sphingomyelin-containing liquid-ordered domains, and generation of gel regions in giant lipidic vesicles. *FEBS Lett* 582: 3230-3236.

Souto, A.A., Acuña, A.U., and Amat-Guerri, F. (1994). A general and practical synthesis of linear conjugated pentaenoic acids. *Tetrahedron Letters* 35: 5907-5910.

Stillwell, W. (2013). An Introduction to Biological Membranes: From Bilayers to Rafts (San Diego: Elsevier).

Thudichum, J.L.W. (1884). A treatise on the chemical constitution of the brain: based throughout upon original researches (London: Bailliere, Tindall, and Cox).

Tristram-Nagle, S., Kim, D.J., Akhunzada, N., Kucerka, N., Mathai, J.C., Katsaras, J., Zeidel, M., and Nagle, J.F. (2010). Structure and water permeability of fully hydrated diphytanoylPC. *Chem Phys Lipids* 163: 630-637.

Urbina, P., Flores-Diaz, M., Alape-Giron, A., Alonso, A., and Goni, F.M. (2009). Phospholipase C and sphingomyelinase activities of the Clostridium perfringens alpha-toxin. *Chem Phys Lipids* 159: 51-57.

Vanderkooi, G., and Green, D.E. (1970). Biological membrane structure, I. The protein crystal model for membranes. *Proc Natl Acad Sci U S A* 66: 615-621.

Veiga, M.P., Arrondo, J.L., Goni, F.M., and Alonso, A. (1999). Ceramides in phospholipid membranes: effects on bilayer stability and transition to nonlamellar phases. *Biophys J* 76: 342-350.

Veiga, M.P., Arrondo, J.L., Goni, F.M., Alonso, A., and Marsh, D. (2001). Interaction of cholesterol with sphingomyelin in mixed membranes containing phosphatidylcholine, studied by spin-label ESR and IR spectroscopies. A possible stabilization of gel-phase sphingolipid domains by cholesterol. *Biochemistry* 40: 2614-2622.

Vieira, C.R., Munoz-Olaya, J.M., Sot, J., Jimenez-Baranda, S., Izquierdo-Useros, N., Abad, J.L., Apellaniz, B., Delgado, R., Martinez-Picado, J., Alonso, A.*, et al.* (2010). Dihydrosphingomyelin impairs HIV-1 infection by rigidifying liquid-ordered membrane domains. *Chem Biol* 17: 766-775.

Wang, S.W., Hojabrpour, P., Zhang, P., Kolesnick, R.N., Steinbrecher, U.P., Gomez-Munoz, A., and Duronio, V. (2015). Regulation of ceramide generation during macrophage apoptosis by ASMase and de novo synthesis. *Biochim Biophys Acta* 1851: 1482-1489.

Wolber, P.K., and Hudson, B.S. (1981). Fluorescence lifetime and time-resolved polarization anisotropy studies of acyl chain order and dynamics in lipid bilayers. *Biochemistry* 20: 2800-2810.

Yarmush, M.L., Golberg, A., Sersa, G., Kotnik, T., and Miklavcic, D. (2014). Electroporation-based technologies for medicine: principles, applications, and challenges. *Annu Rev Biomed Eng* 16: 295-320.

Yeagle, P.L. (2012). The Structure of Biological Membranes, 3rd edn (Boca Raton: CRC Press).

Yingchoncharoen, P., Kalinowski, D.S., and Richardson, D.R. (2016). Lipid-Based Drug Delivery Systems in Cancer Therapy: What Is Available and What Is Yet to Come. *Pharmacol Rev* 68: 701-787.

Zhang, Y., Li, X., Becker, K.A., and Gulbins, E. (2009). Ceramide-enriched membrane domains--structure and function. *Biochim Biophys Acta* 1788: 178-183.

Zitomer, N.C., Mitchell, T., Voss, K.A., Bondy, G.S., Pruett, S.T., Garnier-Amblard, E.C., Liebeskind, L.S., Park, H., Wang, E., Sullards, M.C.*, et al.* (2009). Ceramide synthase inhibition by fumonisin B1 causes accumulation of 1-deoxysphinganine: a novel category of bioactive 1-deoxysphingoid bases and 1-deoxydihydroceramides biosynthesized by mammalian cell lines and animals. *J Biol Chem* 284: 4786-4795.

Zuellig, R.A., Hornemann, T., Othman, A., Hehl, A.B., Bode, H., Guntert, T., Ogunshola, O.O., Saponara, E., Grabliauskaite, K., Jang, J.H.*, et al.* (2014). Deoxysphingolipids, novel biomarkers for type 2 diabetes, are cytotoxic for insulin-producing cells. *Diabetes* 63: 1326-1339.

PUBLICATIONS

PUBLICATIONS

- Artetxe I., Ugarte-Uribe B., Alonso A., García-Sáez A.J. and Goñi F.M. (2017). Does ceramide form channels? The ceramide-induced membrane permeabilization mechanism. *Submitted.*

- Nieves I., Artetxe I., Abad J.L., Alonso A., Busto J.V., Fajarí L., Montes L.R., Sot J., Delgado A. and Goñi F.M. (2015). Fluorescent polyene ceramide analogues as membrane probes. *Langmuir* 31(8): 2484-2492

Additional publications not part of this thesis

- Acosta-Andrade C., Artetxe I., Lete M.G., Ruiz-Mirazo K., Goñi F.M. and Sanchez-Jimenez Francisca. (2016). Polyamine-RNA-membrane interactions: from the past to the future in biology. *Colloid Surface B.* [Under 2nd review]

- Lacalle R.A., de Karam J.C., Martínez-Muñoz L., Artetxe I., Peregil R.M., Sot J., Rojas A.M., Goñi F.M., Mellado M. and Mañes S. (2015). Type I phosphatidylinositol 4-phosphate 5-kinase homo and heterodimerization determines its membrane localization and activity. *FASEB J* 29(6): 2371-2385

- Artetxe, I., Sergelius, C., Kurita, M., Yamaguchi, S., Katsumura, S., Slotte, J. P. and Maula, T. (2013) Effects of sphingomyelin headgroup size on interactions with ceramide. *Biophys J* 104(3), 604-612.

- Maula, T., Artetxe, I., Grandell, P. M. and Slotte, J. P. (2012) Importance of the Sphingoid Base Length for the Membrane Properties of Ceramides. *Biophys J* 103(9), 1870-1879.

ACKNOWLEDGMENTS

ACKNOWLEDGMENTS

The present thesis has been carried out at the Biofisika Institute (UPV/EHU, CSIC), under the supervision of Prof. Félix M. Goñi. The work has been supported by the Basque Government (IT 838-13 and IT 849-13) and the Spanish Government (BFU 2011-28566, BFU 2012-36241 and BFU 2015-66306-P). The author received a research fellowship from the University of the Basque Country (February 2013-January 2017).

The author is grateful to Prof. Alicia Alonso and Dr. Jesús Sot for their valuable assistance throughout the thesis, to Prof. Antonio Delgado and Dr. Ingrid Nieves (Institute of Advanced Chemistry of Catalonia, Barcelona) for their productive collaboration on the work described in chapter 3, to Prof. J. Peter Slotte (Åbo Akademi University, Turku, Finland) for providing the tPA used in chapter 4, to Prof. Ana J. García-Sáez and Dr. Begoña Ugarte-Uribe (Eberhard Karls Universität Tübingen, Tübingen, Germany) for their training in the GUV permeabilization assay used in chapter 5, and to Dr. Rumiana Dimova and Dr. Roland Knorr (Max Plank Institute of Colloids and Interfaces, Potsdam, Germany) for their training in the electroporation technique for measuring bilayer edge tension employed in chapter 6.